

**FINAL REPORT**

**ADVANCED  
COLOR IMAGE ASSESSMENT  
CONCEPTS**

STATINTL

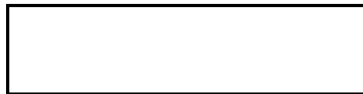
Declass Review by NGA/DOD

FINAL REPORT

ADVANCED COLOR IMAGE ASSESSMENT CONCEPTS

July 1968

by



STATINTL

STATINTL



ACKNOWLEDGMENT

STATINTL

STATINTL

The programming capabilities of [redacted] cannot go unacknowledged. Their efforts have made the theoretical procedures described within this report operational facts.

The optical evaluation of the performance of achromat objectives in a color Micro-Analyzer system was performed by [redacted] His contribution to the understanding of the advantages and disadvantages of the current [redacted] Trichromatic Micro-Analyzer system has been very valuable.

STATINTL

STATINTL

ABSTRACT

Image assessment procedures currently exist for black-and-white materials only. Color image assessment and densitometry are defined only on the macroscale at present. It is the objective of this report to combine these two fields to generate a color image assessment technique based on those current image assessment measures that can be applied to color tripack materials. The vector and matrix properties of color materials are defined and applied to noise assessment, ensemble averaging, and modulation transfer function. The shortcomings of the effective exposure technique are discussed, and a method is described for generating valid effective exposure tables for color materials. It is possible that similar methods may be used in the generation of target spectral signatures from color imagery. Quality control methods applicable for color trichromatic and black-and-white microdensitometers are reviewed. Information concerning the integral to analytical density conversion for three-color material is presented, and all auxiliary experimental work in support of this program is reported. Of particular interest is the investigation of the problems associated with the use of achromat objectives in trichromatic microdensitometers.

(This page is intentionally left blank. )

CONTENTS

<u>Section</u>	<u>Title</u>	<u>Page</u>
I	INTRODUCTION . . . . .	1
II	SPECTRAL PROPERTIES OF COLOR AND COLOR MATERIALS .	3
	A. Properties of Groups . . . . .	3
	1. Closure . . . . .	3
	2. Associativity . . . . .	3
	3. Identity Element . . . . .	3
	4. Inverse . . . . .	4
	5. Commutativity . . . . .	4
	B. Integral and Analytical Densities . . . . .	4
	C. Vector Properties . . . . .	9
III	AVERAGING OF MICRODENSITOMETER RECORDS . . . . .	19
	A. Necessity of Gaussian Assumptions . . . . .	19
	B. Calculating the Gaussian Mean and Standard Deviation . . .	19
IV	NOISE MEASUREMENT . . . . .	27
	A. Classical Methods . . . . .	27
	B. Correlation Method . . . . .	32
	1. Autocorrelation . . . . .	35
	2. Cross Correlation . . . . .	37
	3. Matrix Formulation . . . . .	38
	C. Binomial Methods . . . . .	40
V	EFFECTIVE EXPOSURE CONCEPTS FOR COLOR MATERIALS .	45
	A. Basis for Effective Exposure Concept . . . . .	45
	B. Effective Exposure Concept and Color Materials . . . . .	49
	C. Exposure Table Generation for Color Materials . . . . .	55
	D. Summary . . . . .	61
VI	MODULATION TRANSFER FUNCTIONS FOR COLOR MATERIALS	65
	A. Introduction . . . . .	65
	B. Modulation Transfer Function Generation . . . . .	65
	C. Color Materials . . . . .	67
VII	QUALITY CONTROL OF THE MICRODENSITOMETER . . . . .	69
	A. Introduction . . . . .	69
	B. Ideal Development of Quality Control System . . . . .	69

CONTENTS (cont'd.)

<u>Section</u>	<u>Title</u>	<u>Page</u>
	C. General Program Objectives . . . . .	70
	D. Drift Analysis . . . . .	71
	E. Frequency Response Stability . . . . .	75
	F. Noise Injection Analysis . . . . .	81
	G. Summary of the Quality Control Procedures . . . . .	83
	H. The Quality Control Target . . . . .	85
VIII	LITERATURE REFERENCES . . . . .	91

Appendix

A	INTEGRAL TO ANALYTICAL DENSITY CALIBRATION OF THREE-COLOR TRANSPARENCY MATERIALS . . . . .	A-1
B	COMPUTATION OF ALPHA RISKS FOR VARIOUS DISTRIBUTIONS . . . . .	B-1
C	NOISE MEASUREMENT STUDIES PERFORMED ON COLOR MATERIALS . . . . .	C-1
D	RELATION BETWEEN ANALYTICAL AND INTEGRAL AUTO AND CROSS CORRELATIONS . . . . .	D-1
E	PRODUCTION OF STEP WEDGES FROM NON-NEUTRAL SOURCES . . . . .	E-1
F	SAMPLE PROBLEM IN MULTIVARIATE COMPONENT ANALYSIS	F-1
G	OPTICAL EVALUATION AND RECOMMENDATIONS FOR THE <span style="border: 1px solid black; display: inline-block; width: 150px; height: 1em; vertical-align: middle;"></span> PRECISION TRICHROMATIC MICRODENSI- TOMETER 1032T . . . . .	G-1

STATINTL

ILLUSTRATIONS


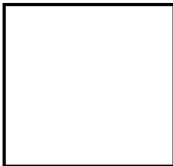
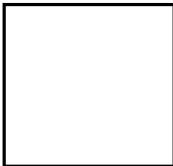
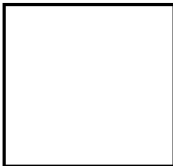
<u>Fig. No.</u>	<u>Title</u>	<u>Page</u>
1	Dye Spectral Density Curves of <span style="border: 1px solid black; display: inline-block; width: 60px; height: 1.2em; vertical-align: middle;"></span> SO-151 Transparency Material . . . . .	STATINTL 5
2	Minor Density as a Function of Major Density: Emulsion 155-16-32	8
3	Idealized Block Dye System . . . . .	11
4a	Two Block Dye System that Obeys Beer's Law . . . . .	13
4b	Two Block Dye System that Does Not Obey Beer's Law . . . . .	14
5	Angular Relationship of Dye Vectors . . . . .	15
6	Spectral Density Curves . . . . .	16
7	Example of Density Frequency Histogram . . . . .	21
8	Selwyn's Relation for Two Black-and-White Materials . . . . .	28
9	RMS Granularity vs Scanning Spot Diameter for Two Color Materials . . . . .	30
10	Differences Between Integral and Analytical Noise Records . . . . .	31
11	Typical Autocorrelation Function for Black-and-White Material at a Given Density Level . . . . .	34
12	Power Spectral Density Functions for Black-and-White Materials .	34
13	Experimental Data and Model Bernoulli Curve (Not Normalized) .	41
14	Callier's Q as a Function of Diffuse Density and Gamma for a Given Material . . . . .	47
15	Characteristic Curve of Cyan Dye Layer of SO-151 Emulsion Exposed to a Neutral and Resulting Exposure Table . . . . .	50
16	Characteristic Curves as a Function of Object Color . . . . .	52
17	Color Samples and Spectral Reflectance Curves . . . . .	53
18	Wavelength Dependence of Yellow Dye Layer of <span style="border: 1px solid black; display: inline-block; width: 60px; height: 1.2em; vertical-align: middle;"></span> 8442 Emulsion . . . . .	STATINTL 54
19	Exposure Table Generation System . . . . .	62
20	Quality Control Computation Flowchart . . . . .	84
21	Fourier Transform of Comb Target . . . . .	86
22	Fourier Transform Envelope Function . . . . .	88
23	Microdensitometer Quality Control Target . . . . .	89



ILLUSTRATIONS (cont'd.)

<u>Fig. No.</u>	<u>Title</u>	<u>Page</u>
A1	Spectral Sensitivity of SO-151 Emulsion . . . . .	A-2
A2	Spectral Sensitivity of SO-155 Emulsion . . . . .	A-3
A3	Spectral Sensitivity of 8442 Emulsion . . . . .	A-4
A4	Minor vs Major Density and Characteristic Curves . . . . .	A-7
A5	Minor vs Major Density and Characteristic Curves . . . . .	A-8
A6	Minor vs Major Density and Characteristic Curves . . . . .	A-9
A7	Minor vs Major Density and Characteristic Curves . . . . .	A-10
A8	Minor vs Major Density and Characteristic Curves . . . . .	A-11
A9	Minor vs Major Density and Characteristic Curves . . . . .	A-12
A10	Minor vs Major Density and Characteristic Curves . . . . .	A-13
A11	Minor vs Major Density and Characteristic Curves . . . . .	A-14
A12	Minor vs Major Density and Characteristic Curves . . . . .	A-15
E1	Optical Arrangement Used to Generate Non-Neutral Microstep Wedges . . . . .	E-2
E2	Spectral Reflectance Curve . . . . .	E-5
E3	Spectral Reflectance Curve . . . . .	E-5
E4	Spectral Reflectance Curve . . . . .	E-5
E5	Spectral Reflectance Curve . . . . .	E-6
E6	Spectral Reflectance Curve . . . . .	E-6
E7	Spectral Reflectance Curve . . . . .	E-6
E8	Spectral Reflectance Curve . . . . .	E-7
E9	Spectral Reflectance Curve . . . . .	E-7
E10	Spectral Reflectance Curve . . . . .	E-7
E11	Spectral Reflectance Curve . . . . .	E-8
E12	Spectral Reflectance Curve . . . . .	E-8
E13	Spectral Reflectance Curve . . . . .	E-8
E14	Spectral Reflectance Curve . . . . .	E-9
E15	Spectral Reflectance Curve . . . . .	E-9

ILLUSTRATIONS (cont'd.)

<u>Fig. No.</u>	<u>Title</u>	<u>Page</u>
E16	Spectral Reflectance Curve . . . . .	E-9
E17	Spectral Reflectance Curve . . . . .	E-10
E18	Spectral Reflectance Curve . . . . .	E-10
E19	Spectral Reflectance Curve . . . . .	E-10
E20	Spectral Reflectance Curve . . . . .	E-11
E21	Spectral Reflectance Curve . . . . .	E-11
E22	Spectral Reflectance Curve . . . . .	E-11
E23	Spectral Reflectance Curve . . . . .	E-12
E24	Spectral Reflectance Curve . . . . .	E-12
E25	Spectral Reflectance Curve . . . . .	E-12
E26	Spectral Reflectance Curve . . . . .	E-13
E27	Spectral Reflectance Curve . . . . .	E-13
E28	Spectral Reflectance Curve . . . . .	E-13
E29	Spectral Reflectance Curve . . . . .	E-14
E30	Spectral Reflectance Curve . . . . .	E-14
E31	Spectral Reflectance Curve . . . . .	E-14
E32	Spectral Reflectance Curve . . . . .	E-15
E33	Spectral Reflectance Curve . . . . .	E-15
G1	Schematic of  Trichromatic Microdensitometer 1032T . . . . .	G-2
G2	Schematic Representation of Wavelength Dependence of Epiplan 8 Focus . . . . .	G-4
G3	 Epiplan 8/0.2 . . . . .	G-6
G4	 Ultrafluor 10/0.2 . . . . .	G-7
G5	 Epiplan 16/0.35 . . . . .	G-8
G6	Defocusing Effect . . . . .	G-9
G7	Schematic Representation of a Multilayer Color Film . . . . .	G-9
G8	Three-Bar Target Focused with 546 Millimicron Filter and Traced with 546 Millimicron Filter . . . . .	G-11
G9	Three-Bar Target Focused with 436 Millimicron Filter and Traced with 546 Millimicron Filter . . . . .	G-13

(This page is intentionally left blank. )

## SECTION I

### INTRODUCTION

Because of increasing utilization, the area of color reconnaissance has come under scrutiny in terms of its operational effectiveness and actual usefulness as a detection tool. Color reconnaissance methods have been pressed into use without detailed evidence of actual enhancement of the photo interpretation results. Because of the subjective factors inherent in photo interpretation tasks, it is questionable if this detailed evidence can be derived. Nevertheless, color imagery is being used, and for this reason it is desirable to assess the quality of this imagery in manners similar to those to which the reconnaissance community is already accustomed in the assessment of black-and-white materials.

Research into color image assessment, with thoughts of retaining the basic methods used in black-and-white image assessment (along with all its problems plus a few more), may not represent the peak of scientific advancement. The basic question, however, is purely pragmatic: "Can we, with suitable modification, develop a color image assessment technique for transparency materials using the accustomed microdensitometric techniques?" The objective of this program is to answer this question and to place constraints, where necessary, upon the answer.

A search of the literature to determine what previous work has been done with this problem has been futile for the most part. The results of this search are cited as references on the following pages. Some work of Russian researchers is applicable. <sup>1, 2, 3, 4</sup> \* In the literature, color density has been studied primarily from the macroscale viewpoint. Whenever color microdensitometry results have been reported, the microdensitometric methods are not given. Thus, the assumption must be made that a standard black-and-white instrument was used to trace color materials. This is commonly accomplished by placing the red, green, or blue filter at the light source or over the photomultiplier (PMT) housing. If red, green, and blue records are desired from

\* For convenience, all references are listed in Section VIII rather than when they occur in the text.

the same sample, then three scans must be performed. Since it cannot be assumed that the sampled points correspond spatially on the three separate records, the use of such techniques as crosscorrelation for granularity analysis is eliminated. The record alignment required in order that analytical filter densities (AFD) may be obtained from integral filter densities (IFD) is also difficult to accomplish. The importance of working with analytical densities is discussed in the following section.

It must be assumed that the red, green, and blue records can be aligned and that AFD's can be used in image assessment; this dictates the use of a trichromatic micro-  
STATINTL densitometer.  present a necessary philosophy to color densitometry in general:

"Mere possession of a good color densitometer is not sufficient. Even the best color densitometer will not be fully effective unless it is used with a complete understanding of its limitations and the care that is necessary to realize its full capabilities."

This report represents a summary of the theoretical routes that may be taken in developing a color image assessment capability similar to presently existing black-and-white capabilities. Many procedures used in black-and-white image assessment have been retained, others changed or broadened, and some new concepts added.

## SECTION II

## SPECTRAL PROPERTIES OF COLOR AND COLOR MATERIALS

## A. PROPERTIES OF GROUPS

Color photography has its basis in the laws of colorimetry. If it can be shown that a set of colors, under the operation of addition or mixing, forms a group, then certain mathematical procedures applicable to groups may be performed<sup>6</sup>. The basic group requirements that must be met are: (1) closure, (2) associativity, (3) an identity element, (4) an inverse. If a fifth condition of commutativity is maintained, the set of colors will form an Abelian group under the operation of addition.

1. Closure

Let  $C_1, C_2, C_3, \dots, C_i, \dots$  be a field of colors.

The rules of closure state that: in a given field, there is an element that exists that is the result of an operation of one element on another, i. e. ,

$$C_1 + C_2 = C_3$$

The experiments of Maxwell confirm that: given any two colors, there is a third color that is the sum of the pair.

2. Associativity

The results of the operation must be identical, independent of the manner of grouping:

$$(C_1 + C_2) + C_3 = C_1 + (C_2 + C_3)$$

Whether we add the first two of three colors together, then add the third; or add the first to the sum of the last two, the result is the same.

3. Identity Element

The existence of an identity element means that the operation of this element upon any other element in the field results in no change in the element operated upon:

$$C_i + I = C_i$$

In colorimetry, the identity element  $I$  is termed a neutral.

4. Inverse

If the inverse of an element operates upon that element, the result is the identity element:

$$C_i + C_i^{-1} = I$$

In colorimetry, the inverse is termed the complementary color.

Hence, colors form a group under the operation of addition.

5. Commutativity

The order of operation of one element upon another must not affect the result:

$$C_i + C_j = C_j + C_i$$

The order of addition is of no importance for nonfluorescent colors. Therefore, nonfluorescent colors meet the requirements of an Abelian group for addition or mixing.

## B. INTEGRAL AND ANALYTICAL DENSITIES

These findings are of significance for they allow the defining of spectrophotometric properties of dyes in terms of an  $N$ -dimensional space and, thereby, allow the generation of critical tests that color materials must meet if image assessment techniques are to be applied.

Figure 1 is a plot of the spectral density curves of the cyan, magenta, and yellow dyes of a typical color material. By adding the densities of these dyes (at 10 millimicron intervals) the upper integral density curve may be generated. If a densitometer were used to read the red, green, and blue densities of this integral tripack, it would be determining not only the major density contribution of the dye having maximum absorption in the waveband being measured, but also the minor contribution to the total density of the other two dyes. Obviously, the total blue density,  $D_b$ , is a sum of the densities of primarily the yellow dye, as well as the magenta and cyan dyes to a lesser extent. Thus:

$$D_b = a_{11} Y + a_{12} M + a_{13} C \quad (1)$$

The individual terms of the equation can be written explicitly because of Beer's law, which states that the narrow-band, or spectral, density of a dye is directly pro-

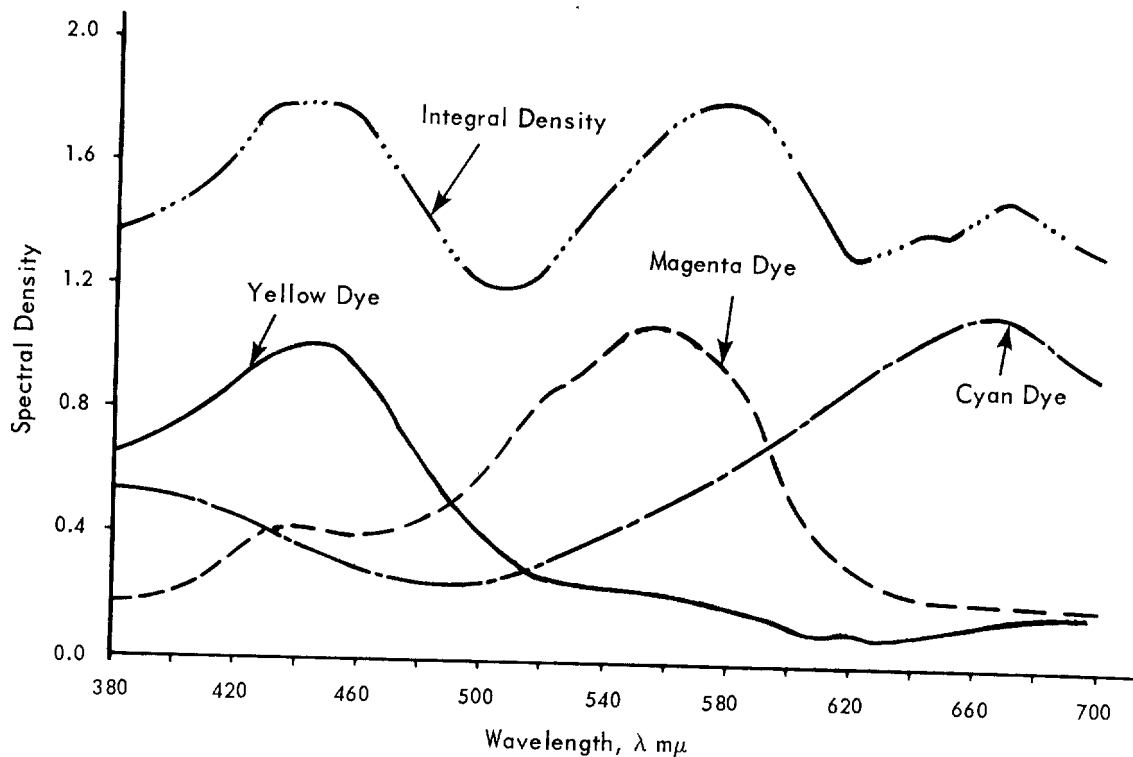


Figure 1. Dye Spectral Density Curves of  SO-151 Transparency Material

STATINTL

proportional to the concentration of the dye, i. e. ,

$$\text{spectral density of cyan dye} = a_{\lambda} Y$$

where  $Y$  is the dye concentration and  $a_{\lambda}$  is termed the spectral absorption coefficient at wavelength  $\lambda$  .

For spectral or narrow-band densitometry, Beer's law holds; and Equation (1) may be written as the sum of the absorption coefficients  $a_{ij}$  of the particular dye. In this case the subscript  $i$  denotes the color being measured;  $j$  denotes the dye with which the absorption coefficient is associated.

Similar equations may be written for the green  $D_g$  and red  $D_r$  densities:

$$D_g = a_{21} Y + a_{22} M + a_{23} C \tag{2}$$

$$D_r = a_{31} Y + a_{32} M + a_{33} C \tag{3}$$

By arranging these three equations into a matrix, one finds that  $D_r$  ,  $D_g$  , and  $D_b$  may be expressed as a multiplication of a column vector of  $C$  ,  $M$  , and  $Y$  concen-



tration elements by a 3 x 3 order matrix of absorption coefficients:

$$\begin{bmatrix} D_b \\ D_g \\ D_r \end{bmatrix} = \begin{bmatrix} a_{11} & a_{12} & a_{13} \\ a_{21} & a_{22} & a_{23} \\ a_{31} & a_{32} & a_{33} \end{bmatrix} \cdot \begin{bmatrix} Y \\ M \\ C \end{bmatrix} \quad (4)$$

By writing the absorption coefficient matrix as **A**, the equation becomes

$$\begin{bmatrix} D_b \\ D_g \\ D_r \end{bmatrix} = \mathbf{A} \cdot \begin{bmatrix} Y \\ M \\ C \end{bmatrix} \quad (5)$$

If the elements of the density matrix  $D_r, D_g, D_b$  are measured with narrow-band filters, they are termed integral filter densities (IFD); if measured on a spectral densitometer or converted from spectrophotometric measurements to density, they are termed integral spectral densities (ISD). The elements of the *YMC* dye matrix are concentrations or densities of individual dyes; hence they are termed analytical densities. The terminology becomes analytical filter densities (AFD) or analytical spectral densities (ASD), with filter and spectral having the same meaning as before. Integral filter densities are the most common measurements and are easily obtained. Analytical densities are impossible to measure directly on imagery without physical destruction of the image. However, analytical densities may be calculated from integral densities if the inverse of the absorption coefficient matrix is computed:

$$\begin{bmatrix} Y \\ M \\ C \end{bmatrix} = \mathbf{A}^{-1} \cdot \begin{bmatrix} D_b \\ D_g \\ D_r \end{bmatrix} \quad (6)$$

Before the description of methods for obtaining the absorption coefficient matrix is undertaken, the necessity of working with analytical densities will be explained.

Let us assume that a trichromatic scan of an edge is performed, and the red record is taken through an appropriate dynamic transfer curve to yield effective exposure values. If the modulation transfer function (MTF) is computed for this red record, it essentially has no meaning, since it is the MTF of the cyan dye layer operated upon in some manner by the MTF of the magenta and yellow layers because of the dye absorption bands in the red of these latter two dyes. The manner in which dye cross absorptions, such as these, affect the MTF is not known. Therefore, at the present time the trans-

form of a red microdensity record has no meaning since no knowledge is gained concerning the emulsion by computing such a transform. If the densities of the red records are mapped using Equation (6) to obtain cyan, magenta, and yellow dye concentration or densities, then the resulting MTF will describe the spatial frequency response of the red-sensitive, cyan dye forming layer only. In this case, something is now known concerning a specific layer in the emulsion. If, at a later time, one learns how one layer of a subtractive color system operates upon another layer in terms of spatial frequency response through the complex arrangement of sensitivity crossover and dye crossover, then perhaps meaningful information may be obtained by transforming integral density records. However, in the initial stages the image assessment work will be accomplished by using analytical densities.

Three methods may be utilized in obtaining the absorption coefficients; all three represent various methods of gaining access to one dye layer of the emulsion. (1) The dye layers may be consecutively removed by gelatin-eating bacteria; (2) the emulsion may be separately coated; or (3) the emulsion layers may be isolated by exposure. Each method presents its inherent difficulty. In the operational case the most feasible method involves exposing two layers of the reversal emulsion, leaving only the one layer of interest unexposed. Obviously, if a wedge is then exposed in the remaining layer using white light, a step wedge modulation of the dye formed in that layer will be obtained. This has been accomplished for three films: SO-151, 8442, and SO-155. The results are listed in Appendix A.

Each of the single dye layers is read on the densitometer or microdensitometer for which the matrix  $\mathbf{A}$  is to provide IFD-to-AFD mapping. It is read for each of the color filters that is to be used in reading or scanning the imagery. This yields three sensitometric curves for each dye layer: one set of major density values is generated when the dye layer is read with the filter that is its complement; the other two sets of densities are generated when the layer is read with the two remaining filters. A plot of the minor densities, determined with the latter two filters, as a function of major density is generated for each of the dye layers. The absorption coefficients of the major densities fall on the main diagonal of the absorption matrix and are all unity ( $a_{11} = a_{22} = a_{33} = 1.00$ ). The secondary absorption coefficients are determined from the slope of the line formed

when a minor density is plotted as a function of the major density. The linearity of this plot confirms the validity of Beer's law. If a straight line is not obtained when minor densities are plotted as a function of major densities, it is an indication that Beer's law is not valid. The reasons for Beer's law failure may be several; for example, the density contribution may not have been reduced to zero through preexposure, or densitometer problems may be the cause. However, when a straight line is obtained, the slope of this line is the corresponding cross absorption coefficient.

Figure 2 is a specific example for the yellow dye layer of SO-155. The cross absorption of the yellow dye to red and green light has been plotted as a function of the blue light density. The absorption coefficient  $a_{11} = 1.00$ . From the graph, the slope of the straight line for green density as the dependent variable is  $a_{21} = 0.12$  and for red plotted as a minor density the absorption coefficient is  $a_{31} = 0.02$ . These relationships, and therefore the absorption coefficients, are valid only on the densitometer and filters, used to determine the IFD's (in this case a  TD-203 and status A-58 filters). In this case the complete absorption coefficient matrix for SO-155 is

STATINTL

$$A = \begin{bmatrix} 1.00 & 0.21 & 0.11 \\ 0.12 & 1.00 & 0.15 \\ 0.04 & 0.17 & 1.00 \end{bmatrix}$$

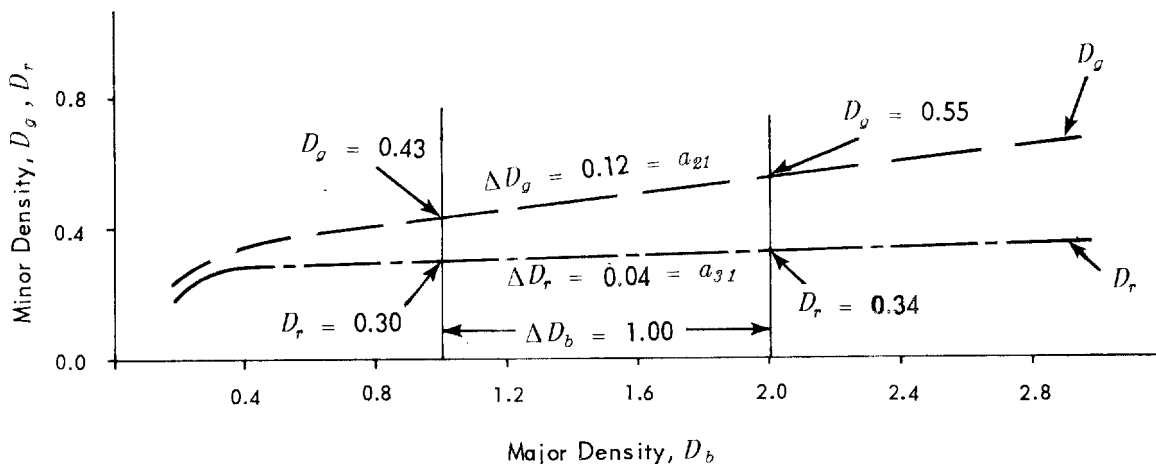


Figure 2. Minor Density as a Function of Major Density; Emulsion 155-16-32

The inverse of the matrix is:

$$A^{-1} = \begin{bmatrix} 1.0276 & -0.2017 & -0.0827 \\ -0.1202 & 1.0498 & -0.1442 \\ -0.0206 & -0.1704 & 1.0279 \end{bmatrix}$$

Let us assume the blue, green, and red densities for SO-155 in a particular instance are 0.24, 0.56, and 0.39 respectively. Solving for the yellow, magenta, and cyan dye concentrations becomes a matrix multiplication problem:

$$\begin{bmatrix} Y \\ M \\ C \end{bmatrix} = \begin{bmatrix} 1.0276 & -0.2017 & -0.0827 \\ -0.1202 & 1.0498 & -0.1442 \\ -0.0206 & -0.1704 & 1.0279 \end{bmatrix} \cdot \begin{bmatrix} 0.24 \\ 0.56 \\ 0.39 \end{bmatrix}$$

$$Y = 1.0276 (0.24) - 0.2017 (0.56) - 0.0827 (0.39) = 0.10$$

$$M = -0.1202 (0.24) + 1.0498 (0.56) - 0.1442 (0.39) = 0.50$$

$$C = -0.0206 (0.24) - 0.1704 (0.56) + 1.0279 (0.39) = 0.30$$

The same principle is used to calibrate a trichromatic color microdensitometer. A microstep wedge is produced separately in each of the single dye layers. These microstep wedges are scanned and the red, green, and blue microdensities of each step are averaged. The minor densities for each dye layer are plotted as a function of the major densities. The slopes of the resulting straight lines (if Beer's law holds) are the elements of the absorption matrix. The inverse of the matrix is taken, thus yielding the mapping matrix of integral filter microdensities (IFMD) to analytical filter microdensities (AFMD).

### C. VECTOR PROPERTIES

Emphasis is placed on the validity of Beer's law because of the necessity of using mathematical models in building an image assessment procedure. If Beer's law is not valid, then models based on the linear additive properties of dye layers are not valid.

Image assessment of color materials includes colorimetric assessment of the dye-forming system. It has been shown that colorimetric procedures for nonfluorescent color meet group requirements. This fact may now be utilized in testing the interrelationships between the dyes.

A spectrophotometric curve for a given dye is generated by reading the transmission of the dye as a function of wavelength, generally in  $10 \text{ m}\mu$  intervals. It is assumed that the measurement intervals are independent and are, therefore, orthogonal. If this assumption is validated by the bandwidth of the measuring equipment, then a unit vector  $\vec{\lambda}_i$  may be defined at each measurement interval (i. e., every  $10 \text{ m}\mu$  over some wavelength closed domain, say  $380 \leq \lambda \leq 700 \text{ m}\mu$ ). Since the absorption coefficients of a dye described completely the behavior of the dye at all concentrations (if Beer's law holds), then the basic dye may be described as a vector quantity. The unit vectors are the set

$$\Lambda = \vec{\lambda}_1, \vec{\lambda}_2, \vec{\lambda}_3, \dots, \vec{\lambda}_i, \dots, \vec{\lambda}_n$$

The subscripts refer to the wavelength measured. The absorption coefficients of, for example, a yellow dye are defined as

$$y_1, y_2, y_3, \dots, y_i, \dots, y_n$$

Therefore, the dye expressed as a vector quantity becomes

$$\mathbf{Y} = y_1 \vec{\lambda}_1 + y_2 \vec{\lambda}_2 + y_3 \vec{\lambda}_3 + \dots + y_i \vec{\lambda}_i + \dots + y_n \vec{\lambda}_n \quad (7)$$

According to Beer's law, a different concentration of the same dye can be expressed by a scalar multiplication:

$$k\mathbf{Y} = k y_1 \vec{\lambda}_1 + k y_2 \vec{\lambda}_2 + k y_3 \vec{\lambda}_3 + \dots + k y_i \vec{\lambda}_i + \dots + k y_n \vec{\lambda}_n \quad (8)$$

The magenta and cyan dyes may be similarly expressed:

$$\mathbf{M} = m_1 \vec{\lambda}_1 + m_2 \vec{\lambda}_2 + m_3 \vec{\lambda}_3 + \dots + m_i \vec{\lambda}_i + \dots + m_n \vec{\lambda}_n \quad (9)$$

$$\mathbf{C} = c_1 \vec{\lambda}_1 + c_2 \vec{\lambda}_2 + c_3 \vec{\lambda}_3 + \dots + c_i \vec{\lambda}_i + \dots + c_n \vec{\lambda}_n \quad (10)$$

The ideal colorant to be used in an image-forming system has been defined as the block dye (Figure 3): a dye that has no off-diagonal term in its red, green, and blue absorption coefficient matrix  $\mathbf{A}$ . Each dye operates independently of the other. Thus, the dyes are orthogonal to one another and the nearer the orthogonality of a dye system, the greater the color saturation that can be attained with the system. Figure 1 exhibits the

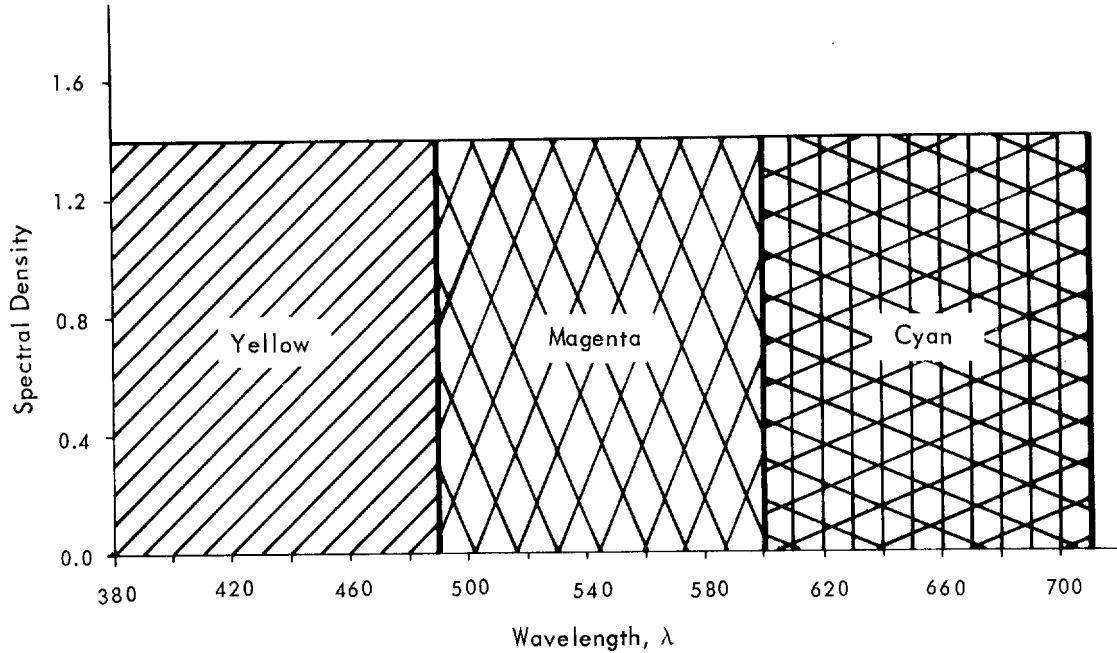


Figure 3. Idealized Block Dye System

STATINTL spectral density curves of  SO-151 material processed in a color Versamat using EA-4 chemistry. It is obvious that, because of the unwanted absorption of these dyes, the system is not orthogonal. Orthogonality defines a 90° angle between the dye vectors or a direction cosine of zero. The direction cosine yields a measure of the independence of one dye layer from another. If two dyes are the same, the vector angle between them is zero or their direction cosine is unity. Three direction cosines may be computed for a tripack emulsion:

$$\cos \theta_{yc} = \frac{Y \cdot C}{|Y| |C|} \quad (11)$$

$$\cos \theta_{mc} = \frac{M \cdot C}{|M| |C|} \quad (12)$$

$$\cos \theta_{ym} = \frac{Y \cdot M}{|Y| |M|} \quad (13)$$

A plot of the angle between two dyes as a function of dye concentration will yield information concerning Beer's law and the formation of stain density, as well as provide a comparison of the dye system of specific emulsions and processes in terms of color saturation capability.

Figure 4a is a polar plot of two dyes that have cross absorption coefficients and obey Beer's law. Figure 4b is a plot of a similar dye pair, except that in this case, the cross absorption is due to a constant stain formation that does not follow Beer's law. Figure 5 represents polar plots of the SO-151 emulsion dye system processed in EA-4 chemistry, the spectral density curve set of which is exhibited in Figure 6 a, b, c. Figure 5 is plotted as a function of visual diffuse density rather than dye concentration. When computing the direction cosines for a real dye system, all stain and base-plus-fog density must be removed from the spectrophotometric data.

STATINTL

The value of direction cosine analysis of a dye system is its ability to supply information concerning the saturation capability of a dye system when processed in a certain manner. Thus, it provides a definite point from which a change in color process variables may be evaluated in terms of color reproduction and saturation capabilities without generation of a complete dye gamut in CIE color space.

If a microdensitometer is to be used in a trichromatic mode, each of the channels and optics must be independent; otherwise, the assumption of a linear additive process is invalidated by the failure of Beer's law. The microdensitometric spectral response vectors  $F_r$ ,  $F_g$  and  $F_b$  to red, green, and blue, respectively, are expressed in a similar manner to the dye vectors:

$$F_r = \sum_{i=1}^n f_{r_i} \vec{\lambda}_i \quad (14)$$

$$F_g = \sum_{i=1}^n f_{g_i} \vec{\lambda}_i \quad (15)$$

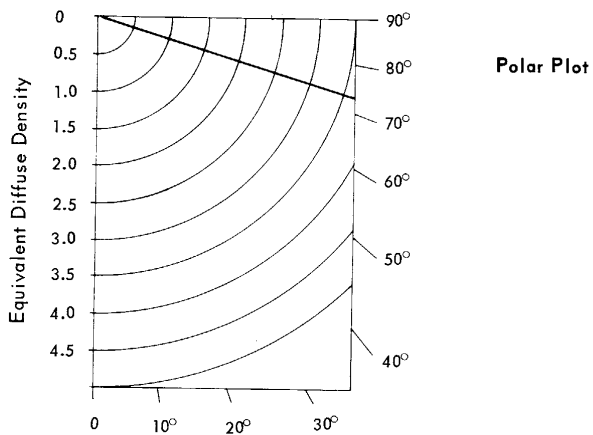
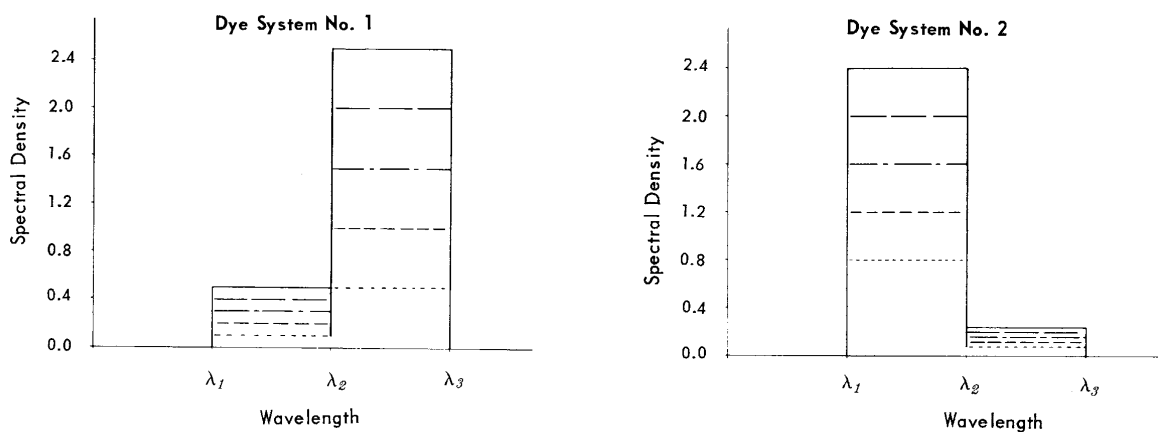


Figure 4a. Two Block Dye System That Obeys Beer's Law



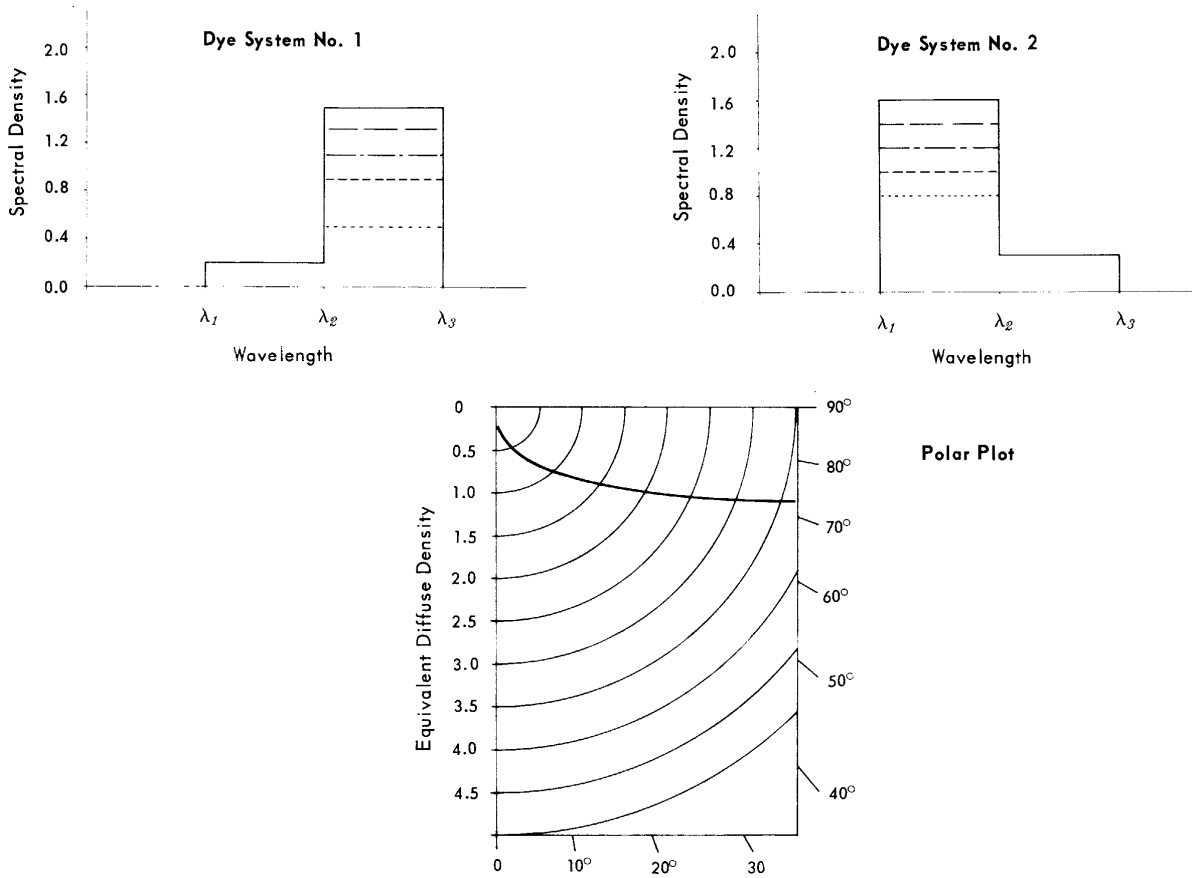


Figure 4b. Two Block Dye System That Does Not Obey Beer's Law

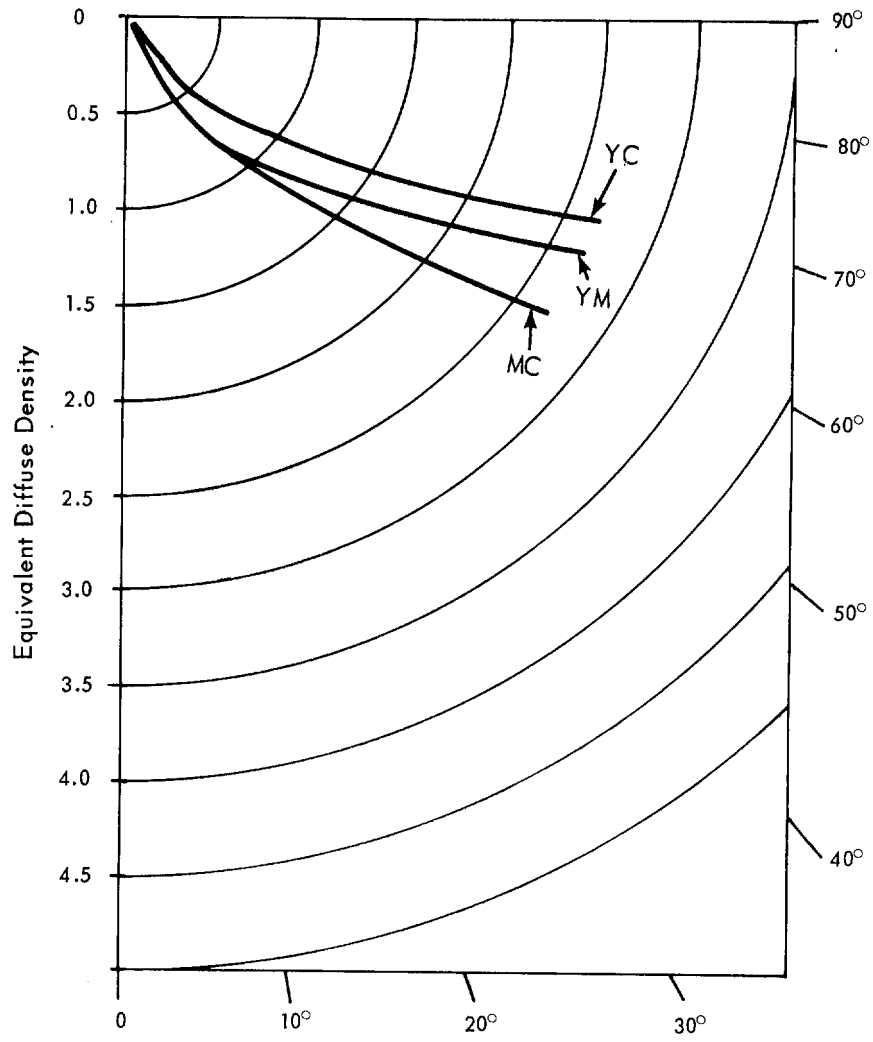


Figure 5. Angular Relationship of Dye Vectors

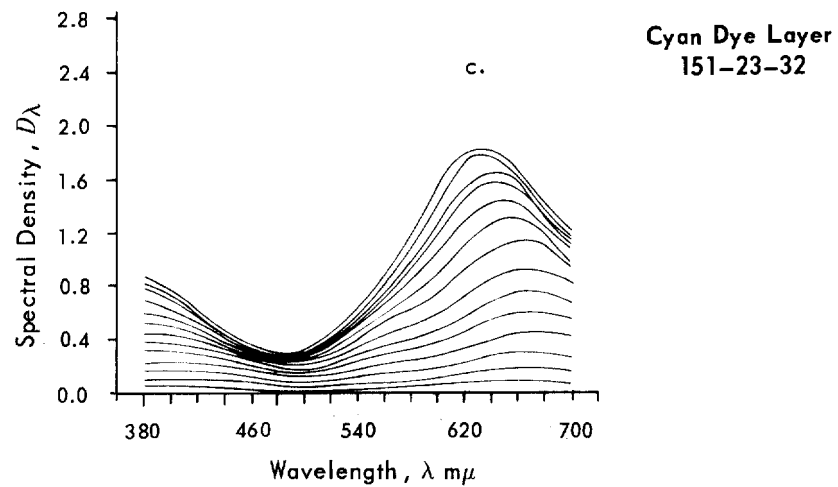
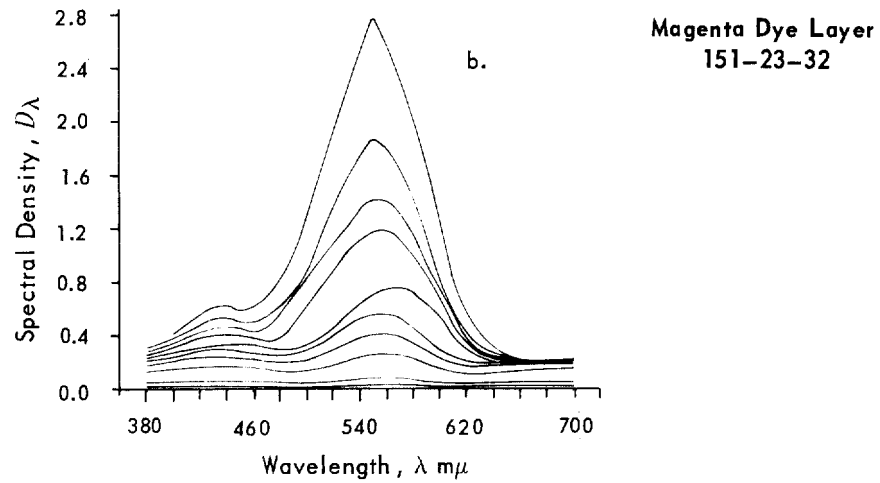
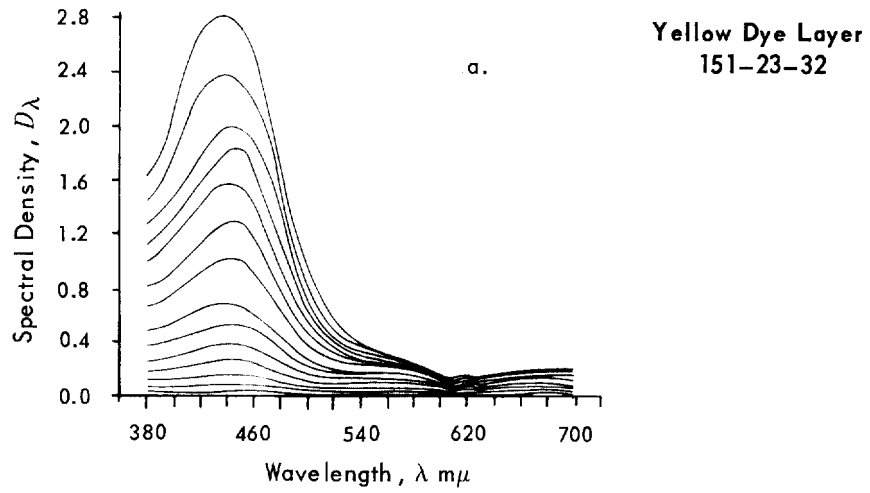


Figure 6. Spectral Density Curves

$$\mathbf{F}_b = \sum_{i=1}^n f_{b_i} \vec{\lambda}_i \quad (16)$$

where  $f$  are the wavelength-dependent logarithmic output values for a nonspectral absorbing sample in the scanning plane of the microdensitometer. Thus, for a microdensitometer to be used for color image assessment, the following condition must be met in terms of direction cosines:

$$\frac{\mathbf{F}_r \cdot \mathbf{F}_g}{|\mathbf{F}_r| |\mathbf{F}_g|} = \frac{\mathbf{F}_r \cdot \mathbf{F}_b}{|\mathbf{F}_r| |\mathbf{F}_b|} = \frac{\mathbf{F}_g \cdot \mathbf{F}_b}{|\mathbf{F}_g| |\mathbf{F}_b|} = 0 \quad (17)$$

(This page is intentionally left blank.)

## SECTION III

## AVERAGING OF MICRODENSITOMETER RECORDS

## A. NECESSITY OF GAUSSIAN ASSUMPTIONS

The scanning of color film samples with a small diameter spot, or a slit of small width, generates a trichromatic record of densities with a significant noise variance. Conversion of the IFD record to an AFD record retains the noise variance but modifies its characteristics as described in the following section. To determine the density level of each layer being scanned, the obvious method is to utilize a simple averaging scheme based on a Gaussian process. In working with black-and-white material, evidence has been presented that the distribution of noise in both density and transmittance is not Gaussian. However, the distributions are not greatly skewed about the mean; hence, a Gaussian assumption may be a good approximation.<sup>7</sup> There is an obvious difference between mean density and mean transmittance of the sample since

$$\langle D \rangle \neq \log_{10} (1/\langle t \rangle) \quad (18)$$

For a microdensitometer operating in a digital mode, the average density corresponds to the left side of Equation (18) and is obtained by computation of the mean of the record. Generally, the photometric large area densitometer determines a spatial transmittance average corresponding to the right side of Equation (18), which is then displayed as density.<sup>8</sup>

The significance of this inequality for color material and the microdensity distribution characteristics have not been reported. Until such information becomes available, it will be necessary to compute the average density of a sample using Gaussian assumptions. It is desirable that the average density of an analytical trichromatic record be determined in an automatic and non-arbitrary manner.

## B. CALCULATING THE GAUSSIAN MEAN AND STANDARD DEVIATION

Let the open domain of analytical filter microdensities (AFMD) be expressed as  $0 \leq D_i \leq 4.00$ , ( $i = 1, 2, 3, \dots, r$ ) the density space being expressible by all densities in the domain that can be grouped in cell interval of width  $\Delta$ . In practice, the recording

precision is two decimal digits; thus, the cell interval is  $\Delta = 0.01$  and  $r = 400$ , yielding an upper density limit of 4.00.

If an analytical microdensity record of  $N$  densities is computed for one dye layer from the IFMD for the tripack, there are two ways the Gaussian mean and standard deviation may be calculated. The most direct method is by averaging the sample and computing the standard deviation by the usual sum of squares technique. The second method retains the actual distribution characteristics of the record by formation of a frequency histogram. The abscissa of the histogram is the previously defined density space arranged from 0 to 4.00 in cell intervals of  $\Delta = 0.01$ . The ordinate of the histogram is the frequency  $f_i$  with which a specific density level  $D_i$  is found within the record.

After formation of the histogram, the least and greatest cell values for which there are entries are determined, and the median cell between these two extremes is computed as  $D_M$ .

The cell values of the histogram are next renumbered with integers,  $l_i$ , taking the median entry  $D_M$  as the origin; the renumeration goes positive with increasing density and negative for densities less than the median (Figure 7).

$$\begin{aligned} D_i = D_M & \quad l_i = 0 \\ D_i < D_M & \quad l_i < 0 \\ D_i > D_M & \quad l_i > 0 \end{aligned}$$

The mean and standard deviation may now be computed from the histogram by the following two equations, respectively:

$$\langle D \rangle = D_M + (\Delta/N) \sum_{i=0}^r f_i l_i \quad (19)$$

$$s = \Delta \left\{ \left[ N \sum_{i=0}^r f_i l_i^2 - \left( \sum_{i=0}^r f_i l_i \right)^2 \right] / [N(N-1)] \right\}^{1/2} \quad (20)$$

The histogram retains the distribution properties of the sample and allows rejection of all anomalous samples that fail to satisfy a criterion such as:

$$\text{for all } |l_i| > 3.5 s/\Delta \quad \text{then } f_i = 0 \quad (21)$$

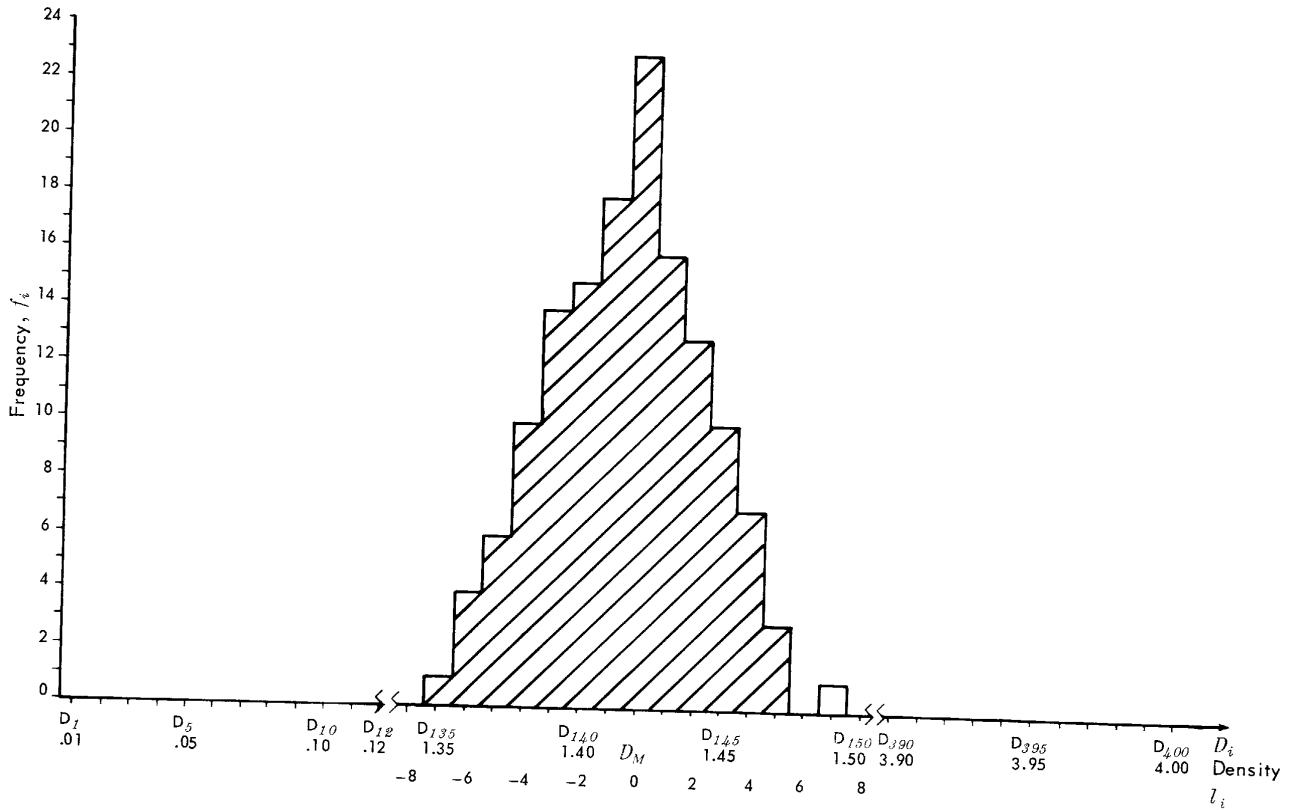


Figure 7. Example of Density Frequency Histogram



This eliminates all large density fluctuations that may be due to dirt particles, emulsion scratches, and other defects.

The alpha risk taken in performing this rejection, at 3.5 times the standard deviation from the mean, is small, as are the consequences of the risk. The mean and standard deviation, as expressed by Equations (19) and (20), are recomputed on the modified frequency histogram.

In this case the modified sample size  $N'$  is used, where:

$$N' = N - \sum_{i=0}^{m_1} f_i - \sum_{i=m_2}^r f_i \quad (22)$$

and

$$m_1 = (D_M - 3.5 s) 100$$

$$m_2 = (D_M + 3.5 s) 100$$

Use of the histogram method also allows computation of the mean transmittance of the standard deviation of the transmittance by the following relations:

$$\langle t \rangle = (1/N') \sum_{i=0}^r f_i \exp(-2.30 D_i) \quad (23)$$

$$s_t = \left\{ \left\{ N' \sum_{i=0}^r f_i \exp(-4.60 D_i) - \left[ \sum_{i=0}^r f_i \exp(-2.30 D_i) \right]^2 \right\} / [N'(N-1)] \right\}^{1/2} \quad (24)$$

The density corresponding to the mean transmittance may be then computed as

$$D_{\langle t \rangle} = \log_{10} (1/\langle t \rangle) \quad (25)$$

Microdensitometry does not concern itself with constant density records but rather with imagery, step wedge, and, in general, records in which different density levels exist. The ensemble averaging concept must be applied so that changes in density levels may be detected.

Since the density sample rate and the approximate dimension of the smallest object to be detected are known variables, this allows the selection of a subsample of densities  $n_j$  from the total record  $N$ . The histogram technique is used for the determination

of the AFMD subsample mean  $\bar{D}_j$  and standard deviation  $s_j$  (or variance  $s_j^2$ ). To detect changes in density level or in standard deviation, it is necessary to define an ensemble average and variance  $\bar{D}_{e_j}$  and  $s_{e_j}^2$  as running values determined by pooling past subsample values that are of the same population.

Initially, a subsample mean and variance are computed for the first subsample ( $j = 1$ ). The next mean and variance are computed for the record sample ( $j = 2$ ) and compared to the initial values, which are taken to be the ensemble parameters. If the just-computed values are the same as the ensemble values, then standard pooling techniques are used. The new ensemble average becomes

$$\bar{D}_{e_{j+1}} = (n_{e_j} \bar{D}_{e_j} + n_{j+1} \bar{D}_{j+1}) / (n_{e_j} + n_{j+1}) \quad (26)$$

where the new ensemble sample size is

$$n_{e_{j+1}} = n_{e_j} + n_{j+1} \quad (27)$$

The new ensemble variance is

$$s_{e_{j+1}}^2 = [(n_{e_j} - 1) s_{e_j}^2 + (n_{j+1} - 1) s_{j+1}^2] / (n_{e_j} + n_{j+1} - 2) \quad (28)$$

The pooling procedures are identical in transmittance values. The criterion for determining if the subsample average differs from the ensemble average, or if the subsample variance differs from the variance of the ensemble, is based on normal statistical test procedures for a Gaussian-distributed population.

The test procedure requires that an F-test be performed on the variance of the subsample, as compared to the ensemble variance. The null hypothesis in this case is that the ensemble and subsample variances are equal:

$$H_0 : \sigma_{e_j}^2 = \sigma_{j+1}^2 \quad (29)$$

The alternative is that an inequality exists:

$$H_1 : \sigma_{e_j}^2 \neq \sigma_{j+1}^2 \quad (30)$$

The F-ratio formed is subject to the following constraints:

if  $s_{e_j}^2 > s_{j+1}^2$

then  $F_{cal} = s_{e_j}^2 / s_{j+1}^2$

if  $s_{e_j}^2 \leq s_{j+1}^2$

then  $F_{cal} = s_{j+1}^2 / s_{e_j}^2$

The critical F-value may be selected from tabulated values<sup>9</sup> and is based on the degrees of freedom of each variance and the alpha risk desired. Alternatively, the alpha risk incurred with the rejection of the null hypothesis, for any computed F-value, may be computed from the equations given in Appendix B. This procedure is more amenable to computer operation.

If the variances can be taken to be equal, then they are pooled by using Equation (28), provided the mean density level has not shifted.

A shift in density level is detectable using a calculated T-distribution value:

$$T_{cal} = (\bar{D}_{e_j} - \bar{D}_{j+1}) \{ [n_{e_j} - 1] s_{e_j}^2 + (n_{j+1} - 1) s_{j+1}^2 \} / (n_{e_j} + n_{j+1} - 2) \}^{-1/2} \\ \times [ (1/n_{e_j}) + (1/n_{j+1}) ]^{-1/2} \quad (31)$$

with  $\nu = n_{e_j} + n_{j+1} - 2$  degrees of freedom. The best procedure in running this test is to compute the alpha risk associated with  $T_{cal}$  and  $\nu$  (Appendix B) and compare the computed risk value with the acceptable risk. The null hypothesis in this case is that the two means are the same:

$$H_0 : \mu_{e_j} = \mu_{j+1} \quad (32)$$

The alternative is that the mean density level has shifted:

$$H_1 : \mu_{e_j} \neq \mu_{j+1} \quad (33)$$

If both the mean and variance tests indicate no change between the ensemble and the subsample, then the pooling of both the variance and mean density is allowable

to form a revised estimate of the ensemble average.

If either the variance or mean density of a subsample is significantly different from the ensemble values, then the ensemble values are set aside (stored, printed out, etc.) and the new ensemble average is taken as the subsample parameters just computed, i. e. ,

if

$$\sigma_{e_j}^2 \neq \sigma_{j+1}^2$$

or

$$\mu_{e_j} \neq \mu_{j+1}$$

then

$$\bar{D}_{e_{j+1}} = \bar{D}_{j+1}$$

and

$$s_{e_{j+1}}^2 = s_{j+1}^2$$

and the subsample averaging and variance computation and comparisons are carried out using the next subsample  $j + 2$ . This procedure essentially "walks through" the entire record and detects all shifts in mean and variance and sets aside the ensemble average and variance for any stationary ensemble. Obviously, if there is a monotonic trend in density level or variance throughout the record, then each subsample will differ from the previous one, and no ensemble value with a large degree of freedom will be found.

This procedure may be used in the determination of RMS granularity, as will be explained in the next section.

Since trichromatic records are involved here, this procedure must be accomplished for each of the dye layers. A detection of density or variance shift in any one or two dye layers, or differential shifts between dye layers, indicates that a change in hue has been encountered. To detect hue shifts requires that all three dye layers be entered into separate histograms on an individual spatial trichromatic sample basis (the trichromatic values must first be converted from IFMD to AFMD).

If one or two layers shift in density, then a hue shift has occurred. If shifts occur in all three layers, a hue shift or a neutral density shift may have occurred. If no shift occurs in any of the three layers, then no hue shift has occurred.

The necessity and explicit method of detecting hue shifts within a density record will be explained in Section V.

(This page is intentionally left blank.)

## - SECTION IV

## NOISE MEASUREMENT

## A. CLASSICAL METHODS

Processing a negative or positive black-and-white material produces particles of essentially opaque silver. The growth of these silver particles and their form, spatial constraints, and filamentary construction are determined by the gelatin environment and the conditions and type of development. Since (1) the grains are individually opaque, (2) the grains are small with respect to the diameter of the scanning aperture, and (3) the grains are randomly distributed, then Selwyn's law is obeyed. This law states that for a given material at a given density the product of the standard deviation of the density  $\sigma(D)$  and the scanning aperture diameter  $d_\mu$  is a constant, i. e. ,

$$\sigma(D) \cdot d_\mu = G \quad (34)$$

where  $G$  = Selwyn's granularity constant. (A plot of this relation for two typical black-and-white materials appears in Figure 8.) This permits computation of the RMS granularity of a material for any given scanning aperture once  $G$  is obtained. To realize the full usefulness of this relation, granularity — a purely objective, numerical measure of noise — must be related to the subjective measure of noise: graininess. Stultz and Zweig<sup>10</sup> stated this relationship by defining the viewing magnification,  $V_m$ , under which the material was to be viewed and the effective point spread function of the eye. The result is the simple computation of the aperture with which the material must be scanned in order to obtain a measure of granularity that best corresponds to graininess. This relationship

$$d_\mu = \frac{513}{V_m} \quad (35)$$

is valid whether or not Selwyn's law holds. (In Equation (35)  $d_\mu$  is the required scanning aperture in microns.)

Positive or negative dye-forming systems, based on a silver halide as the photoreceptor, form a dye image around the silver developed in the color developer stage. Since the dye formation is a coupling reaction with the oxidized developing agent,

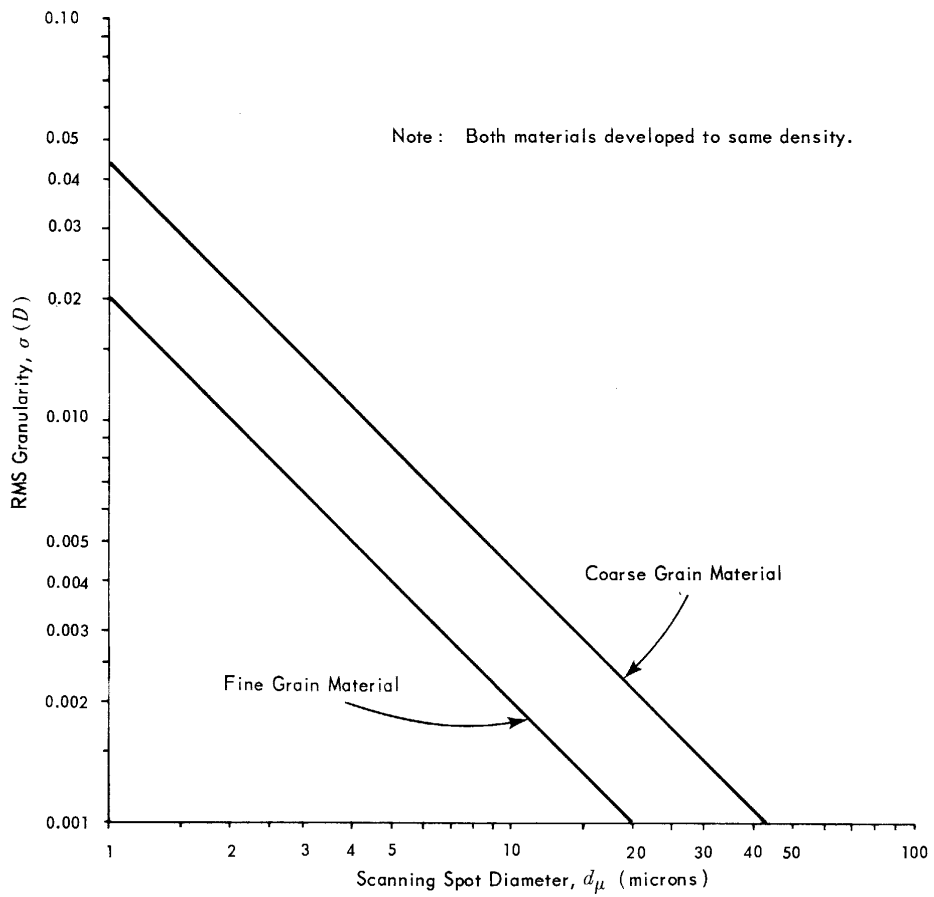


Figure 8. Selwyn's Relation for Two Black-and-White Materials

the dye is formed in the vicinity of the grain being developed although obviously it cannot be formed in the exact location. This fact, plus diffusion of the oxidized developing agent away from the reaction site, means that the image-forming unit in modern color materials is a cloud of dye formed around the image silver. Of course, the bleaching of silver leaves only the dye. Because of the diffusion condition, the assumption of randomness of the image-forming units cannot be made. Because of the failure of its basic assumption, Selwyn's law does not hold in the case of dye image-forming systems<sup>11</sup>. The relation between  $\sigma(D)$  and  $d_\mu$  takes the form shown in Figure 9. Since this means that the granularity of color materials cannot be computed, it therefore must be measured by using the aperture that will best simulate the effective aperture properties of the system in which the material will be used (for human interpretation see Equation (35)). There is some question concerning the validity of Equation (35) in color materials since the fundamental unit visualized as grain is not a fundamental granular unit but may be an agglomeration of dye clouds<sup>12</sup>. Because of the transparency of the dyes, the agglomeration is not necessarily confined to dyes in one layer of the emulsion but may be dye clouds in other layers (Figure 10).

Because of the possible spatial superposition of dye units in different layers of the film and because of the dye cross absorption, it is actually misleading to express granularity in terms of red, green, and blue densities.

The ensemble averaging methods, explained in the last section, will actually yield the RMS granularity,  $\sigma(D)$ , as output. It is the simple standard density deviation of a constant density sample of sample size  $N_e \approx 5000$ . In other words, to adequately estimate the RMS granularity of a material the sample size must be at least 5000. If each density sample is taken through the mapping function  $A^{-1}$  (see Equation 6) to obtain analytical filter microdensities (AFMD), then three analytical RMS granularity values — namely  $\sigma(C)$ ,  $\sigma(M)$ , and  $\sigma(Y)$  — are determined in place of the integral RMS granularity values  $\sigma(D_r)$ ,  $\sigma(D_g)$ , and  $\sigma(D_b)$ . The latter values contain errors due to cross absorption of underlying dye clouds, as just explained. Using AFMD conversion of each density sample, before computation of the RMS granularity, allows the noise to be attributed to the proper layer of the emulsion. To recognize the significance of this, the use of autocorrelation and cross correlation functions in noise measurement must be discussed.



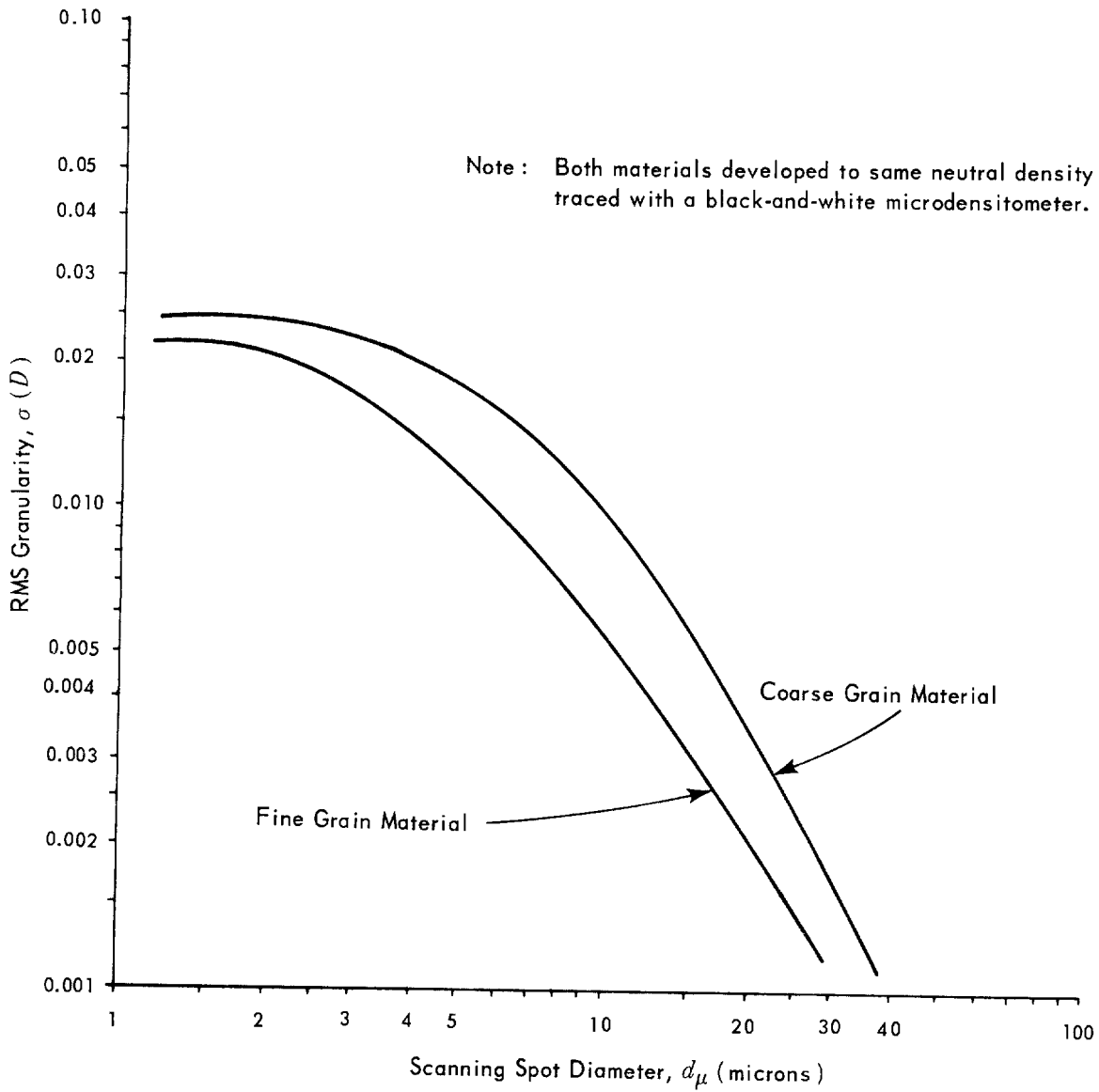


Figure 9. RMS Granularity vs Scanning Spot Diameter for Two Color Materials

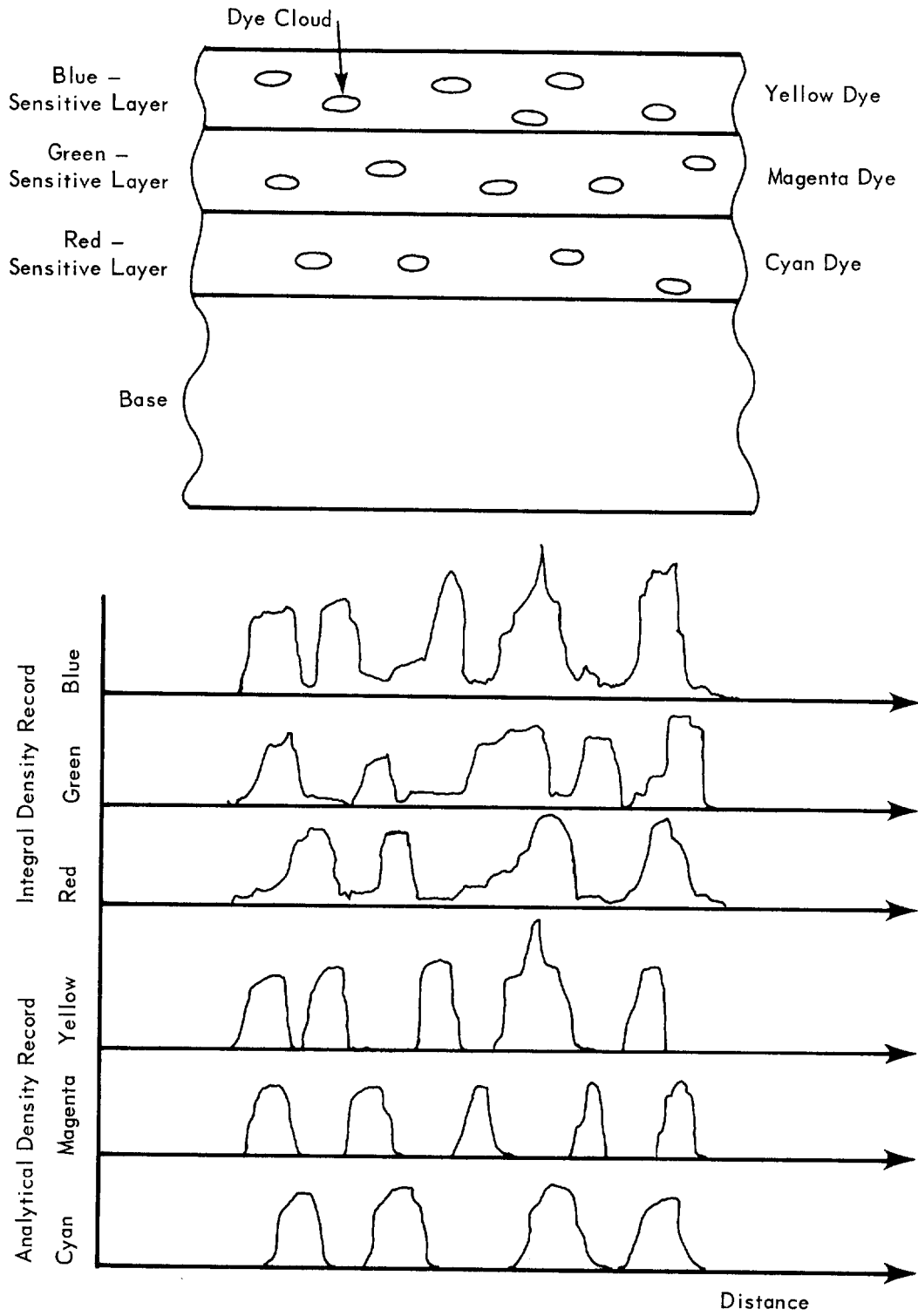


Figure 10. Differences Between Integral and Analytical Noise Records

## B. CORRELATION METHOD

Consider two continuous density records as a function of distance, namely  $f_1(x)$  and  $f_2(x)$ . The autocorrelation function of either of these records is defined as

$$\rho_{11}(\tau) = \lim_{T \rightarrow \infty} \frac{1}{2T} \int_{-T}^T f_1(x) f_1(x + \tau) dx \quad (36)$$

The cross correlation of these two records, i. e., the correlation of the first with the second, is

$$\rho_{12}(\tau) = \lim_{T \rightarrow \infty} \frac{1}{2T} \int_{-T}^T f_1(x) f_2(x + \tau) dx \quad (37)$$

or the second with the first:

$$\rho_{21}(\tau) = \lim_{T \rightarrow \infty} \frac{1}{2T} \int_{-T}^T f_2(x) f_1(x + \tau) dx \quad (38)$$

in which case

$$\rho_{12}(-\tau) = \rho_{21}(\tau) \quad (39)$$

Equivalent information results from use of auto and cross correlation functions as from a determination of the RMS granularity as a function of aperture diameter<sup>13</sup>. However, the correlation method allows easier visualization of the influence of the individual components of the photographic system on granularity. Explaining the interpretation of correlation functions requires the definition of the power spectral density of the noise, i. e., the Fourier transform of the autocorrelation function:

$$\begin{aligned} P_{11}(\omega) &= \lim_{T \rightarrow \infty} \int_{-\infty}^{\infty} \frac{1}{2T} \int_{-T}^T f_1(x) f_1(x + \tau) \exp(-j\omega\tau) dx d\tau \\ &= \int_{-\infty}^{\infty} \rho_{11}(\tau) \exp(-j\omega\tau) d\tau \end{aligned} \quad (40)$$

and its inverse

$$\rho_{11}(\tau) = \frac{1}{2\pi} \int_{-\infty}^{\infty} P_{11}(\omega) \exp(j\omega\tau) d\omega \quad (41)$$

giving the transform pair

$$\rho_{11}(\tau) \longleftrightarrow P_{11}(\omega) \quad (42)$$

The same definition exists for the cross power density spectrum:

$$\begin{aligned} P_{12}(\omega) &= \lim_{T \rightarrow \infty} \int_{-\infty}^{\infty} \frac{1}{2T} \int_{-T}^T f_1(x) f_2(x+\tau) \exp(-j\omega\tau) dx d\tau \\ &= \int_{-\infty}^{\infty} \rho_{12}(\tau) \exp(-j\omega\tau) d\tau \end{aligned} \quad (43)$$

and its inverse

$$\rho_{12}(\tau) = \frac{1}{2\pi} \int_{-\infty}^{\infty} P_{12}(\omega) \exp(j\omega\tau) d\omega \quad (44)$$

yielding the transform pair

$$\rho_{12}(\tau) \longleftrightarrow P_{12}(\omega) \quad (45)$$

No great physical significance can be associated with the autocorrelation formula other than it indicates the likelihood of correlation between the function at  $f_i(x)$  with a value of the function  $f_i(x+\tau)$  at the location  $x+\tau$ . Of course, when  $\tau=0$ , the correlation should be perfect since

$$\rho_{11}(0) = \lim_{T \rightarrow \infty} \frac{1}{2T} \int_{-T}^T f_1(x) f_1(x+0) dx = \lim_{T \rightarrow \infty} \frac{1}{2T} \int_{-T}^T f_1^2(x) dx \quad (46)$$

which is a maximum. Of course, correlation should be expected throughout the interval

$$\tau < d$$

in other words, when the lag variable  $\tau$  is less than the aperture diameter. The reason for this is that the aperture is of finite width, and several points on the emulsion may appear in the aperture at one time<sup>14</sup>. These effects can be seen in the correlation function for a typical black-and-white emulsion in Figure 11. It has been

Declass.  
Review by

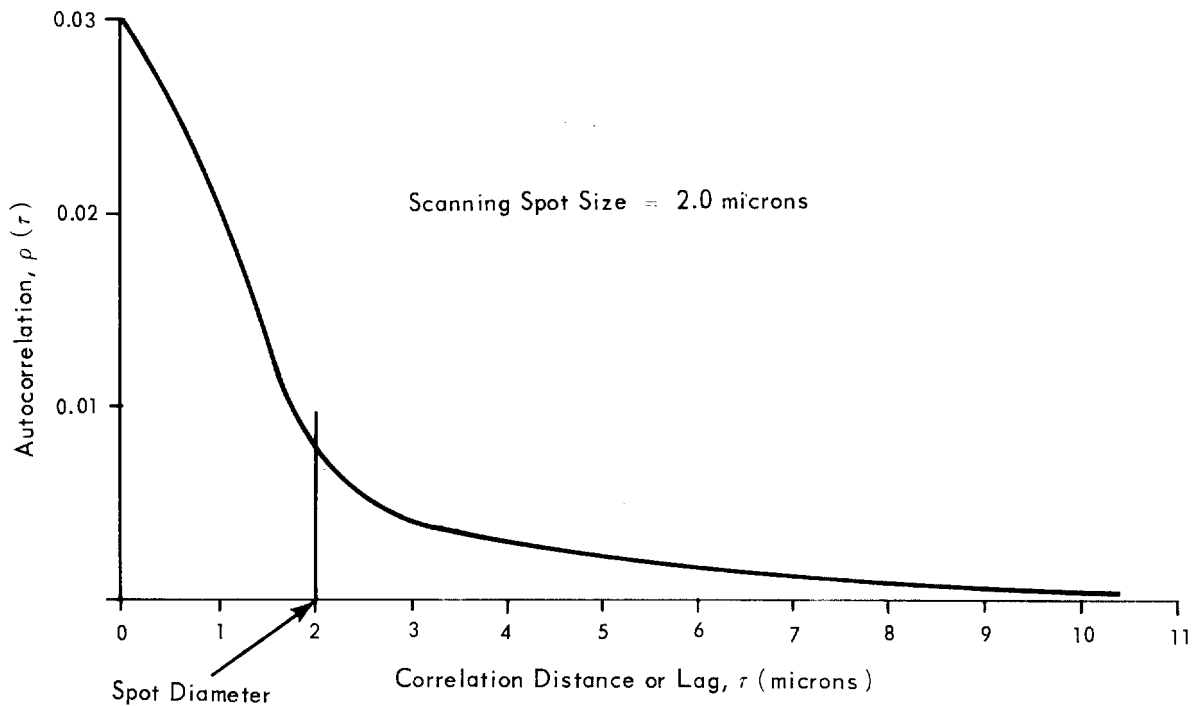


Figure 11. Typical Autocorrelation Function for Black-and-White Material at a Given Density Level

observation<sup>15</sup> that the autocorrelation function of a print equals the autocorrelation of the positive stock plus the autocorrelation of the negative stock, as modified by the modulation transfer characteristics of the printer. The transfer of granular noise in black-and-white materials can best be visualized by use of the power spectral density function (Wiener spectrum). A hypothetical example of this function for a coarse- and fine-grain emulsion, and a print of the former on the latter, is shown in Figure 12.

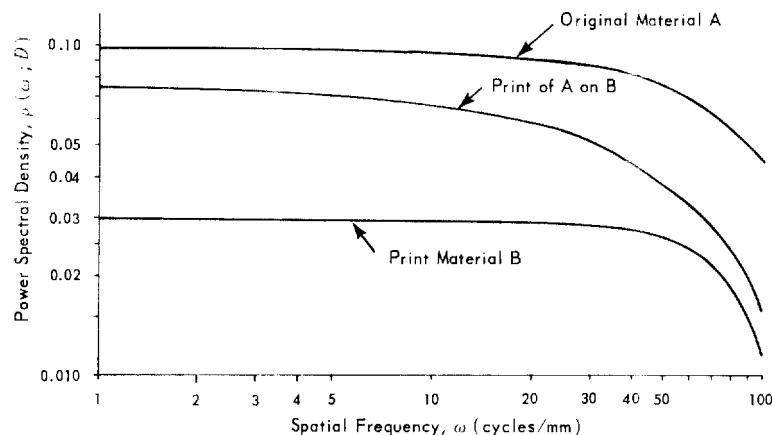


Figure 12. Power Spectral Density Functions for Black-and-White Materials

The falloff of the function at the higher frequencies is due to the filtering effect of the aperture. Doerner<sup>16</sup> derived the relation for the determination of the Wiener spectrum for a print  $P_r(\omega_j D)$ , as a function of the gamma  $\gamma$  to which the positive material is developed, the Wiener spectrum of the positive material  $P_P(\omega_j D)$  and original negative material  $P_N(\omega_j D)$  and the combined modulation transfer function of the negative material and the printer  $|M(\omega)|$ :

$$P_r(\omega; D) = P_N(\omega; D) [\gamma |M(\omega)|]^2 + P_P(\omega; D) \quad (47)$$

Obviously density,  $D$ , must be introduced as a parameter since the Wiener spectra of the materials and the print are dependent upon the density level.

This type of granularity transfer analysis is important from the standpoint of the determination of noise propagation characteristics through printing or reproduction systems.

#### 1. Autocorrelation

Published research<sup>17, 18, 19, 20</sup> does not deal directly with the noise propagation of color reproduction systems. It does not even deal satisfactorily with the color noise analysis of camera original materials. It is, therefore, necessary to initiate color image noise assessment techniques for camera original and reproduction materials. The first step is the examination of autocorrelation techniques for individual dye layers of the color emulsion. In terms of analytical filter microdensity records, the autocorrelation function may be written for each of the three dye layers:

yellow

$$\rho_{yy}(\tau) = \lim_{T \rightarrow \infty} \frac{1}{2T} \int_{-T}^T Y(x) Y(x + \tau) dx \quad (48)$$

magenta

$$\rho_{mm}(\tau) = \lim_{T \rightarrow \infty} \frac{1}{2T} \int_{-T}^T M(x) M(x + \tau) dx \quad (49)$$

cyan

$$\rho_{cc}(\tau) = \lim_{T \rightarrow \infty} \frac{1}{2T} \int_{-T}^T C(x) C(x + \tau) dx \quad (50)$$

In addition, six cross correlation functions may be written. First the cross correlation of the noise record of the yellow layer with that of the magenta layer:

$$\rho_{ym}(\tau) = \lim_{T \rightarrow \infty} \frac{1}{2T} \int_{-T}^T Y(x) M(x + \tau) dx \quad (51)$$

and similarly the yellow layer cross correlated with the cyan layer:  $\rho_{yc}(\tau)$  (the cyan record contains the lag variable); and the magenta layer cross correlated with the cyan layer:  $\rho_{mc}(\tau)$ . The three remaining cross correlation functions are the same as the above three except that the other AFMD record contains the lag variable, i. e. ,

$$\rho_{my} = \lim_{T \rightarrow \infty} \frac{1}{2T} \int_{-T}^T M(x) Y(x + \tau) dx \quad (52)$$

From Equation (39) it follows that

$$\rho_{my}(\tau) = \rho_{ym}(-\tau) \quad (53)$$

It will be standard procedure in this report to express the correlation function such that the lower of the two dye layers contains the lag variable. When this cannot be accomplished, the notation of Equation (53) will be utilized. Then the remaining two correlation functions are

$$\rho_{cy}(\tau) = \rho_{yc}(-\tau) \quad (54)$$

and

$$\rho_{cm}(\tau) = \rho_{mc}(-\tau) \quad (55)$$

The description of the experiment and preparation of samples to evaluate all analytical density autocorrelation and cross correlation functions for three emulsion types is included in Appendix C. Interpretation and duplication of color materials involves integral densities; thus it is necessary that the noise in a color dye system be expressed in integral terms that can be broken into analytical components. The autocorrelation and cross correlation of integral red, green, and blue densities are more complex than the equivalent analytical density expressions. For example, the autocorrelation of the blue density record is expressed as

$$\rho_{bb}(\tau) = \lim_{T \rightarrow \infty} \frac{1}{2T} \int_{-T}^T D_b(x) D_b(x + \tau) dx \quad (56)$$

However, integral densities are expressible as a linear combination of the yellow, magenta, and cyan layer with the latter two layers contributing unwanted absorption to the blue record:

$$D_b(x) = a_{11} Y(x) + a_{12} M(x) + a_{13} C(x) \quad (57)$$

Inserting (37) into (56) yields :

$$\rho_{bb}(\tau) = \lim_{T \rightarrow \infty} \frac{1}{2T} \int_{-T}^T [a_{11} Y(x) + a_{12} M(x) + a_{13} C(x)] [a_{11} Y(x+\tau) + a_{12} M(x+\tau) + a_{13} C(x+\tau)] dx$$

and expanding inside the integral, we have

$$\begin{aligned} \rho_{bb}(\tau) = \lim_{T \rightarrow \infty} \frac{1}{2T} \int_{-T}^T [a_{11}^2 Y(x) Y(x+\tau) + a_{12}^2 M(x) M(x+\tau) + a_{13}^2 C(x) C(x+\tau) \\ + a_{11} a_{12} Y(x) M(x+\tau) + a_{11} a_{13} Y(x) C(x+\tau) + a_{11} a_{12} M(x) Y(x+\tau) \\ + a_{12} a_{13} M(x) C(x+\tau) + a_{11} a_{13} C(x) Y(x+\tau) + a_{12} a_{13} C(x) M(x+\tau)] dx \end{aligned} \quad (58)$$

Since the integral of the sum equals the sum of the integrals, this becomes (using (39)):

$$\begin{aligned} \rho_{bb}(\tau) = a_{11}^2 \rho_{yy}(\tau) + a_{12}^2 \rho_{mm}(\tau) + a_{13}^2 \rho_{cc}(\tau) + a_{11} a_{12} [\rho_{ym}(\tau) + \rho_{ym}(-\tau)] \\ + a_{11} a_{13} [\rho_{yc}(\tau) + \rho_{yc}(-\tau)] + a_{12} a_{13} [\rho_{mc}(\tau) + \rho_{mc}(-\tau)] \end{aligned} \quad (59)$$

It can now be seen that an integral density autocorrelation is a weighted sum of all possible analytical autocorrelation and cross correlation functions. The weighting functions are the elements of the dye absorption coefficient matrix  $\mathbf{A}$ . The above procedure may be continued for the remaining two autocorrelation functions for the green and red record.

## 2. Cross Correlation

The procedure is basically the same for the cross correlation of integral microdensity records. For example, the cross correlation of blue and green noise records:

$$\rho_{bg}(\tau) = \lim_{T \rightarrow \infty} \frac{1}{2T} \int_{-T}^T D_b(x) D_g(x+\tau) dx \quad (60)$$



in which  $D_b(x)$  is that expressed in equation (57), and

$$D_g(x) = a_{21} Y(x) + a_{22} M(x) + a_{23} C(x) \quad (61)$$

where  $a_{21}$ ,  $a_{22}$  and  $a_{23}$  are the dye absorption coefficients.

Substituting (57) and (61) into (60) yields:

$$\begin{aligned} \rho_{bg}(\tau) &= \lim_{T \rightarrow \infty} \frac{1}{2T} \int_{-T}^T [a_{11} Y(x) + a_{12} M(x) + a_{13} C(x)] \\ &\quad [a_{21} Y(x+\tau) + a_{22} M(x+\tau) + a_{23} C(x+\tau)] dx \\ &= \lim_{T \rightarrow \infty} \frac{1}{2T} \int_{-T}^T [a_{11} a_{21} Y(x) Y(x+\tau) + a_{12} a_{21} M(x) M(x+\tau) \\ &\quad + a_{13} a_{21} C(x) C(x+\tau) + a_{11} a_{22} Y(x) M(x+\tau) + a_{11} a_{23} Y(x) C(x+\tau) \\ &\quad + a_{12} a_{21} M(x) Y(x+\tau) + a_{12} a_{23} M(x) C(x+\tau) + a_{13} a_{21} C(x) Y(x+\tau) \\ &\quad + a_{13} a_{22} C(x) M(x+\tau)] dx \\ &= a_{11} a_{12} \rho_{yy}(\tau) + a_{12} a_{13} \rho_{mm}(\tau) + a_{13} a_{23} \rho_{cc}(\tau) + a_{11} a_{22} \rho_{ym}(\tau) \\ &\quad + a_{12} a_{21} \rho_{ym}(-\tau) + a_{11} a_{23} \rho_{yc}(\tau) + a_{13} a_{21} \rho_{yc}(-\tau) + a_{12} a_{23} \rho_{mc}(\tau) \\ &\quad + a_{13} a_{22} \rho_{mc}(-\tau) \end{aligned} \quad (62)$$

The same analytical correlation terms are present as for the integral autocorrelation; however, the spectral absorption weighting coefficients are different.

Five remaining cross correlation functions exist for integral microdensity records, namely  $\rho_{br}(\tau)$ ,  $\rho_{gr}(\tau)$ ,  $\rho_{by}(-\tau)$ ,  $\rho_{br}(-\tau)$ , and  $\rho_{gr}(-\tau)$ . The complete analytical expressions for all integral microdensity cross correlations and autocorrelations are listed in Appendix D.

### 3. Matrix Formulation

All possible analytical cross correlation and autocorrelation functions may be expressed, for a color tripack, by defining the matrix  $L(\tau)$  such that

$$L(\tau) = \begin{bmatrix} \rho_{yy}(\tau) & \rho_{ym}(\tau) & \rho_{yc}(\tau) \\ \rho_{ym}(-\tau) & \rho_{mm}(\tau) & \rho_{mc}(\tau) \\ \rho_{yc}(-\tau) & \rho_{mc}(-\tau) & \rho_{cc}(\tau) \end{bmatrix} \quad (63)$$

All autocorrelation terms lie on the main diagonal. This matrix may be formed from two analytical microdensity matrices: first, the analytical density column matrix

$$J(x) = \begin{bmatrix} Y(x) \\ M(x) \\ C(x) \end{bmatrix} \quad (64)$$

and the transpose of this same matrix with the lag  $\tau$  added

$$\mathbf{J}'(x + \tau) = \begin{bmatrix} Y(x + \tau) \\ M(x + \tau) \\ C(x + \tau) \end{bmatrix}' = [Y(x + \tau) M(x + \tau) C(x + \tau)] \quad (65)$$

where the prime notation designates the transpose.

The matrix  $\mathbf{L}(\tau)$  may be simply expressed as

$$\mathbf{L}(\tau) = \lim_{T \rightarrow \infty} \frac{1}{2T} \int_{-T}^T \mathbf{J}(x) \cdot \mathbf{J}'(x + \tau) dx \quad (66)$$

The same procedure may be used to form the similar matrix  $\mathbf{I}(\tau)$ , composed of all integral auto and cross correlations for a color tripack. Again, the autocorrelation functions are found on the main diagonal.

$$\mathbf{I}(\tau) = \begin{bmatrix} \rho_{bb}(\tau) & \rho_{bg}(\tau) & \rho_{br}(\tau) \\ \rho_{bg}(-\tau) & \rho_{gg}(\tau) & \rho_{gr}(\tau) \\ \rho_{br}(-\tau) & \rho_{gr}(-\tau) & \rho_{rr}(\tau) \end{bmatrix} \quad (67)$$

This matrix may likewise be simply expressed as the correlation integral of the matrices  $\mathbf{J}(x)$  and  $\mathbf{J}(x + \tau)$ , each multiplied by the dye absorption coefficient matrix  $\mathbf{A}$ :

$$\mathbf{I}(\tau) = \lim_{T \rightarrow \infty} \frac{1}{2T} \int_{-T}^T [\mathbf{A} \cdot \mathbf{J}(x)] \cdot [\mathbf{A} \cdot \mathbf{J}(x + \tau)]' dx \quad (68)$$

The elements of  $\mathbf{I}(\tau)$  are found in Appendix D.

The significance of these equations lies in the fact that they provide a means for forming cross and autocorrelation functions for dye layers and for their interpretation in terms of the interactions between the three dye layers. Combining this ability with advanced duplication theory will allow the study of noise propagation throughout an  $N$ -generation duplication system. These procedures also allow the evaluation of processing condition changes (such as competing coupler addition, temperature changes etc.) as a cause of grain noise changes in color materials. The signal-to-noise ratio problem may now be expressed and examined in terms of both analytical and integral

microdensity terminology with an understanding of how unwanted dye cross absorption affects the signal-to-noise ratio.

The Wiener spectrum for color materials is now expressible, in a complete form, as

$$P_L(\omega) = \frac{1}{2\pi} \int_{-\infty}^{\infty} L(\tau) \exp(-j\omega\tau) d\tau \quad (69)$$

in the analytical microdensity case, and as

$$P_L(\omega) = \frac{1}{2\pi} \int_{-\infty}^{\infty} l(\tau) \exp(-j\omega\tau) d\tau \quad (70)$$

in the integral case.

The use of the Wiener spectrum has already been discussed for black-and-white systems. Research should continue to determine the applicability of Equation (47) to color duplication systems.

### C. BINOMIAL METHODS

As previously mentioned, photographic grain noise does not follow a strictly Gaussian distribution. Attempts to elucidate the distribution associated with black-and-white photographic systems have resulted in some success.

STATINTL

The applicability of the binomial distribution has been noted in the literature<sup>21,22</sup>.

demonstrated the adherence of the grain noise, in transmittance, to the binomial or Bernoulli distribution function. He demonstrated that the black-and-white photographic material could be represented by plotting the transmittance variance of the sum of  $N$  binomially distributed layers as a function of the mean transmittance (Figure 13).

In color materials the grains are not opaque but are transparent dye clouds that exhibit optical absorption. The applicability of the binomial distribution to this situation has not been examined, but the mathematical background for a system with non-opaque basic image elements was studied by

STATINTL

Assume a probability density for an emulsion layer of unit (one dye element)

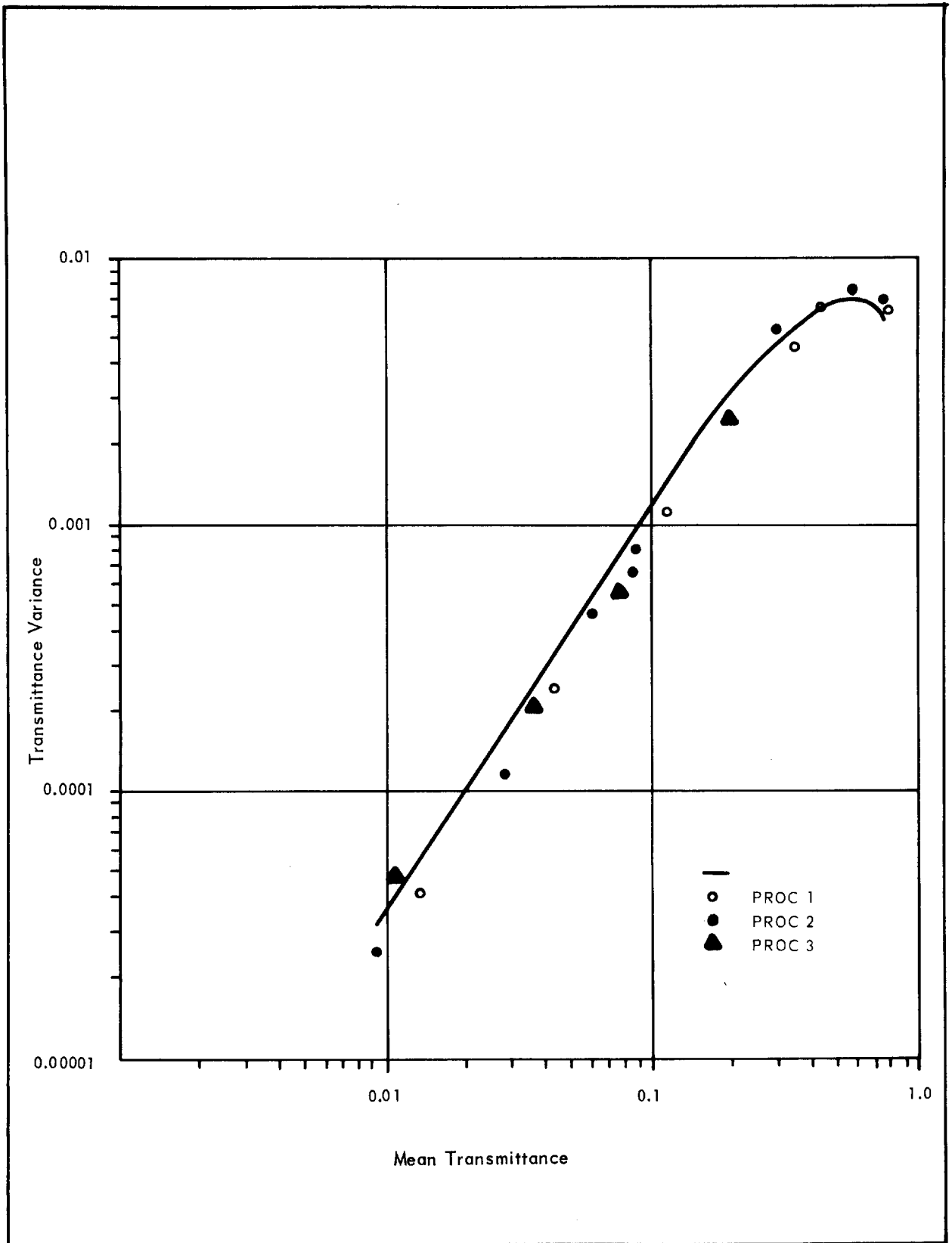


Figure 13. Experimental Data and Model Bernoulli Curve (Not Normalized)

thickness to be

$$W(t) = p \delta(\alpha) + q \delta(\beta) \quad (71)$$

where  $t$  = transmission

$\alpha$  = maximum transmission of an image element

$\beta$  = minimum transmission of an image element

$p$  = probability of  $\alpha$

$q$  = probability of  $\beta$

$\delta$  = Dirac function

also, assume

$$q + p = 1$$

Then, for  $N$  layers

$$\bar{t} = k \prod_{i=1}^N \bar{t}_i \quad (72)$$

where  $k$  is base plus stain transmission.

By the sifting properties of the Dirac function

$$\bar{t}_i = \int_t t W(t) dt = \{ p \alpha + q \beta \} \quad (73)$$

The variance may be shown to be equal to

$$\sigma^2(\bar{t}) = N k^2 [ \alpha (\bar{t}/k)^2 - 1/N - (\bar{t}/k)^2 ] [ 1 - \beta (\bar{t}/k)^{-1/N} ] \quad (74)$$

This may be arbitrarily referenced for aperture size of the microdensitometer by

$$K = N k^2$$

so that

$$\sigma^2(\bar{t}) = K [ \alpha (\bar{t}/k)^2 - 1/N - (\bar{t}/k)^2 ] [ 1 - \beta (\bar{t}/k)^{-1/N} ] \quad (75)$$

In the case of compact, opaque grains  $\alpha = 1$  and  $\beta = 0$  so that

$$\sigma^2(\bar{t}) = K [ (\bar{t}/k)^2 - 1/N - (\bar{t}/k)^2 ] \quad (76)$$

STATINTL

Of the equations developed by  Equation (74) is most useful as it utilizes the maximum and minimum transmission ( $\alpha$  and  $\beta$ , respectively) of image-forming elements and allows the determination of the effective number of binomially distributed layers  $N$  that a given image-forming layer simulates.

At this point, research concerning the implications of using average transmission and transmission variance information in noise studies of color materials has not been undertaken. However, as described in the previous section, the necessary information, either in terms of AFMD or IMFD, is provided if automatic ensemble averaging techniques are used.

(This page is intentionally left blank.)

## SECTION V

## EFFECTIVE EXPOSURE CONCEPTS FOR COLOR MATERIALS

## A. BASIS FOR EFFECTIVE EXPOSURE CONCEPT

The effective exposure concept is based on the assumption that a density-exposure relationship (D-log E curve or dynamic transfer function) can be expressed such that for any density observed on the photographic material the exposure given to obtain that density may be determined. Thus, if  $f$  is the functional relationship between density  $D$  and exposure  $E$ , then:

$$D = f(E) \quad (77)$$

and the effective exposure concept is expressible as:

$$E = f^{-1}(D) \quad (78)$$

The validity of this assumption will be dealt with later in this report.

There are two basic reasons why the effective exposure concept is utilized. First, since the dynamic transfer function is nonlinear, it allows the removal of these nonlinearities prior to the determination of modulation transfer functions. Secondly, density calibration of black-and-white microdensitometers has been shown to be a fallacious concept. Through use of the effective exposure principle the microdensitometer is employed as a function generator, thus bypassing the absolute microdensity calibration problem.

The photographic system has been described as a linear transformation (modulation transfer function of the photographic material) followed by a nonlinear transformation (dynamic transfer function). Theoretically, after the densities of the image are taken through the inverse D-log E curve, the frequencies present in the image should be the same as were present in the object since the modulation transfer function is linear. This model was examined  by exposing pure sine waves to a black-and-white emulsion and determining the distortion,  $D$ , as the percentage of the harmonic content present in the effective exposure:

STATINTL

$$D = \left[ \left( \sum_{m=2}^{\infty} c_m c_m^* \right) / c_1 c_1^* \right]^{1/2} \quad (79)$$



where the asterisk (\*) denotes complex conjugate and  $c_m$  are the Fourier coefficients of the image, expressed as effective exposure. In  work the higher order terms of the transform were ignored, thus limiting the sum of the numerator of (79) to the third harmonic. The conclusion was that significant distortion was present even after removal of the nonlinearities of the characteristic curve by using the effective exposure principle. This distortion varied — as a function of exposure, modulation, and frequency — from a maximum of 8 percent to a minimum of 3 percent. This research was performed using black-and-white materials only. The validity of effective exposure for color materials has not been investigated at all.

STATINTL

Absolute density calibration of microdensitometers is exceedingly difficult in concept and accomplishment. The differences between a diffuse reading macrodensitometer and a specular reading microdensitometer have already been described in Section III. Considering the error  $\epsilon$  between average density and the log of average transmittance, i. e. ,

$$\epsilon = \langle \log_{10} (1/t) \rangle - \log_{10} (1/\langle t \rangle) \quad (80)$$

is not sufficient. The Callier  $Q$  coefficient of the material being scanned must also be taken into consideration. This quantity is defined as the ratio of diffuse to specular density:

$$Q = D_{\text{specular}}/D_{\text{diffuse}} = D_{\mu}/D_{\text{macro}} \quad (81)$$

For black-and-white materials this ratio varies as a function of the gamma, to which the material is developed, and of the density level (Figure 14).  studied this relationship for color dye systems. The field of specular densitometry in general is not well defined. As is stated in Mees<sup>28</sup> :

STATINTL

"To date, no standard method or apparatus has been generally adopted for the measurement of specular density... It is desirable that standard terms be adopted which would serve to differentiate the limiting true specular density from densities lying between this and totally diffuse density".

The general conclusion to be drawn is that microdensitometer calibration by density correlation with a diffuse macro-reading instrument is not meaningful. Simulation of the specular characteristics of a microdensitometer requires the same numerical

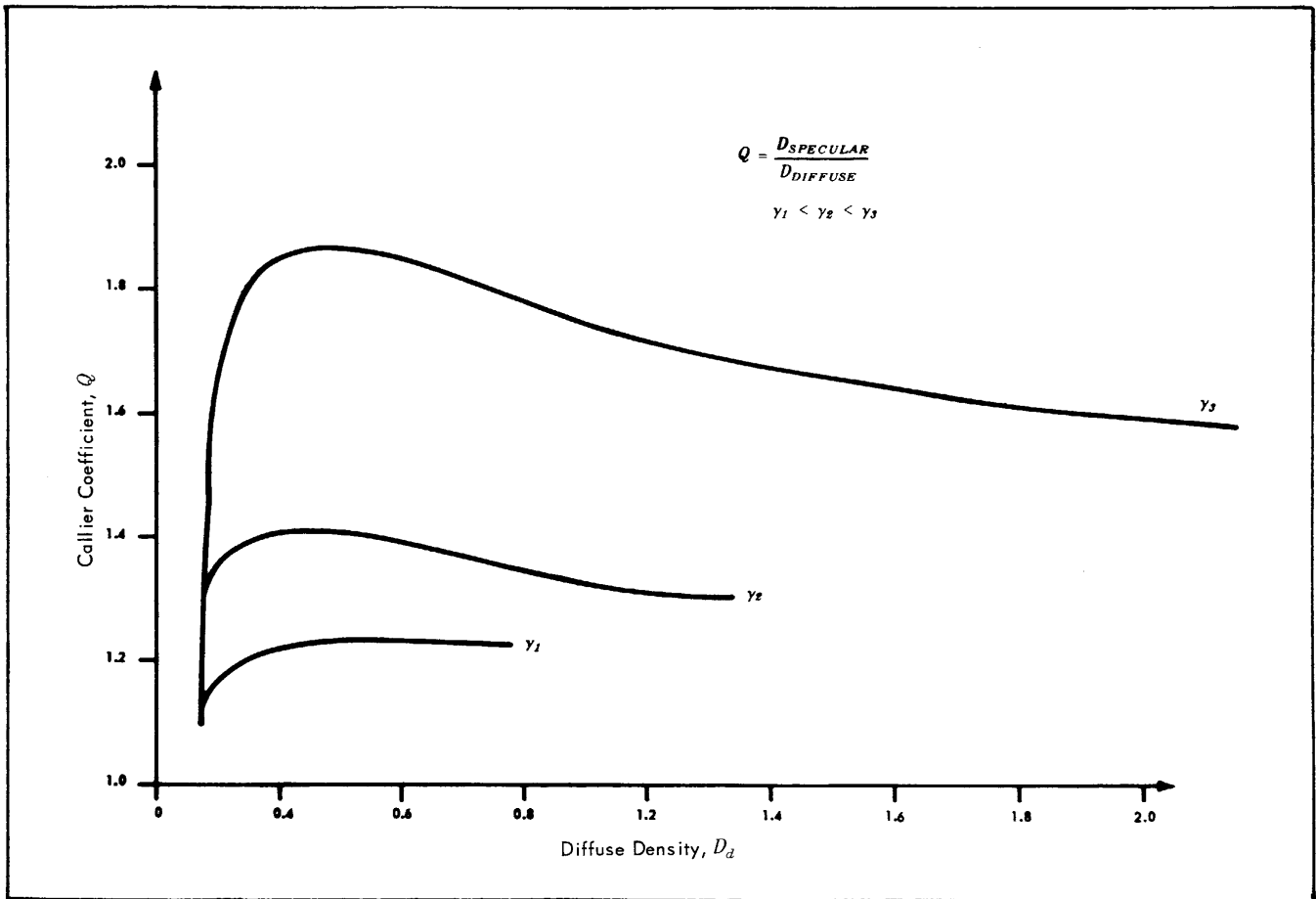


Figure 14. Callier's Q as a Function of Diffuse Density and Gamma for a Given Material

aperture as the microdensitometer being simulated and, hence, requires high magnification.

The most reasonable procedure to use is acceptance of the output of a microdensitometer as purely microdensities, distinct and separate from macrodensities. The two may be related most validly through the principle of effective exposure.

The effective exposure concept is utilized first and primarily as a means of eliminating the nonlinearities introduced by the dynamic transfer characteristics of the photographic materials. This it does to some degree; however, at high frequencies ( $\omega \geq 120$  cycles/mm) the harmonic distortion may be worse than if density units had been transformed directly. At lower frequencies, effective exposure yields less distortion than density units transformed directly<sup>29</sup>.

There are, of course, other variables whose significance are as yet unknown. Coherency of the microdensitometer beam at the film plane has been mentioned as a possible source of nonlinearity; on the other hand, mention has also been made that the microdensitometer may suppress the harmonic content. Nevertheless, this problem of the interference of the measuring instrument with the results is not an easily solved problem.

Large scale nonlinearities, such as adjacency effects in black-and-white materials, have been investigated mathematically. Simonds<sup>30</sup> demonstrated that the linear terms of the Maclaurin expansion could not adequately account for a system containing adjacency effects. Let  $e_0$  be the true exposure given at point  $i = 0$  and let  $E_i, i = -n, -n+1, \dots, 0, \dots, n-1, n$  be the apparent effective exposure values at points adjacent to  $i = 0$  (we are dealing with a one-dimensional exposure distribution). Since development nonlinearities arise from the fact that exposures adjacent to a point, say  $i = 0$ , generate changes in developing agent concentration through by-product diffusion, then the true exposure at point  $i = 0$  is a function of the effective exposure at adjacent points:

$$e_0 = g(E_{-n}, E_{-n+1}, \dots, E_0, \dots, E_{n-1}, E_n) \quad (82)$$

This function of several variables can be expressed as a Maclaurin series if it can be assumed that all derivatives are continuous and the series is convergent. Thus:

$$e_0 = \sum_{i=-n}^n a_i E_i + \sum_{j=-n}^n \sum_{i=-n}^n b_{ij} E_i E_j + \text{higher order terms} \quad (83)$$

Simonds<sup>31</sup> found that the following condensed Maclaurin expansion was adequate to describe the effective exposure perturbation by adjacency effects:

$$e_0 = (a_{-n} E_{-n} + a_{-n+1} E_{-n+1} + \dots + a_n E_n) + (b_{-n} E_0 E_{-n} + b_{-n+1} E_0 E_{-n+1} + \dots + b_0 E_0^2 + \dots + b_n E_0 E_n) \quad (84)$$

The point to be made is that the effective exposure principle, although it has its shortcomings, is a first and necessary step in the elimination of the nonlinearities inherent in the photographic process. Work has been performed in dealing with higher order effects; however, this work supplements the effective exposure principle. The same problems beset the effective exposure concept in color materials, with the added problem of not being able to state a valid dynamic transfer function.

## B. EFFECTIVE EXPOSURE CONCEPT AND COLOR MATERIALS

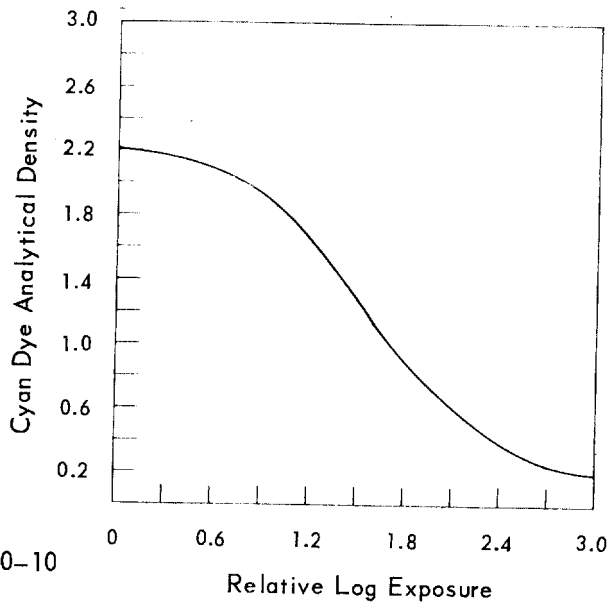
To recognize the problems involved, it is first necessary to state the basic procedure used in generating an effective exposure table.

To generate exposure tables for color materials, it is first necessary to obtain a characteristic curve for each dye layer of the material. Thus, it is necessary to work with analytical densities. Figure 15 is the characteristic curve for the cyan dye layer of SO-151 when the material is exposed to a neutral. Two third-order polynomials are fitted to the characteristic curve: one polynomial fitted to the toe and lower straight line portion of the curve, the other fitted to the upper straight line and shoulder portion of the curve. Thus:

$$D = (a_0 + a_1 E + a_2 E^2 + a_3 E^3) + [b_0 + b_1 (E + E_0) + b_2 (E + E_0)^2 + b_3 (E + E_0)^3] \quad (85)$$

$$= f(E)$$

The inverse of this function is taken, and for each density increment  $\Delta D = 0.01$  in the range  $0 < D \leq 4.00$  a corresponding exposure value is determined. This generates the



Note: Curve is for SO-151 emulsion exposed to a neutral.

Figure 15. Characteristic Curve of Cyan Dye Layer of SO-151 Emulsion Exposed to a Neutral and Resulting Exposure Table

EFFECTIVE EXPOSURE TABLE

DENSITY	EFFECTIVE EXPOSURE	DENSITY	EFFECTIVE EXPOSURE
4.00	.00788	2.05	.0316
3.99	.00788	2.04	.0331
3.98	.00788	2.03	.0339
3.97	.00788	2.02	.0355
⋮	⋮	2.01	.0356
⋮	⋮	2.00	.0389
2.20	.00788	1.99	.0398
2.19	.00955	⋮	⋮
2.18	.0110	⋮	⋮
2.17	.0126	.30	2.34
2.16	.0145	.29	2.40
2.15	.0155	.28	2.50
2.14	.0170	.27	2.69
2.13	.0182	.26	2.82
2.12	.0195	.25	2.95
2.11	.0218	.24	3.32
2.10	.0240	.23	3.63
2.09	.0251	⋮	⋮
2.08	.0263	⋮	⋮
2.07	.0282	.02	5.75
2.06	.0302	.01	5.75

exposure table, a portion of which is shown accompanying Figure 15. Computer usage of this table is made in the following manner. The table is read into the computer such that the exposure value corresponding to a density of 4.00 is stored as the 400th value of a 400 x 1 array. Likewise, the 50th value of the array corresponds to a density of 0.50, and a density of 0.01 is the first value of the array. The incoming digital densities are, therefore, multiplied by 100, converted to a fixed point number, and used as a subscript to index the exposure table. Thus, once the exposure table is available, converting from density to corresponding exposure can be accomplished very rapidly. Generation of the exposure table, however, is a time-consuming task.

A problem arises with color film as no unique dynamic transfer function exists. The shape of the analytical characteristic curve for the dye layers of a color tripack changes as a function of the color of the object photographed. Therefore, a single set of exposure tables, say for a neutral, will not suffice or offer valid exposure values since naturally occurring neutrals are not very numerous. If purely black-and-white images are photographed on a color material, then a single set of exposure tables — one each for the red-, green-, and blue-sensitive layer — would be sufficient.

Figures 16a, b, c are characteristic curves for the cyan, magenta, and yellow dye layers, respectively, of  emulsion 151-23-32. The curves have been generated from step wedges produced by neutrally modulating the colors shown in Figure 17. The procedure for generating these wedges is described in Appendix E.

The actual changes in curve shape are more important than the lateral curve shifts. These curve shape changes are due to interimage effects and the effect of the wavelength of the exposing light on gamma.

Interimage effects are best understood by considering the arrangement of the conventional color tripack. Consider, for example, the curves for the blue exposure. In this case, the top layer of the tripack will require a great deal of first developer and will produce more by-products than the bottom two green- and red-sensitive layers. The top layer will also produce more developer by-products than if the material had been exposed to a neutral. Diffusion of these first developer by-products into the lower layers will retard the first development in these layers. The sensitometric result will

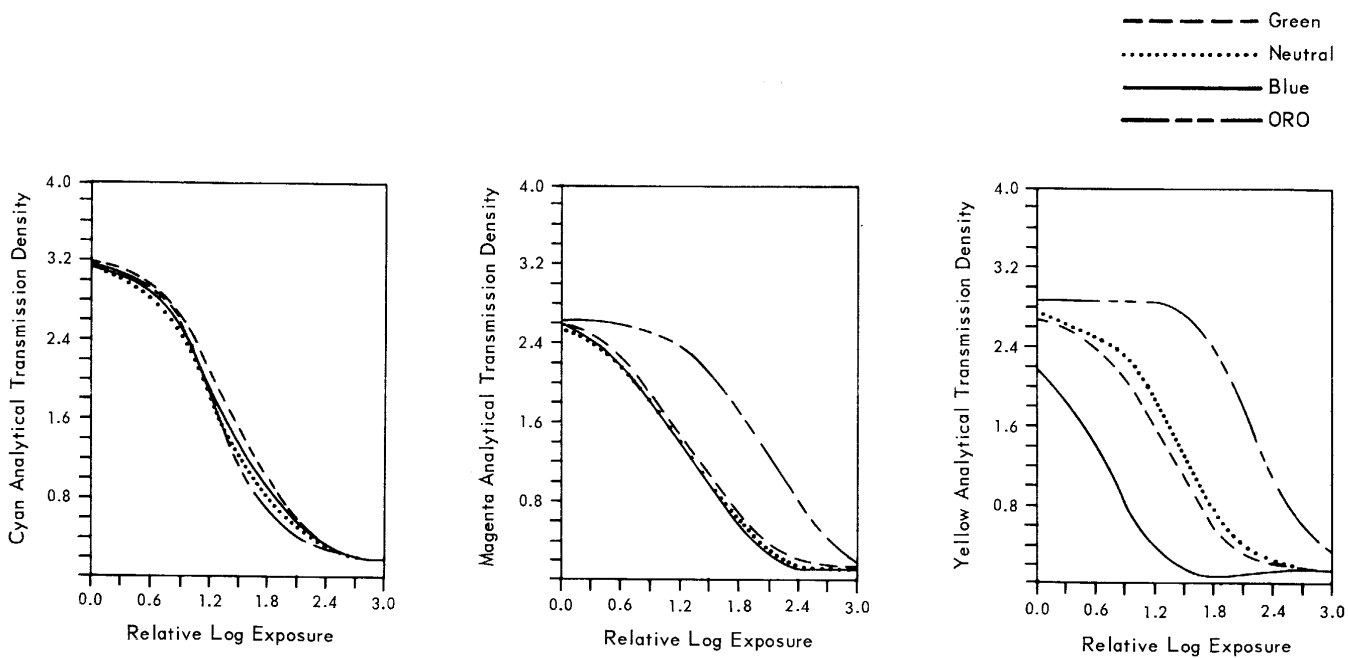
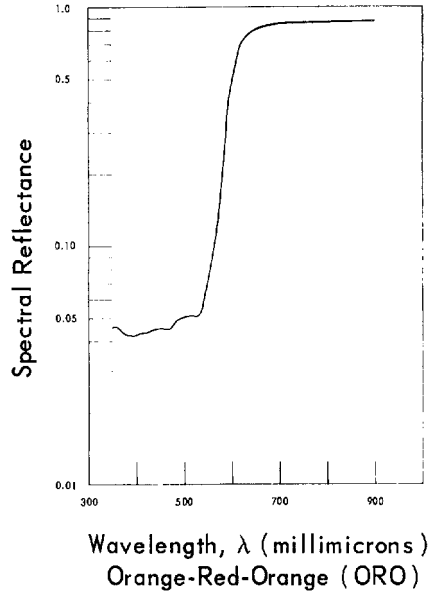
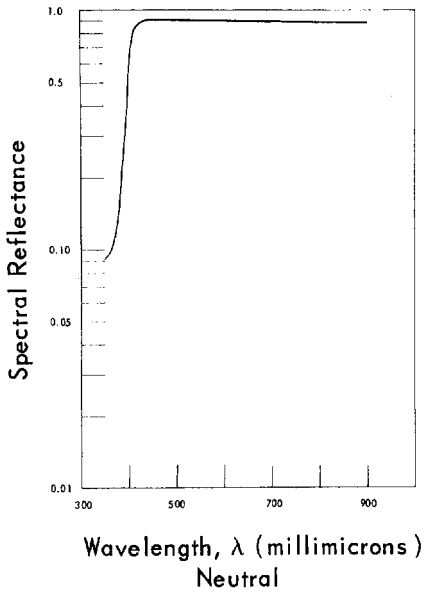


Figure 16. Characteristic Curves as a Function of Object Color



Notes :

1. These colors were neutrally modulated to produce the characteristic curves in Figure 16.
2. Exposure adjustments were based on integrated reflectance of sample.

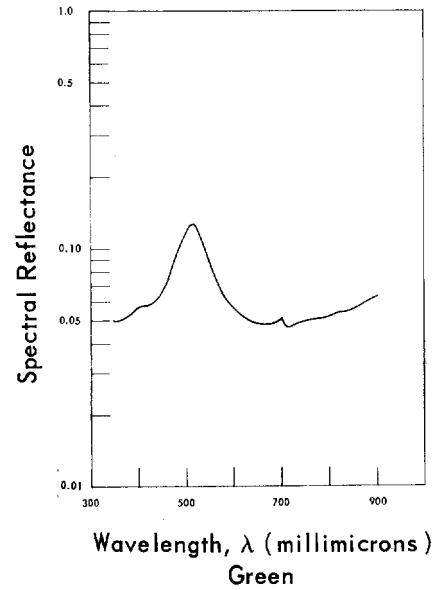
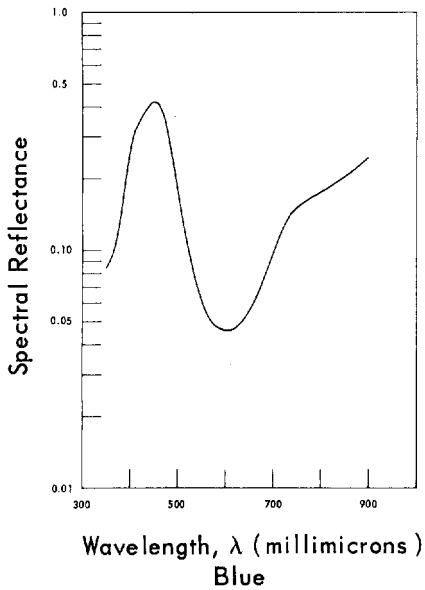


Figure 17. Color Samples and Spectral Reflectance Curves



be a higher Dmax and gamma in these layers. In addition, as development progresses in the bottom two layers, by-products must diffuse from these layers and through the top, blue-sensitive layer. This retards development in the blue-sensitive layer, especially if the bottom two layers are heavily exposed by a red or orange object (see example curve Figure 16). Retarding the blue-sensitive layer in the first developer means that a higher blue density and gamma will be obtained in the blue layer (yellow dye layer) when a red object is photographed than when a blue object is photographed.

These interimage effects are more significant when they occur in the first developer than when they occur in the color development stage<sup>32, 33</sup>.

As can be seen in Figure 16c, the curve of the yellow dye layer, when exposed to a blue object, exhibits marked interimage effects in the toe. In this region of the curve, the densities drop below the final Dmin dye density for the yellow layer. The other curves exhibit drastic change in the shape of the toe or shoulder portion of the curve.

The second reason for curve shape changes can be found by examining the relation between the gamma obtained in a dye layer and the wavelength of the exposing source. Figure 18 shows this relationship for the yellow dye layer of type 8442 color aerial

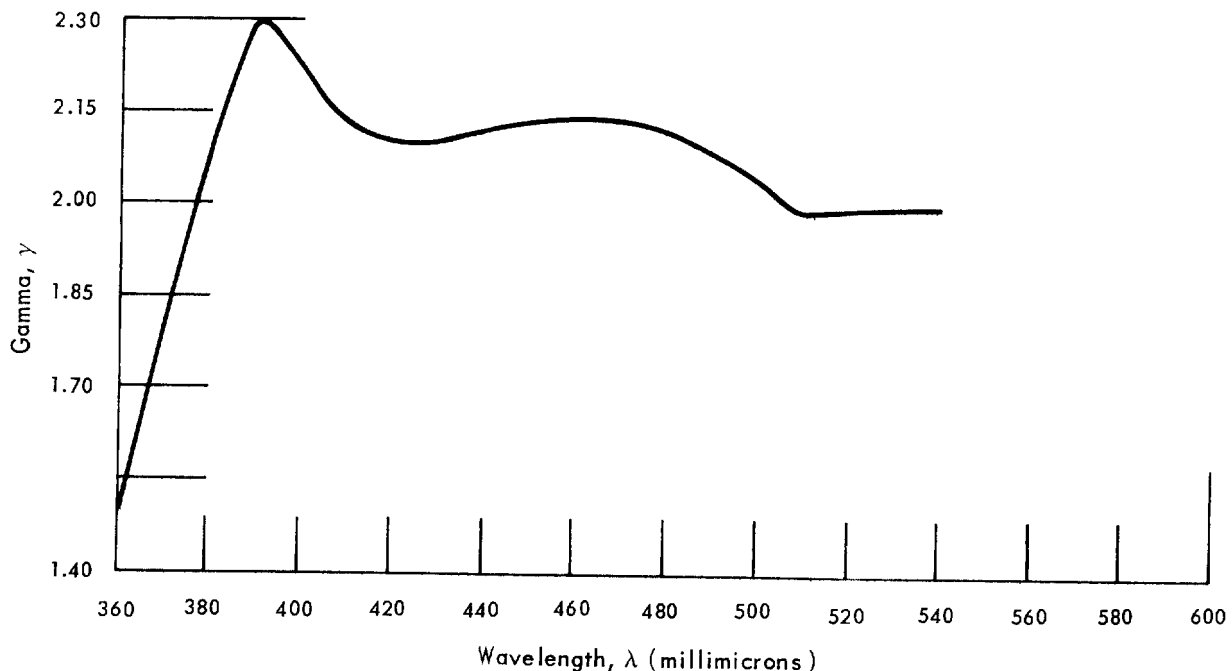


Figure 18. Wavelength Dependence of Yellow Dye Layer of  8442 Emulsion

STATINTL

reconnaissance material. Since (in operational situations) broadband selective reflectors are encountered, and since the sensitivity functions of the emulsion layers overlap, exposure of layers in wavebands away from the peak sensitivity is quite likely to occur. This means that layer gamma changes can be expected purely as a function of the dominant wavelength and purity of the exposing radiation.

Thus, these two effects — one inherent to the emulsion, the other processing oriented — mean that if effective exposure values are determined for a non-neutral color, whereas the exposure table was computed from a neutral curve, then the effective exposures will be incorrect.

### C. EXPOSURE TABLE GENERATION FOR COLOR MATERIALS

Obviously, the correct characteristic curve or exposure table, associated with the color of the object being scanned on the microdensitometer, must be utilized. Selection of the proper set of characteristic curves implies that a set of exposure tables must be computed for each set of curves — a time-consuming task. Use of the proper methods of detecting changes in the relationship between the yellow, magenta, and cyan dye layers will result in the entire set of 400 values for the exposure table for each of the dye layers being regenerated or perturbed from a neutral in approximately 1/1000 of the time it takes to generate the exposure tables from the characteristic curve. The procedure of regeneration makes use of the features of multivariate component analysis. To establish the logic behind the selection and generation of the correct exposure table, it is first necessary to set forth the operational and substantive hypotheses.

The substantive hypothesis is that the dynamic transfer function of color photographic materials undergoes perturbations as a function of the spectral characteristics of the color of the object photographed and that these perturbations can be expressed by a linear combination of a unique set of characteristic vectors.

The operational hypotheses are:

1. A set of characteristic vectors is valid for a given emulsion type, processed

in a specified manner. Changing either the emulsion type or the processing condition requires a recomputation of the characteristic vectors.

2. Batch-to-batch variation in emulsion and normal processing variance at any given time may be taken into account through the addition of the neutral reproduction characteristics of the system.

The procedure of exposure table regeneration will be described in two parts: first, the determination of the characteristic vectors of the system (equivalent to calibration) and, secondly, the functioning of the operational system.

The determination of the set of characteristic vectors requires that a set of exposure tables be generated from non-neutral characteristic curves. These curves must be generated from sensitometric strips that are neutral modulations of representative colors that will be photographed. In other words, if jungle scenes are to be photographed, the set of characteristic curves from which the exposure tables will be generated should be neutral modulations of foliage colors (dark and light greens, browns, yellows, and any other colors that may be expected). The set of sample exposure tables are generated from these curves by the curve-fit and inversion procedure previously described. Obviously there will be three (  $C$  ,  $M$  , and  $Y$  ) exposure tables for each sensitometric strip. A set of exposure tables will, therefore, exist as determined from the cyan, magenta, and yellow characteristic curves for each of the samples. Let  $E_c$  represent this sample matrix for the cyan dye layer;  $E_m$  and  $E_y$  will be the corresponding sets for the magenta and yellow layers, respectively. In describing the procedure, only one of the matrices  $E_c$  will be used as an example, since the procedure is the same for the other two matrices.

The matrix  $E_c$  is a  $400 \times n$  array, where  $n$  is the number of cyan exposure tables generated for  $n$  sample colors. For example:

	← object color →							
	green	yellow-green	blue	red	orange			
$E_c =$	$e_{11}$	$e_{12}$	$e_{13}$	$\dots$	$e_{1j}$	$\dots$	$e_{1n}$	0.01
	$e_{21}$	$e_{22}$	$e_{23}$	$\dots$	$e_{2j}$	$\dots$	$e_{2n}$	0.02
	$e_{31}$	$e_{32}$	$e_{33}$	$\dots$	$e_{3j}$	$\dots$	$e_{3n}$	0.03
	.	.	.	.	.	.	.	.
	.	.	.	.	.	.	.	.
	.	.	.	.	.	.	.	.
	$e_{i1}$	$e_{i2}$	$e_{i3}$	$\dots$	$e_{ij}$	$\dots$	$e_{in}$	$i/100$
	.	.	.	.	.	.	.	.
	.	.	.	.	.	.	.	.
	$e_{400_1}$	$e_{400_2}$	$e_{400_3}$	$\dots$	$e_{400_j}$	$\dots$	$e_{400_n}$	4.00

From this matrix a 400 x 1 array is subtracted; this array is the cyan exposure table for a neutral exposure:  $E_{cn}$ . The result is a matrix describing the perturbation from a neutral, produced in the cyan dye layer by each object color. This matrix  $P$  is a 400 x  $n$  matrix and may be termed a natural corrected perturbation matrix:

$$P = E_c - E_{cn} \tag{86}$$

The variance-covariance matrix  $S$  of  $P$  is formed:

$$S = PP' \tag{87}$$

There are several methods by which the principal components of  $S$  may be determined; the procedure used herein is iterative<sup>34</sup>. Let  $B^{(1)}$  represent the first principal component, and let  $x_{(0)}$  be any vector not orthogonal to  $B^{(1)}$ . Then  $x_{(i)}$  may be defined as

$$x_{(i)} = S y_{(i-1)} \tag{88}$$

where

$$y_{(i)} = x_{(i)} (x_{(i)}' x_{(i)})^{-1/2} \tag{89}$$

It can be shown that

$$\lim_{i \rightarrow \infty} \mathbf{y}^{(i)} = \pm \mathbf{B}^{(1)} \quad (90)$$

and

$$\lim_{i \rightarrow \infty} \mathbf{x}^{(i)} \mathbf{x}^{(i)'} = \lambda_1^2 \quad (91)$$

where  $\lambda_1$  is the first principal root.

In actual practice the limit is not infinity, but iteration is continued until no difference exists between  $\mathbf{x}^{(i)}$  and  $\mathbf{x}^{(i+1)}$  to a specified precision. The percentage  $R$  of the variance accounted for by the first principal component is simply the ratio of the characteristic root to the trace of the covariance matrix  $\mathbf{S}$  :

$$R_1 = \lambda_1 / \text{tr } \mathbf{S} \quad (92)$$

If a sufficient percentage of the trace is accounted for by the first principal component, then computation of the remaining orthogonal principal components need not be accomplished. However, the variance present in a covariance matrix, computed from a neutral corrected perturbation matrix, generally requires at least three principal components to account for a sufficient percentage (99.99%) of the trace.

The second characteristic matrix is computed from the covariance matrix  $\mathbf{S}_2$  with the variance of the first principal component removed; hence

$$\mathbf{S}_2 = \mathbf{S} - \lambda_1 \mathbf{B}^{(1)} \mathbf{B}^{(1)'} \quad (93)$$

The iteration procedure described by (88), (89), (90), and (91) is repeated for  $\mathbf{S}_2$  to obtain  $\mathbf{B}^{(2)}$  and  $\lambda_2$ . The percentage of the trace now accounted for is

$$R_2 = (\lambda_1 + \lambda_2) / \text{tr } \mathbf{S} \quad (94)$$

If desired, the third characteristic vector  $\mathbf{B}^{(3)}$  is similarly computed from the covariance  $\mathbf{S}_3$ , where the latter is  $\mathbf{S}$  deleted by the variance of the first two principal components:

$$\mathbf{S}_3 = \mathbf{S}_2 - \lambda_2 \mathbf{B}^{(2)} \mathbf{B}^{(2)'} = \mathbf{S} - \lambda_1 \mathbf{B}^{(1)} \mathbf{B}^{(1)'} - \lambda_2 \mathbf{B}^{(2)} \mathbf{B}^{(2)'} \quad (95)$$

Obviously, the limiting situation is to determine all characteristic roots of  $\mathbf{S}$  such that

$$\lim_{j \rightarrow \infty} R_j = \lim_{j \rightarrow \infty} \left( \sum_j \lambda_j / \text{tr } \mathbf{S} \right) = 1 \quad (96)$$

Simonds<sup>35</sup> describes an equivalent procedure, only with the normalization of each iterate estimate  $\mathbf{y}^{(i)}$  such that the largest element of this estimate  $\text{max } x^{(i)}$  is normalized to unity. He defines  $\mathbf{y}^{(0)}$  as an arbitrary starting array not orthogonal to  $\mathbf{B}^{(1)}$ ; thus (88) is the same as previously stated. However, the normalization takes the form

$$\mathbf{y}^{(i)} = (1/\text{max } x^{(i)}) \mathbf{x}^{(i)} \quad (97)$$

This means that

$$\lim_{i \rightarrow \infty} \text{max } x^{(i)} = \lambda_1$$

and

$$\lim_{i \rightarrow \infty} (\text{max } x^{(i)} / \mathbf{x}'^{(i)} \mathbf{x}^{(i)})^{1/2} \mathbf{x}^{(i)} = \lambda_1^{1/2} \mathbf{B}^{(1)} = \mathbf{V}^{(1)} \quad (98)$$

This means that the sum of the squares of the elements of  $\mathbf{V}^{(1)}$  equals  $\lambda_1$  since

$$\mathbf{B}^{(1)'} \mathbf{B}^{(1)} = 1 \quad (99)$$

Using Simond's notation, the modified covariance matrix  $\mathbf{S}_2$  for the computation of the second characteristic vector is

$$\mathbf{S}_2 = \mathbf{S} - \mathbf{V}^{(1)} \mathbf{V}^{(1)'} \quad (100)$$

The finite number of characteristic vectors (each a 400 x 1 array) extracted from  $\mathbf{S}$  may be arrayed to form a character matrix  $\mathbf{V}$ . An example of this procedure is given in Appendix F.

The physical significance associated with the characteristic matrix is that each 400 x 1 characteristic vector comprising the matrix describes a "principal source" of variance of a sample exposure table from the neutral exposure table. Any exposure table in the group of sample exposure tables may be regenerated by adding together

certain multiples of the characteristic vectors. This is equivalent to stating that a particular scalar multiple  $y_l, l = 1, 2, 3, \dots, p$  (where  $p$  is the number of characteristic vectors) of the characteristic vector  $\mathbf{V}^{(l)}$  plus the amount  $y_{(l+1)}$  of vector  $\mathbf{V}^{(l+1)}$  will, when added to the neutral exposure table, generate a perturbed sample exposure table. Thus, the set  $\mathbf{E}_c$  may be regenerated by the simple matrix equation

$$\mathbf{E}_c = \mathbf{V}_c \mathbf{Y}_c + \mathbf{E}_{cn} \quad (101)$$

where  $\mathbf{Y}$  is the  $p \times 1$  array of scalar multiples. (Note: Subscript  $c$  denotes the equation representing the exposure table regeneration for the cyan dye.)

Equation (101) is the key to the exposure table regeneration routine. If the array of scalars  $\mathbf{Y}$  can be determined as a function of dominant wavelength and purity of the image, then the correct exposure table can be generated and the effective exposure concept retained in color microdensitometry. Obviously the scalar multiples must be determined as a function of the analytical densities  $Y, M,$  and  $C$ . This may be accomplished by regression techniques, which implies that a sample of scalar multiples must be generated. This, in turn, may be readily accomplished by defining the weighting values  $\mathbf{W}$  from the characteristic matrix. As stated by Simonds

$$\mathbf{W}^{(l)} = \mathbf{V}^{(l)} / \lambda_l = \mathbf{B}^{(l)} / \lambda_l^{1/2} \quad (102)$$

From (101), then,

$$\mathbf{Y}_c = \mathbf{W}_c (\mathbf{E}_c - \mathbf{E}_{cn}) \quad (103)$$

Through regression analysis, the scalar multiples  $y_l, l = 1, 2, 3, \dots, p$  may be related to the  $Y, M,$  and  $C$  analytical dye densities by determination of the coefficients  $z_{jl}, j = 0, 1, 2, \dots, 9$  of the following equation:

$$y_l = z_{0l} + z_{1l} Y + z_{2l} M + z_{3l} C + z_{4l} M/Y + z_{5l} Y/C + z_{6l} C/M + z_{7l} Y^2/MC + z_{8l} M^2/YC + z_{9l} C^2/YM \quad (104)$$

Once  $\mathbf{V}_c, \mathbf{V}_m, \mathbf{V}_y$ , and the set of coefficients for determining scalar multiples (namely  $z_{jlc}, z_{jlm}, z_{jly}, l = 1, 2, 3, \dots, p$ , where  $p =$  the number of charac-

teristic vectors in each  $V$ ) have been established, the calibration procedure is completed.

The operational system for the generation of the correct set of effective exposure tables is presented in the flowchart in Figure 19.

#### D. SUMMARY

Knowledge of the emulsion type and processing conditions allows the selection of the appropriate data base from which the system works. This data base consists of, first, the characteristic matrices for each of the analytical dye layers:  $V_c$  for the cyan or red sensitive layer,  $V_m$  and  $V_y$  for the magenta and yellow layers, respectively. Each of the matrices is composed of  $p$  characteristic vectors, each characteristic vector being a  $400 \times 1$  array of values. Thus, each characteristic matrix is of dimension  $400 \times p$ . Secondly, the coefficients for scalar multiple computation (Equation (104)) are required. There are nine coefficients for each equation and  $p$  equations for each characteristic matrix.

The system neutral wedge analytical microdensities, representing the sensitometric characteristics of the particular emulsion batch in use, are used to compute the set of neutral exposure tables  $E_{cn}$ ,  $E_{mn}$ ,  $E_{yn}$  by the standard curve fit and inversion procedure. Once this information is known, the system is ready to operate with image microdensity records.

Incoming integral microdensities (IFMD) are converted to analytical microdensities (AFMD) through Equation (6). The resulting  $Y$ ,  $M$ ,  $C$  densities are used to determine the scalar multiples from the set of equations represented by (104), using the coefficients as described above. This computation results in three matrices of scalar multiples:  $Y_c$ ,  $Y_m$ , and  $Y_y$ , each of dimension  $p \times 1$ . Each exposure table is then regenerated, the cyan exposure table by (101) and the magenta and yellow tables, respectively, by

$$E_m = V_m Y_m + E_{mn} \quad (105)$$

$$E_y = V_y Y_y + E_{yn} \quad (106)$$



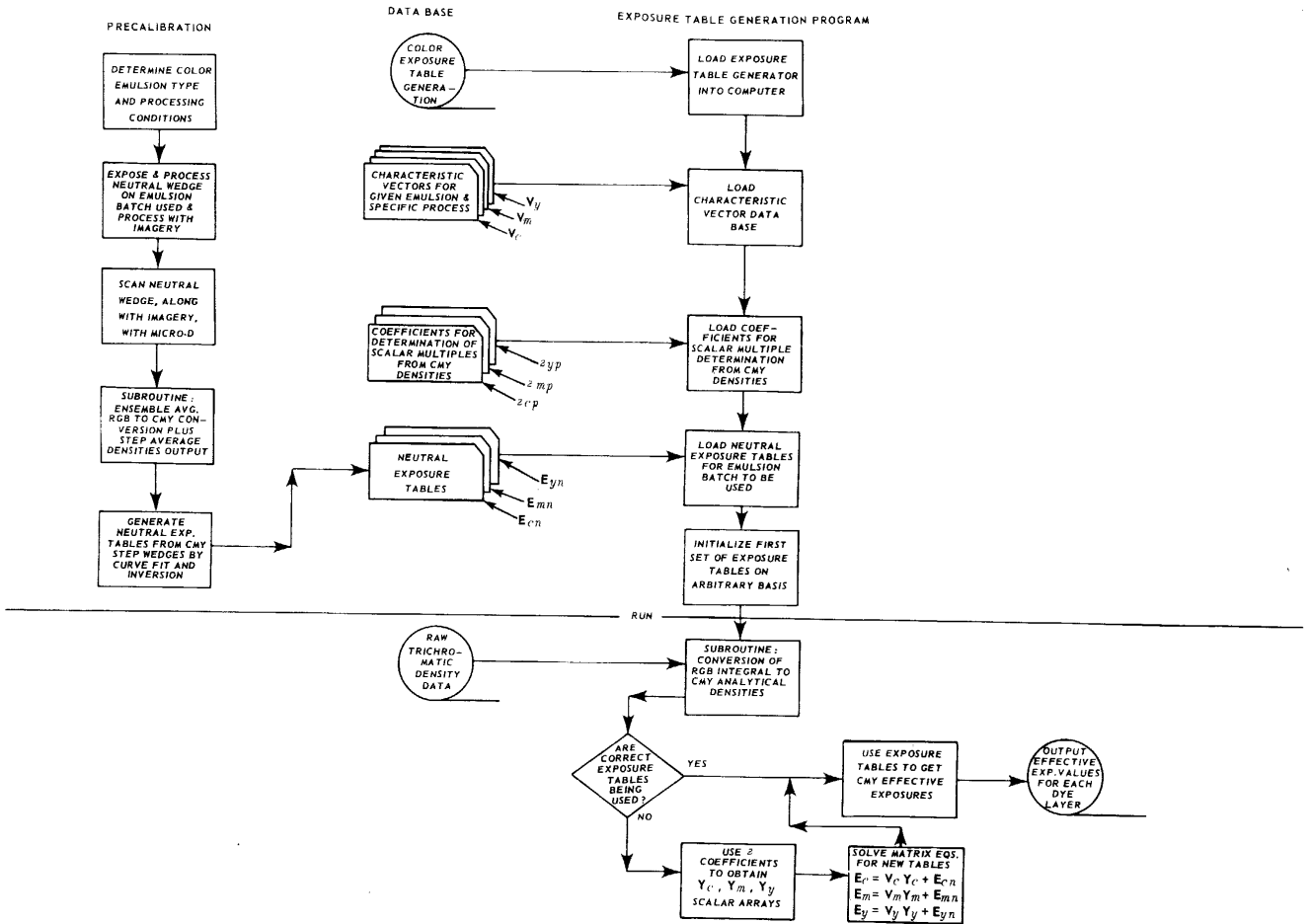


Figure 19. Exposure Table Generation System

The regeneration of the exposure tables is thus based solely on the incoming image densities. Should the "color" of the image being processed change (a color change being any change except the effective addition of neutral density), then the correct set of exposure tables are generated. The procedure described allows generation of these tables in 1/1000 the time required to generate the exposure tables from a set of characteristic curves.

One problem remains unsolved at this time: what is the criterion to be used to detect specifically when a new set of exposure tables should be generated? This criterion is very situation dependent insofar as its method of solution depends on the errors and risks that are allowable and the use to which the effective exposures will be placed. Visual measures based on the CIE MacAdam system and MacAdam units may be desirable, or a non-visual statistical detection method may be employed.

The procedure of exposure table generation may possibly be applied to the generation of the spectral signature of targets; however, no work has been performed along this line within this program.

(This page is intentionally left blank.)

## SECTION VI

## MODULATION TRANSFER FUNCTIONS FOR COLOR MATERIALS

## A. INTRODUCTION

Articles and information dealing with the theory and uses of modulation transfer functions abound in the literature and will not be discussed in detail within this report.

The program, which has just been completed, devoted little time to the investigation of color modulation transfer functions on an empirical basis. A few theoretical concepts were generated that are of importance when considering the modulation transfer function of color tripacks. These are described below.

As already mentioned in Section V, the photographic system may be considered to be a linear process (point or line spread function) combined with a nonlinear process (dynamic transfer function). The modulation transfer function (MTF) allows description of the linear process in terms of spatial frequency. It has also been mentioned that there is evidence that nonlinearities do exist in the amount of 3-8% distortion when the first three harmonics are considered. The cause of this apparent nonlinearity in black-and-white materials has not been investigated. It may result from inadequacies in the effective exposure concept, use of incorrect effective exposure tables, nonlinearities inherent in the emulsion proper, or the microdensitometer.

## B. MODULATION TRANSFER FUNCTION GENERATION

There are basically three methods by which the MTF of an emulsion may be evaluated. The first, and simplest in terms of computation, is to image sine waves directly on the emulsion<sup>37, 38</sup>. Since the exposure is known, the input modulation for a given frequency is computed as

$$M_{in} = (E_{max} - E_{min}) / (E_{max} + E_{min}) \quad (107)$$

The modulation transfer factor is defined as the ratio of output modulation to input modulation and is a function of spatial frequency,  $\omega$  :

$$\text{Modulation transfer factor} = M_{out}(\omega) / M_{in}(\omega) \quad (108)$$

This function, when normalized to unity at  $\omega = 0$ , is termed the MTF.

A second method of MTF generation is the utilization of an edge or step function exposed on the photographic material. Assume that a perfect edge can be exposed on the film, then the Fourier transform of the output edge derivative yields the impulse response function of the material. Of course, the output edge function  $H(x)$  is expressed in terms of effective exposure.

Then

$$G(\omega) = \int_{-\infty}^{\infty} [dH(x)/dx] \exp(-j\omega x) dx \quad (109)$$

Normalization at  $\omega = 0$  then yields the MTF:

$$MTF = G(\omega)/G(0) \quad (110)$$

Other methods involve the use of special functions which are imaged on the photographic material. These functions are divided into two groups: continuous and discontinuous. A sinc function is a prime example of the former, and the various bar targets are examples of the latter.

Sinc functions<sup>39</sup>  $\text{sinc}(x) = (\sin x)/x$  have been acclaimed as an optimum target for the evaluation of the spatial frequency response of the photographic material. Problems exist, however, in the generation of this function as a continuous tone image; therefore, widespread use of this function has not occurred.

Two types of bar targets are currently under investigation, the comb<sup>40, 41</sup> and the binary comb<sup>42</sup>. These targets are easily produced on photographic materials. However, to determine the MTF of the system the target transform must be removed from the Fourier transform of the photographic output. If  $H_T(x)$  is the target function and  $H_I(x)$  is the resulting image function expressed in terms of effective exposure, then the Fourier transforms are simply

$$G_T(\omega) = \int_{-\infty}^{\infty} H_T(x) \exp(-j\omega x) dx \quad (111)$$

$$G_I(\omega) = \int_{-\infty}^{\infty} H_I(x) \exp(-j\omega x) dx \quad (112)$$

for the target and image functions, respectively. The normalized MTF of the photographic material is

$$MTF = G_I(\omega) / G_T(\omega) G(0) \quad (113)$$

The computation of the MTF is performed using effective exposures derived from the microdensity records. This, of course, assumes that the proper inverse dynamic transfer function or exposure table was used in converting from analytical microdensities to exposure values.

### C. COLOR MATERIALS

The application of modulation transfer functions to color tripacks introduces a significant complexity into their interpretation. Examples exist in which color MTF curves have been reported. Verbrugghe<sup>43</sup> has reported red, green, and blue integral modulation transfer functions for color materials. However, to go from integral MTF to analytical modulation transfer functions, at the present time, is not as easy as it is to obtain analytical Wiener noise spectra from integral data. This is because the sensitivity crossovers for the three layers are operating in the exposure-optical diffusion process and because the MTF curves are computed from effective exposure values rather than density values.

It is suggested that in future programs the relation between integral and analytical modulation transfer functions be investigated from both an empirical and analytical standpoint. This research becomes essential once color photographic materials are used in the estimation of spectral signatures.

Up to this time, a search of the literature reveals that consideration has only been given to the neutral modulation of color materials. However, from an operational standpoint this is almost a trivial case. There are several parameters that must be more fully understood than at present. Not only does the output modulation vary as a function of the input modulation, but the dominant wavelength and purity (or hue and chroma) of the input modulation must also be considered. For example, in an operational situation the critical situation may be the detection of an edge generated by a

green object on a greenish-brown background. Neutral modulation transfer functions convey, at present, no information concerning the detectability of this situation with a given material under given exposure conditions. The added dimension of the "color" of the target then becomes a nontrivial operational parameter which is extremely significant in the proper assessment of color imagery.

SECTION VII

QUALITY CONTROL OF THE MICRODENSITOMETER

STATINTL

STATINTL

A. INTRODUCTION

STATINTL

Techniques for the quality control of microdensitometers were developed at   under Air Force contract . This study<sup>44</sup> resulted in a procedure requiring the existence of a computer facility and the development of a quality control target. It is a description of this program that is presented in this section. The fact that the procedure was developed for black-and-white microdensitometers is of no significance, as it may be adapted directly for trichromatic use. A neutral target must still be used because the high resolution quality control target can be produced to sufficient quality and stability only on black-and-white glass plates at the present time. This target would be traced, however, in a trichromatic mode and the trichromatic data analyzed to obtain quality control on each channel of the microdensitometer.

B. IDEAL DEVELOPMENT OF QUALITY CONTROL SYSTEM

In an ideal situation (one that conforms to theory), a quality control system would be established in accordance with the following sequence<sup>45</sup>.

Establishment of Policy. A decision to establish a quality control system represents the initial desire for knowledge concerning the past, probable present, and probable future status of a process or instrument.

Establishment of Objectives. In the second phase, the goals of the quality control system are dictated. If possible, the level of performance that the completed control system is to achieve should be stated.

Adoption of a Plan. The next logical step is to formulate and adopt a plan whereby the established objectives can be attained. (The establishment of a plan to meet the quality control objectives is the goal of this section.)

Organization. Organization to carry out the plan is accomplished in basically two phases: research and implementation. Research concerning the nature of the vari-



ables of microdensitometry and how these variables are reflected in a quality control measure is necessary prior to finalization and implementation of a quality control plan.

Personnel Selection and Training. The selection and training of people to operate the system are, indeed, important phases in making a quality control system design an operational entity meeting the initial objectives. The operators must be sufficiently informed to maintain the quality control system, and they must be unbiased to the point that they will not force out-of-control conditions to in-control situations by arbitrarily resetting the limits.

Motivation. Stimulating people to meet the planned objectives may become a large problem, especially if many people utilize an instrument which is monitored on a quality control basis. Rather than allow the quality control procedure to be handled by many or by whomever is utilizing the machine at the time, it is desirable to assign this task either to a single individual or to a department handling all such tasks.

Reevaluation. Once established, the quality control system should not be abandoned, unless the system does not meet the planned objectives or unless the basic quality policy changes. Continued updating of expectations and control limits must be part of the system procedure. Reviewing the system against its objectives and attempting to correct its deficiencies are time consuming steps whose accomplishment may require considerable control system background history. Nevertheless, the reevaluation of the system is necessary, not only to approach the final objectives of the program but also to streamline the system to an efficient procedure.

### C. GENERAL PROGRAM OBJECTIVES

The establishment of a quality control system for a microdensitometer must be based on a meaningful measure of system performance, such that the information gained from the control system will be useful in the diagnosis of machine failures. This system must be designed to allow cross comparison of quality control information between machines, thus allowing relative calibration on this basis. The procedure for obtaining the basic (raw) control data must involve as little setup time and run time as possible. Likewise, mathematical computations or manipulations must be computer programmable for short throughput times. The output from the program must be

readily interpretable in terms of the status of the system as well as the diagnosis of machine failure. In other words, the quality control system for the microdensitometer must operate with the utmost efficiency in order to generate a maximum of useful information with the minimum possible expenditure of energy in man-hours (training and running), microdensitometer time, computer time, etc.

The following results are anticipated from the implementation of the proposed quality control system.

1. It will increase reliance on the data taken from a microdensitometer to which the control system has been rigorously applied, since the probable operational status of the instrument will be known at a time not remote from the time of measurement.
2. It will give assurance that data taken from any single microdensitometer may be mapped to correlate with data taken from the same input to a second microdensitometer, providing that the quality control system has been applied to both instruments and that both are in control. (This concept arises from a hypothesis that microdensitometers are not easily calibrated on an absolute density basis and that an ensemble average taken from a finite record is not directly relatable to the diffuse density value determined from a standard large area or macrodensitometer, except perhaps on an effective exposure basis.)
3. It will establish routines for the diagnosis of causes of machine failures in situations considered out of control.

#### D. DRIFT ANALYSIS

In the evaluation of standard diffuse macrodensitometers, quality control efforts are generally concerned with maintaining the dc response of the instrument. In the general case, control information is gathered in three portions of the dynamic range of the instrument, i. e., high, medium and low densities. Drifting of the instrument response can be detected by zeroing and recalibrating (rereading a "calibrated" step wedge or a series of selected points from a step wedge) periodically. The length of this calibration period is determined by the risk the operator wishes to take in the detection of short-term drift errors.

Similar dc problems disturb the world of microdensitometry, but in this case there is also a lateral, longitudinal, or rotational translation of the image during the measurement period. This gives rise to concern for the spatial frequency response characteristics of the microdensitometer. However, it is reasonable to assume that shifts in the spatial frequency response characteristics of the microdensitometer will be of a long term nature and will be caused either by improper operation of the instrument or by operational failure of the instrument.

Shifts and changes in the spatial frequency response of the system may be detected, providing that any dc drifting is first detected and removed from the data. Given a specific image to be scanned, the drift of the instrument during the scanning period may be reasonably estimated by observing the initial dc calibration or setup points and then recalibrating at the end of the image scan. Observing the differences between the initial and final calibration points yields an indication of the drift of the instrument over the measurement period.

From these observations, a basic procedure may be evolved for collecting quality control information from a microdensitometer. The basic procedure encompasses an initial setup or scanning of a step wedge, so that the zero point and dynamic range of the instrument may be established. This may then be followed by the scanning of a target suitable for the measurement of the spatial frequency response characteristics of the instrument. Following this, a rescan of the step wedge or of a selected number of setup calibration points may be accomplished, thus providing a determination of the amount of dc drift in the instrument during the intervening time. (Short term instabilities would not be detected by this method but would be reflected in the spatial frequency response variations of the instrument.) If the drift interval is constant (i. e., if the measurement interval  $\Delta t$  is constant), then a determination of the difference between the first and second dc calibrations will measure the average drift rate. This involves an assumption of a drift function that is linear with time. Estimation of the drift rate may be a trivial point, as any detectable dc shift during the measurement period is undesirable. In testing for the presence of dc drift, it is necessary to realize that such shifts may be detectable only on a statistical basis.

The dc calibration of a microdensitometer is performed on an effective exposure

basis. This means that the establishment of the calibration curve for the microdensitometer is performed from a constant input, just prior to the scanning of the test target. Generally, this input consists of a step wedge of  $i = 1, 2, 3, \dots, n$  discrete levels, such that the input function range is compatible with the dynamic range of the microdensitometer. After the scanning of the "unknown" sample, the step wedge is again scanned. The data so determined are taken through the initial calibration curve, so that drift errors appear as effective exposure errors.

Let  $\langle E_{i0} \rangle$  represent the initial calibration value for the  $i$ th step. This is an ensemble average effective exposure taken over the  $i$ th step of finite width. After the scanning of the unknown sample, the step wedge is again scanned, and the effective input value for the  $i$ th step is again determined as  $\langle E_{i \Delta t} \rangle$ .

A correlated pair analysis<sup>46</sup> (paired observation analysis) may be performed upon the differences  $\Delta \langle E_i \rangle = \langle E_{i \Delta t} \rangle - \langle E_{i0} \rangle$ . This type of analysis will permit the detection and estimation of the probable magnitude of any drift occurring during the measurement interval  $\Delta t$ . To perform this analysis, two parameters are computed: one is the average difference,  $\bar{d}$ , across the  $n$  steps of the calibration wedge,

$$\bar{d} = \frac{1}{n} \sum_{i=1}^n \Delta \langle E_i \rangle \quad (114)$$

The second parameter is the standard deviation of the differences across the calibration wedge

$$s_d = \left[ \sum_{i=1}^n \frac{(\Delta \langle E_i \rangle - \bar{d})^2}{n-1} \right]^{1/2} \quad (115)$$

The main assumption in this case is that the values obtained for the average deviation estimates  $\bar{d}$  are distributed normally about the true mean difference  $\delta$ . This being the case, from the above values a test statistic may be calculated which follows a student's  $T$ -distribution function with  $n-1$  degrees of freedom:

$$T_{CAL} = \frac{\bar{d} \sqrt{n}}{s_d} \quad (116)$$

In all cases, the null hypothesis  $H_0$  is that no drift  $\delta$  occurred during the interval  $\Delta t$ :

$$H_0 : \delta = \delta_0 = 0 \quad (117)$$

The alternate hypothesis that must be accepted, if the null hypothesis is rejected, is that drifting of the instrument occurred over the interval in which the ac response characteristics of the microdensitometer were evaluated, i. e. , during the interval  $\Delta t$

$$H_1 : \delta \neq \delta_0 \quad (118)$$

Rejection of  $H_0$  then indicates acceptance of the occurrence of a significant amount of drift during the estimation of the ac response characteristics of the instrument and brings into play the alpha risk taken when the null hypothesis is rejected. In this case, a rejection, or alpha error, occurs when a set of ac response data is rejected as containing microdensitometer drift when, in truth, no drifting occurred. In stating the rejection error or the specific alpha probability that would be acceptable, two factors come into play: the first of these concerns the alpha risk directly, and the second takes into account the allowable beta or acceptance risk. The two factors, considered together, determine the magnitude of the drift error that can be detected.

The consequence of rejecting a set of data as containing microdensitometer drift, when actually it does not (alpha risk), requires the rescanning of the quality control target and a loss of man-hours, microdensitometer time, and a small amount of computer time. On the other hand, acceptance of a set of data containing drift (beta risk) could (1) indicate an out-of-control situation in the analysis of the ac response of the system, thus bringing into play the diagnostic program with the consequences of closing down the system until the problem is diagnosed (the only actual machine error, in this case, being dc drift); or (2) the drift problem could remain undetected, thus influencing production data; or (3) the machine could stabilize, and the drift problem could disappear in future time. The only data influenced in this case would be the ac quality control data. (As can be seen, the time of day when quality control data are gathered from the machine may influence the result obtained.)

In terms of consequences, the risk involved in accepting the existence of dc drift, when in truth there is none, is less than the risk involved in accepting data as being drift-free when, in truth, it is not. Thus, the acceptable alpha and beta risk probabilities may be set on a relative basis as  $\alpha \geq \beta$ .

## E. FREQUENCY RESPONSE STABILITY

The mention of quality control monitoring of the ac response characteristics of the microdensitometer system involves many implications and problems. The first of these is that it is, at best, an exceedingly difficult problem to assess the absolute frequency response of a microdensitometer in terms of spatial frequencies. However, by placing quality control restrictions upon the utilization of frequency response data, the problem becomes of lesser magnitude in that the stability of the response can be monitored without regard to the absolute frequency transfer function of the apparatus. The observation that spatial frequencies, when scanned, are mapped into temporal frequencies brings into consideration the flutter and wow idiosyncracies of the drive mechanism. Drive instabilities may be diagnosed through proper inspection of the quality control data.

A possible error source exists in the ability of the operator to focus the instrument; if the focus is far from optimum, attenuation of the higher spatial frequencies results. This leads to questions concerning what optics and what slit dimensions or spot diameter should be utilized in the quality evaluation procedure. Since there are many possible combinations of slit size, spot size, scan speed, digital conversion rate, and chart velocity, quality control information obviously cannot be generated for all possible permutations. The alternative is a practical choice of one or a few conditions based on some criteria such as a median condition, a most often utilized situation, or an extreme condition that is likely to illustrate system problems with a high sensitivity.

The method of approach to developing the basic diagnostic and quality control procedure is threefold. First, we must develop a method of relating, numerically, the information gained through frequency plane analysis of a specific target to the operational status of the microdensitometer. Ideally, this basic quality control measure would be a single number reflecting the effects of all the critical parameters of the microdensitometer. Once a mathematical method of dealing with spatial frequency data, on a quality control basis, has been established, the second step then consists of applying this knowledge to the design of a specific quality control target configuration that will satisfy the demands of the mathematics of the quality control procedure. The

third step is the simulation of machine failures on a mathematical basis, resulting in the establishment of the diagnostic procedure to be utilized when the general quality control measure indicates an out-of-control situation.

The basic quality control target will be a configuration that varies as some function of distance in the  $xy$  plane. It is desirable that the  $y$  domain of the target be so defined that to the microdensitometer it would appear that the configuration is constant in the  $y$  direction, that is,  $F(y) = \text{constant}$  for  $-\infty \leq y \leq \infty$ . For the present, let  $F(x)$  represent the optical density of the target as a function of the spatial dimension  $x$ . This target will be defined to exist over a closed domain  $-L/2 \leq x \leq L/2$ , such that the output record will exist only within this spatial domain. The Fourier transform of  $F(x)$  is

$G_F(\omega)$ :

$$G_F(\omega) = \int_{-\infty}^{\infty} F(x) \exp(-j\omega x) dx = \int_{-L/2}^{L/2} F(x) \exp(-j\omega x) dx \quad (119)$$

or  $F(x) \leftrightarrow G_F(\omega)$ , i. e., the Fourier transform pairs. In the process of scanning the target with the microdensitometer, a convolution of the slit illuminance function  $S(x)$  with the target function  $F$  occurs, so that the output signal becomes

$$Q(\tau) = \int_{-\infty}^{\infty} F(x) S(\tau - x) dx \quad (120)$$

where  $\tau$  is the lag variable, and the output transform becomes

$$G(\omega) = G_F(\omega) G_S(\omega) = \int_{-\infty}^{\infty} \int_{-\infty}^{\infty} F(x) S(\tau - x) dx e^{-j\omega\tau} d\tau \quad (121)$$

where

$$S(x) \leftrightarrow G_S(\omega)$$

$G(\omega)$  may be computed from the digital sampling of the function  $Q(\tau)$  over the closed domain  $-L/2 \leq x \leq L/2$ . If a number  $n$  of repetitive scans are performed in successive determinations of  $Q(\tau)$ , differences between scans would be expected, due to random machine and operator errors. In this case, a mean transform  $\overline{G}(\omega)$  becomes a useful representation of the expected transform of  $Q(\tau)$ . For the present, the mean transform will be defined as the simple average of the sample of  $n$  transform estimates:

$$\overline{G}(\omega) = \frac{1}{n} \sum_{j=1}^n G_j(\omega) \quad (122)$$

The vector difference between any estimate of  $G(\omega)$  in the frequency plane and the mean transform may be defined as

$$\Delta G(\omega) = G(\omega) - \overline{G(\omega)} \quad (123)$$

In basing a quality control estimate upon the transform of a specific target, as produced by a given microdensitometer at a specific time, concern is not for the nature of that particular transform but for the stability of that transform, i. e., the important factor is  $\Delta G(\omega)$ . If  $\Delta G(\omega) = 0$ , the past and the immediate past averages correspond, on the average, and the assumption is made that this state will continue to be true for a finite interval of time in the future.

Since the function  $G(\omega)$  actually will be represented by a finite number of frequencies  $\omega_i$ ,  $i = 1, 2, 3, \dots, \Omega$ , the modulus of the vector difference between the sample transform and the mean will be

$$|\Delta G(\omega_i)| = \{ [G(\omega_i) - \overline{G(\omega_i)}] [G^*(\omega_i) - \overline{G^*(\omega_i)}] \}^{1/2} \quad (124)$$

Random fluctuations of the phase  $\Delta \Phi(\omega_i)$  will be associated with random fluctuations of the modulus about the mean. It is possible to simplify matters to a considerable degree by placing restrictions upon the target design  $F(x)$  such that  $F(x) = F(-x)$ , thus yielding only real terms in the transform. This eases the problem of defining phase errors since the phase at any spatial frequency is equal to zero, i. e.,  $\Phi(\omega_i) = 0$ . (This is true at least from an idealistic viewpoint.)

It is now necessary to place quality control constraints upon the modulus difference  $|\Delta G(\omega_i)|$  and the phase fluctuations  $\Delta \Phi(\omega_i)$ . In a normal (in-control) operating situation, we would expect random fluctuations in phase and modulus about their respective expectations. The expected phase deviation from the average phase would be

$$E[\Delta \Phi(\omega_i)] = 0 \quad (125)$$

since

$$-\pi < \Delta \Phi(\omega_i) \leq \pi \quad (126)$$

which follows from the definition of the average transform  $\overline{G(\omega_i)}$ .

The range of values that can be taken by  $|\Delta G(\omega_i)|$  may be stated as  $0 \leq |\Delta G(\omega_i)| \leq \infty$ . Hence, the expectation cannot be zero since this would imply the expectation of zero



error; thus

$$E [ | \Delta G (\omega_i) | ] > 0 \quad (127)$$

It is now necessary to state, as a hypothesis, that if the microdensitometer is operating in control, then a value obtained for  $|\Delta G (\omega_i)|$  will show little correlation with  $|\Delta G (\omega_{i+j})|$ , where  $j > 0$ . In other words, if the microdensitometer is operating in control, it is hypothesized that any absolute deviation in the amplitude of the transform, from the mean amplitude at a given frequency, will show little correlation with the absolute deviation from the mean amplitude at any other frequency. Since the expectation for  $|\Delta G (\omega_i)|$  is greater than zero, this implies that the deviations from the mean transform amplitude will exhibit a small serial correlation,  $\rho_{GG} \neq 0$ , in terms of the frequency domain. The reason that a non-zero serial correlation coefficient  $\rho_{GG}$  is expected is that the modulus of the vector difference is defined as an absolute value, thus disallowing the assumption of a symmetrical probability density function of  $|\Delta G (\omega_i)|$  about the expectation  $E [ |\Delta G (\omega_i)| ]$ . We would expect the serial correlation coefficient to exceed a critical value whenever the microdensitometer, or the operation thereof, is not in-control.

A similar, and perhaps more important, point may be made that a lack of serial correlation should occur in terms of the random phase shifts at any given frequency with respect to any given frequency, i. e., between  $\Delta \Phi (\omega_i)$  and  $\Delta \Phi (\omega_{i+j})$ . Thus, it is hypothesized that the magnitude of the phase shift or the random deviations of the phase from the expected phase, at any given frequency, will be uncorrelated ( $\rho_{\Phi} = 0$ ) with the phase deviation at any other frequency, providing the instrument is operating and is being operated in-control.

The test hypotheses for the quality control statistics may now be defined. Let  $\rho_G$  be the true value, and let  $\rho_{GG}$  be the expected value of the serial correlation coefficient of the absolute magnitude of the deviation of the sample transform from the expected magnitude of the transform. Let  $\rho_{\Phi}$  represent the true value of the serial coefficient of correlation across the frequency domain for the deviations in phase from the expected phase.

1. It has been stated that the microdensitometer is operating and is being operated in-control if

$$H_{0G} : \rho_G = \rho_{G0} \quad (128)$$

and

$$H_{0\Phi} : \rho_\Phi = 0$$

(a necessary and sufficient condition for consideration of an in-control status).

2. At this point we shall only state that the operational status of the machine will be questioned if

$$H_{1G} : \rho_G > \rho_{G0} \quad (129)$$

or

$$H_{1\Phi} : \rho_\Phi \neq 0$$

that is, if either of these alternate hypotheses is accepted, this represents a sufficient condition for questioning the operational status of the machine.

3. If both of the alternate hypotheses of (129) are accepted as true, then the operational status of the machine must be considered out-of-control (a sufficient condition for declaring the microdensitometer to be in an out-of-control status and for initiating a diagnostic procedure).

The procedure for calculating the serial correlation coefficients on the modulus and phase components of a set of quality control sample data is as follows. For computational convenience in the estimation of the density function of the serial correlation coefficients, a circular universe will be assumed for the series of phase and modulus deviations at the discrete frequencies  $\omega_i, i = 1, 2, 3, \dots, \Omega$ . Further, in the computation of the circular serial correlation coefficient, a unity lag will be utilized<sup>47</sup>. The sample estimate of the circular correlation  $\bar{r}$  from a given quality control evaluation of  $G(\omega_i)$  at  $\Omega$  discrete frequencies is determined by the equation

$$\bar{r}_G = \left\{ \left[ \sum_{i=1}^{\Omega-1} |\Delta G(\omega_i)| |\Delta G(\omega_{i+1})| \right] + |\Delta G(\omega_\Omega)| |\Delta G(\omega_1)| \right\} \left[ \sum_{i=1}^{\Omega} |\Delta G(\omega_i)| \right]^{-2} \quad (130)$$

for the modulus of the vector difference between the amplitude of a given sample and that of the average transform. The circular serial coefficient of correlation on the phase difference between the same sample and the expected phase is

$$\bar{r}_\Phi = \left\{ \left[ \sum_{i=1}^{\Omega-1} \Delta \Phi(\omega_i) \Delta \Phi(\omega_{i+1}) \right] + \Delta \Phi(\omega_\Omega) \Delta \Phi(\omega_1) \right\} \left[ \sum_{i=1}^{\Omega} \Delta \Phi(\omega_i) \right]^{-2} \quad (131)$$

In the two equations above,  $\bar{r}_G$  is the sample estimate of the true circular correlation coefficient  $\rho_G$ , and  $\bar{r}_\Phi$  is the sample estimate of the true circular serial correlation coefficient  $\rho_\Phi$ .

Actually, defining  $|\Delta G(\omega_i)|$  and  $\Delta\Phi(\omega_i)$  as belonging to a circular stochastic process may affect the power of the test of significance on the value obtained for the coefficient of serial correlation from a given sample<sup>48</sup>. The degree to which the significance test is affected is unknown, but it is believed to be slight; the simplification gained, in the definition of the density function of  $\bar{r}$  by working in a circular universe, is significant<sup>49</sup>.

There will be a distribution of  $\bar{r}$  values around the true correlation coefficient  $\rho$ . The approximate marginal distribution  $R_\rho(\bar{r})$  is

$$\tilde{R}_\rho(\bar{r}) = \frac{\Gamma\left(\frac{\Omega}{2} + 1\right)}{\Gamma\left(\frac{1}{2}\right) \Gamma\left(\frac{\Omega + 1}{2}\right)} (1 - \bar{r}^2)^{\frac{\Omega-1}{2}} (1 + \rho^2 - 2\rho\bar{r})^{-\frac{\Omega}{2}} \quad (132)$$

where  $\Omega$  is the number of discrete points correlated<sup>50</sup>.

By definition of the average transform  $\overline{G(\omega_i)}$ , we have stated as the null hypotheses that

$$\rho_G = \rho_{G0} > 0 \quad (133)$$

and

$$\rho_\Phi = \rho_{\Phi0} = 0$$

These are the necessary and sufficient conditions for an in-control process.

The marginal distribution for each quality control parameter must be defined on the basis of the null hypothesis, i. e., on the basis of the expected circular serial correlation. Hence, the approximate marginal distribution function of  $\bar{r}_G$  becomes

$$\tilde{R}_{\rho_{G0}}(\bar{r}_G) = \frac{\Gamma\left(\frac{\Omega}{2} + 1\right)}{\Gamma\left(\frac{1}{2}\right) \Gamma\left(\frac{\Omega+1}{2}\right)} (1 - \bar{r}_G^2)^{\frac{\Omega-1}{2}} (1 + \rho_{G0}^2 - 2\rho_{G0}\bar{r}_G)^{-\frac{\Omega}{2}} \quad (134)$$

The approximate marginal distribution function for the circular serial correlation coefficients calculated for the phase deviations becomes

$$\tilde{R}_0(\bar{r}_\Phi) = \frac{\Gamma\left(\frac{\Omega}{2} + 1\right)}{\Gamma\left(\frac{1}{2}\right) \Gamma\left(\frac{\Omega+1}{2}\right)} (1 - \bar{r}_\Phi^2)^{\frac{\Omega-1}{2}} \quad (135)$$

which corresponds to the Dixon distribution<sup>51</sup> for  $\rho = 0$ .

The critical test values, upon which the acceptance or rejection of the null hypothesis is based, may be calculated. For the cumulative distribution of  $\bar{r}_\Phi$  we are faced with a two-tailed situation since  $-1 \leq r \leq 1$ . The total rejection risk probability may be determined for a given domain  $-\bar{r}_{\Phi\alpha} \leq \bar{r}_\Phi \leq \bar{r}_{\Phi\alpha}$  by integration across the  $\bar{r}_\Phi$  axis:

$$\alpha_\Phi = 1 - \frac{\int_{-\bar{r}_{\Phi\alpha}}^{\bar{r}_{\Phi\alpha}} (1 - \bar{r}_\Phi^2)^{\frac{\Omega-1}{2}} d\bar{r}_\Phi}{\int_{-1}^1 (1 - \bar{r}_\Phi^2)^{\frac{\Omega-1}{2}} d\bar{r}_\Phi} \quad (136)$$

The two-tailed rejection risk is thus  $\alpha/2$ .

Looking at the cumulative distribution for the values of  $\bar{r}_G$ , it must be noted that  $-1 \leq \bar{r}_G \leq 1$ . The rejection risk probability may be defined similarly by evaluating the area between the  $-1$  and the specific  $\bar{r}_{G\alpha}$  value,  $\bar{r}_{G\alpha}$ , i. e.,

$$\alpha_G = 1 - \frac{\int_{-1}^{\bar{r}_{G\alpha}} (1 - \bar{r}_G^2)^{\frac{\Omega-1}{2}} (1 + \rho_{G0}^2 - 2\rho_{G0}\bar{r}_G)^{-\frac{\Omega}{2}} d\bar{r}_G}{\int_{-1}^1 (1 - \bar{r}_G^2)^{\frac{\Omega-1}{2}} (1 + \rho_{G0}^2 - 2\rho_{G0}\bar{r}_G)^{-\frac{\Omega}{2}} d\bar{r}_G} \quad (137)$$

Once  $\Omega$  is specified, these integrals may be evaluated and the critical  $\bar{r}_{\Phi\alpha}$  and  $\bar{r}_{G\alpha}$  values estimated for a given alpha risk.

#### F. NOISE INJECTION ANALYSIS

The quality control checks thus far established have not taken into consideration the problem of monitoring the noise injection characteristics of the microdensitometer system. It is desirable to separate the noise characteristics of the amplifiers and the photomultiplier of the microdensitometer from the granular noise of the film or photographic quality control target. The separation can be effected by allowing the digitizer to run without scanning the target. Since the signal-to-noise ratio decreases

at high photometric densities, it is at a high photometric density that the instrument scan should be halted. Allowing the digitizer to run at this point will establish a data record of the noise characteristics being injected at a low input signal level. The amplifier and photomultiplier are not easily separable as noise sources.

It appears necessary to monitor only one density level in order that knowledge of the changes in noise characteristics, particularly a significant increase in the noise level at a given density input, may be detected.

Let  $N_j$ ,  $j = 1, 2, 3, \dots, M$ , be the set of noise data. The allowable noise variance may be stated as  $\sigma_N^2$ ; if the noise variance taken over any time interval is greater than the allowable variance, then the microdensitometer must be checked to determine the cause for the increase in noise injection. On this basis the null hypothesis becomes

$$H_0 : \sigma^2 \leq \sigma_N^2 \quad (138)$$

where  $\sigma^2$  is the true noise variance. The acceptance of the null hypothesis indicates that the noise injection characteristics are nominal. The rejection of the null hypothesis forces the acceptance of the alternate hypothesis

$$H_1 : \sigma^2 > \sigma_N^2 \quad (139)$$

in which case the instrument is declared to be out of control. A rejection (alpha) risk is operating in the latter case, that is, there is a finite probability that we may state that the noise variance has increased above the allowable standard  $\sigma_N^2$  when, in truth, it has not. This risk probability will be stated as  $\alpha$ .

Since  $N_j$ ,  $j = 1, 2, 3, \dots, M$ , are independent and identically distributed random variables following a normal distribution, then a chi-square test value may be computed as

$$\chi_{TEST}^2 = \frac{\sum_{j=1}^M (N_j - \bar{N})^2}{\sigma_N^2} \quad (140)$$

where  $\bar{N}$  is the input average determined for the sample.

The actual alpha probability associated with the chi-square test value may be calculated by integrating across the chi-square distribution function (see Appendix B).

Once  $M$  and  $\sigma_N^2$  are set, the critical chi-square value  $\chi_\alpha^2$  may be set as a constant upper quality control limit on the value  $\chi_{TEST}^2$ , such that if  $\chi_{TEST}^2 > \chi_\alpha^2$ , then the alternate hypothesis is accepted with a known  $\alpha$ .

This completes the establishment and definition of the quality control parameters to be utilized in monitoring the microdensitometer.

#### G. SUMMARY OF THE QUALITY CONTROL PROCEDURES

The following ten-step procedure implements the criteria derived above (see Figure 20).

1. The machine is set up and calibrated on a microstep wedge; the average ensemble input  $\langle E_{i0} \rangle$  is determined for each step of the wedge.
2. A high spatial frequency target of a specific configuration is scanned, and the data are digitized. The digital values are taken back through the characteristic setup curve to determine the equivalent input.
3. The microstep wedge is again scanned and digitized, and the amount of dc drift is evaluated at each step as  $\Delta \langle E_i \rangle = \langle E_{i \Delta t} \rangle - \langle E_{i0} \rangle$ .
4. The average drift over all steps is calculated as  $\bar{d}$ , and if it can be taken as significantly not zero, then the data collected in step 2 above are rejected as containing dc drift. The cause for the occurrence of dc drift is determined. If no significant drift is detected, then the data collected in step 2 are taken as containing no drift.
5. The digitized data collected in step 2 are transformed into the frequency plane and compared in modulus and phase at selected frequencies  $\omega_i, i = 1, 2, 3, \dots, \Omega$ , to a mean transform  $\overline{G(\omega_i)}$  previously determined.
6. The difference functions  $|\Delta G(\omega_i)|$  and  $\Delta \Phi(\omega_i)$  are computed as the difference between the sample transform and the mean transform modulus and phase.
7. The circular coefficients of correlation,  $\bar{r}_G$  and  $\bar{r}_\Phi$ , are computed for the modulus difference function and for the phase difference function, respectively.
8. If  $\bar{r}_G < \bar{r}_{G\alpha}$  (where  $\bar{r}_{G\alpha}$  is the critical circular serial correlation coefficient at a probability of rejection risk  $\alpha$ ) and if  $\bar{r}_\Phi < \bar{r}_{\Phi\alpha}$  (where  $\bar{r}_{\Phi\alpha}$  is the critical correlation coefficient for the phase difference function), then the instrument is said to be in-control. If either or both of these values, i. e.,  $\bar{r}_G$  and  $\bar{r}_\Phi$ , are greater than or

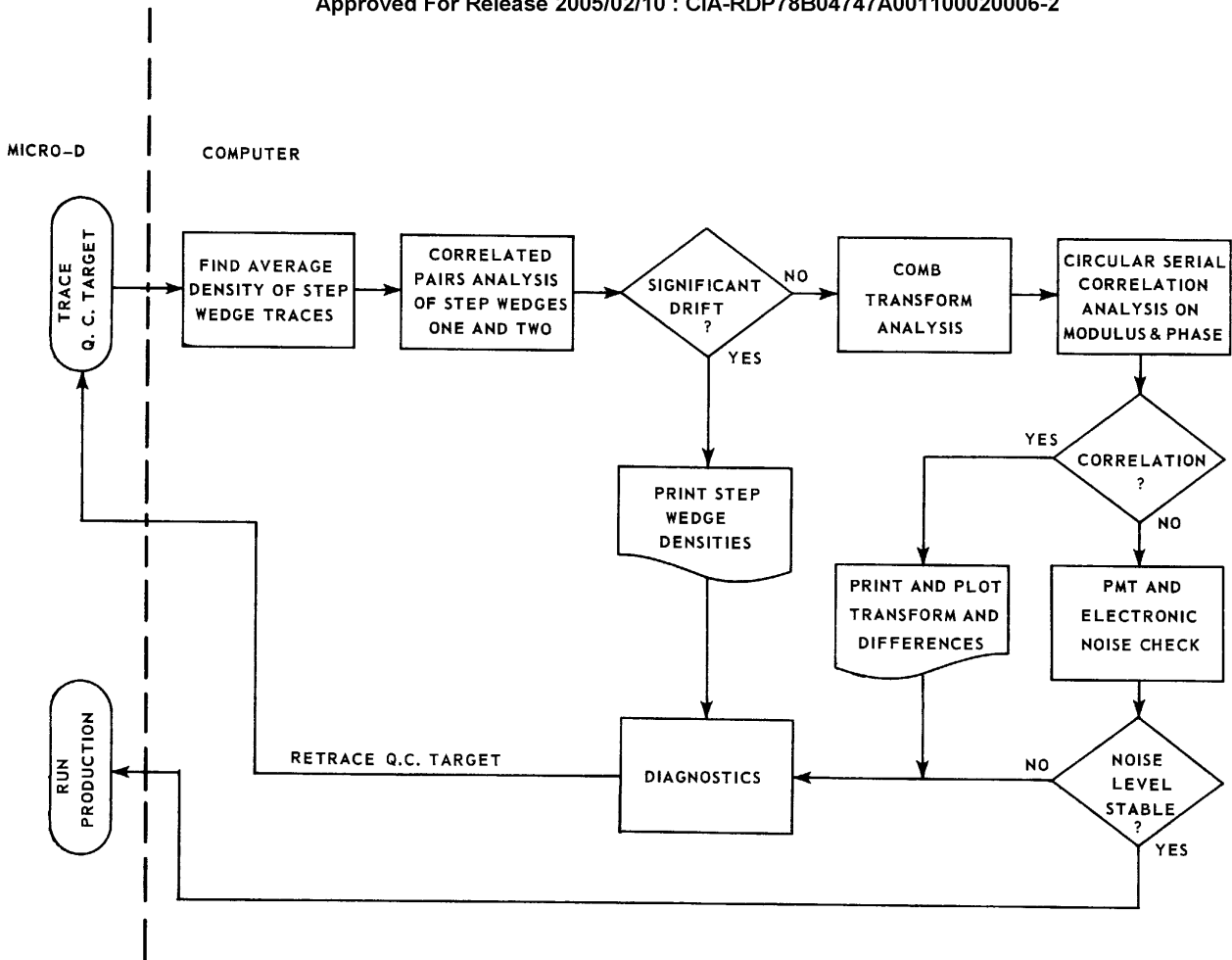


Figure 20 . Quality Control Computation Flowchart

equal to their respective critical values, then the operational status of the machine is questioned, and a diagnostic procedure is brought into play.

9. The scanning of the microdensitometer is halted at a high-density step on the quality control target; however, the digitizer is allowed to run in order to sample the noise characteristics of the instrument.

10. From the digital data collected in step 9 the sample variance is estimated, and it is tested against the allowable standard variance. Rejection of the sample, as being of a population with a greater noise variance than the standard, is done on the basis of the chi-square distribution function. If the estimated noise variance is greater than the acceptable noise variance  $\sigma_N^2$ , the microdensitometer is tested to determine the cause for the increase in its noise injection characteristics.

#### H. THE QUALITY CONTROL TARGET

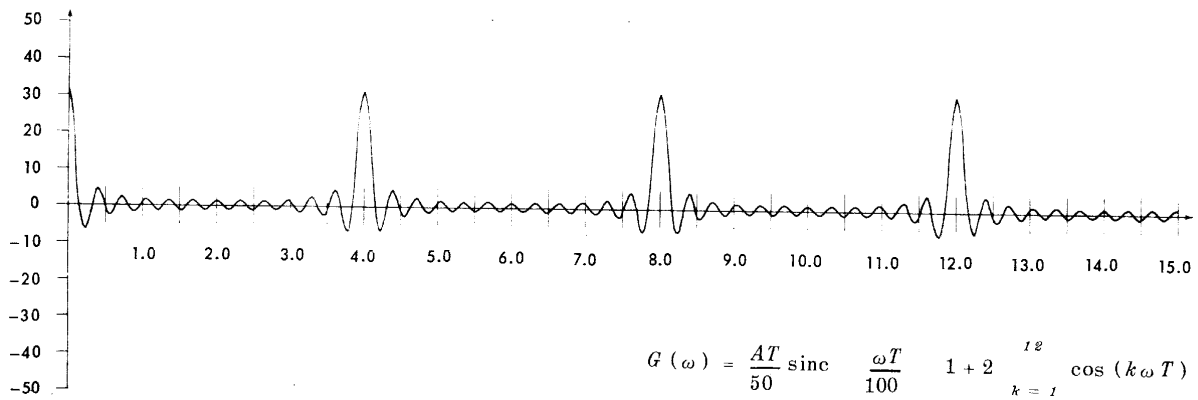
At this point the design of the quality control target follows logically from the above procedure. There must be a step wedge on either side of a target used in the frequency analysis of the system. These step wedges should be short enough not to require a great deal of tracing time, yet each should contain a sufficient number of steps to allow a reasonable degree of freedom in the pair-comparison drift analysis check. Initially, a five step microstep wedge was chosen with a  $D_{max} = 4.00$  and remaining steps of 2.00, 1.00, 0.50, and 0.25 density. Each of the two step wedges are made as identically as possible with a 600-micron step width and a 50-micron step spacing. The frequency plane stability of the microdensitometer is monitored by using a comb target, which is simply an array of pulses equally spaced throughout the domain  $-L/2 \leq x \leq L/2$ . In this case a bar spacing of  $T$  is desirable, where  $T/50$  is the bar width in millimeters. The bar amplitude is  $A$ . The Fourier transform of this array may be easily calculated by applying a symmetrical set of shift functions to the basic square pulse of width  $T/50$ . The Fourier transform for a 25-bar comb is

$$G(\omega) = \frac{AT}{50} \operatorname{sinc} \left( \frac{\omega T}{100} \right) \left[ 1 + 2 \sum_{k=1}^{12} \cos(k\omega t) \right] \quad (141)$$

where  $\omega$  is the spatial frequency in cycles/millimeter. Figure 21 is a graph of a small portion of this transform for a target of 25 bars, with  $T = 0.250$ . Note that a pulse occurs in the positive transform amplitude every  $\Delta\omega$  cycles/millimeter, where



98



where:  $A = 250$   
 $T = .250 \text{ mm}$

Figure 21. Fourier Transform of Comb Target

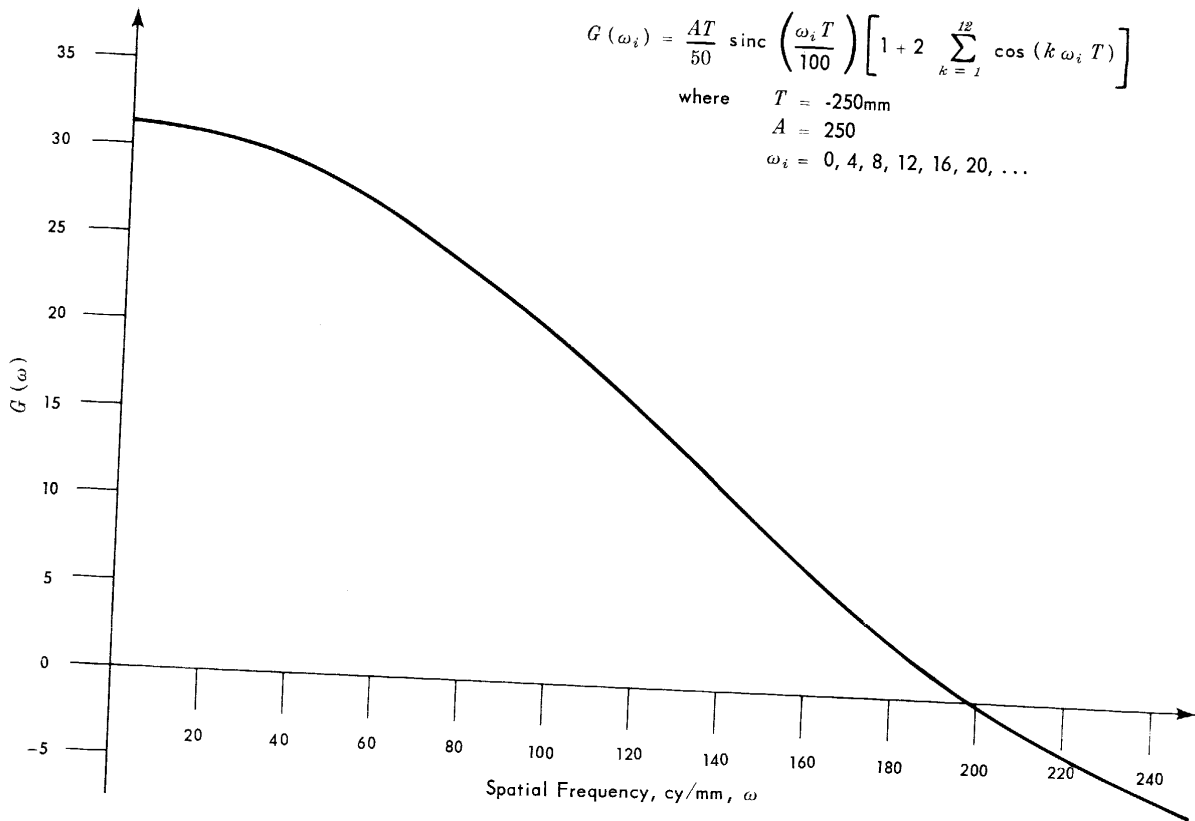
$$\Delta\omega = 1/T \quad (142)$$

It is at these peaks that the values of the transform are subtracted from the mean transform, and the serial correlation coefficient is computed on the phase and modulus differences.

The envelope of this transform follows a basic sinc function with the first zero crossing at  $50/T$  cycles/millimeter (Figure 22).

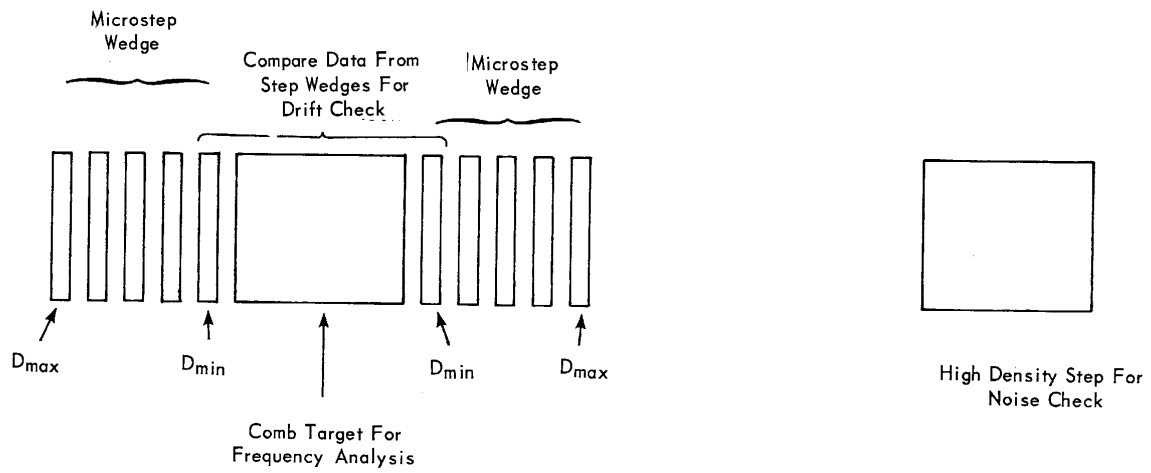
The final test concerns the noise insertion properties of the microdensitometer system. The scan of the machine may be halted either on the final Dmax step of the microstep wedge or a high density noise patch located a remote distance (10 millimeters) from the end of the second wedge. The target shown in Figure 23 incorporates this design.

This same target design may be used in the quality control of the trichromatic microdensitometer as well as black-and-white systems. Extension of the quality control procedure to the trichromatic system merely means that the data analysis must be accomplished for each channel of the system.



88

Figure 22. Fourier Transform Envelope Function



Note: Printed on 2 In. x 2 In. or 4 In. x 5 In. Plate.

Figure 23. Microdensitometer Quality Control Target

(This page is intentionally left blank.)

SECTION VIII

LITERATURE REFERENCES

1. Adashev, N. D. and Gorokhouskii, Yu. N., "A Statistical Analysis of the Densitometric Properties of Color and Motion Picture Images", Usp. Nauch. Foto. Vol. 8 (1962), pp. 134-135.
2. Bakhvalov, V. M., "Some Factors in the Densitometry of Color Photographic Papers and the Determination of the Concentration of Dyes in the Separate Layers", Usp. Nauch. Foto. Vol. 8 (1962), pp. 216-244.
3. Kirillov, N. I., "The Ratio of Optical Densities of Color and Silver Images with Different Methods of Processing Color Positive Film", Zhur. Nauch. i Priklad. Fotografii i Kinematografii Vol. 6, No. 4 (1961), pp. 296-298.
4. Krupenin, L. K. and Baranov, G. S., "Methods of Graduating Color Densitometers", Usp. Nauch. Foto. Vol. 8 (1962), pp. 263-272.
5. Powers, S. A. and Miller, O. E., "Pitfalls of Color Densitometry", PS & E Vol. 7, No. 1 (1963), p. 59.
6. Voglesong, W. F., Color Process Lecture Notes, Rochester Institute of Technology; Rochester, N. Y., (1963), pp. 21-23.

STATINTL



9. Beyer, W. H., Handbook of Tables for Probability and Statistics, The Chemical Rubber Co.; Cleveland, Ohio (1966), pp. 240-246.
10. Stultz, K. F. and Zweig, H. J., "Relation Between Graininess and Granularity for Black and White Samples with Nonuniform Granularity Spectra", JOSA Vol. 49, No. 7 (July 1959), pp. 693-702.
11. Mees, C. E. K. and James, T. H., Theory of the Photographic Process, 3rd ed., MacMillan Company; N. Y. (1966), p. 528.
12. Zwick, D., "Color Granularity and Graininess", J. Photo. Sci. Royal Photographic Society of Great Britain, Vol. 11 (1963), p. 275.
13. Mees, C. E. K. and James, T. H., op. cit., p. 532.

14. Ibid., pp. 505-506.

15. Zweig, H. J., "Autocorrelation and Granularity, III. Spatial Frequency Response of the Scanning System and Granularity Correlation Effects Beyond the Aperture", JOSA Vol. 49, No. 3 (March 1959), pp. 238-244.

16. Doerner, E. C., "Wiener Spectrum Analysis of Photographic Granularity", JOSA Vol. 52, No. 6 (June 1962), pp. 669-672.

17. Zwick, D., op. cit., pp. 269-275.

18. Stultz, K. F. and Koch, D. A., "Role of Chromaticity Difference in Color Graininess Judgements", JOSA Vol. 56, No. 10 (Oct. 1956), pp. 832-837.

19. Zwick, D., "Quantitative Studies of Factors Affecting Granularity", PS & E Vol. 9, No. 3 (May-June 1965), pp. 145-148.

20. Verbrugge, R., DeBelden, M., and Langner, G., "Influence of the Color Coupling Process on Granularity and Sharpness in Color Films", PS & E Vol. 11, No. 6 (Nov. - Dec. 1967), pp. 379-384.

21. Gurevich, S. B., Breido, I. I., and Garrilov, G. A., "The Distribution of the Number of Developed Grains and the Relation Between Photographic Noise and Optical Density", Usp. Nauch. Foto. Vol. 10 (1964), pp. 171-174.

22. Berwart, L., "Statistical Study of the Distribution of the Transmittance Deviations Due to Granularity", Bul. Soc. Roy Sci. Liege. Vol. 34, No. 5-6 (1965), pp. 266-283.

STATINTL

STATINTL

24. Ibid., pp. 8-10.

STATINTL

27. Heiland, W. and Vieth, G., "Determination of the Callier Coefficient of Color Reversal Films", Photographische Korrespondenz Vol. 100 (Jan. 1964), pp. 3-6.

28. Mees, C. E. K. and James, T. H., op. cit., p. 426.

30. Simonds, J. L., "Analysis of Nonlinear Photographic Systems", PS & E Vol. 9, No. 5 (Sept.-Oct. 1965), p. 294.

31. Ibid., p. 295.

STATINTL



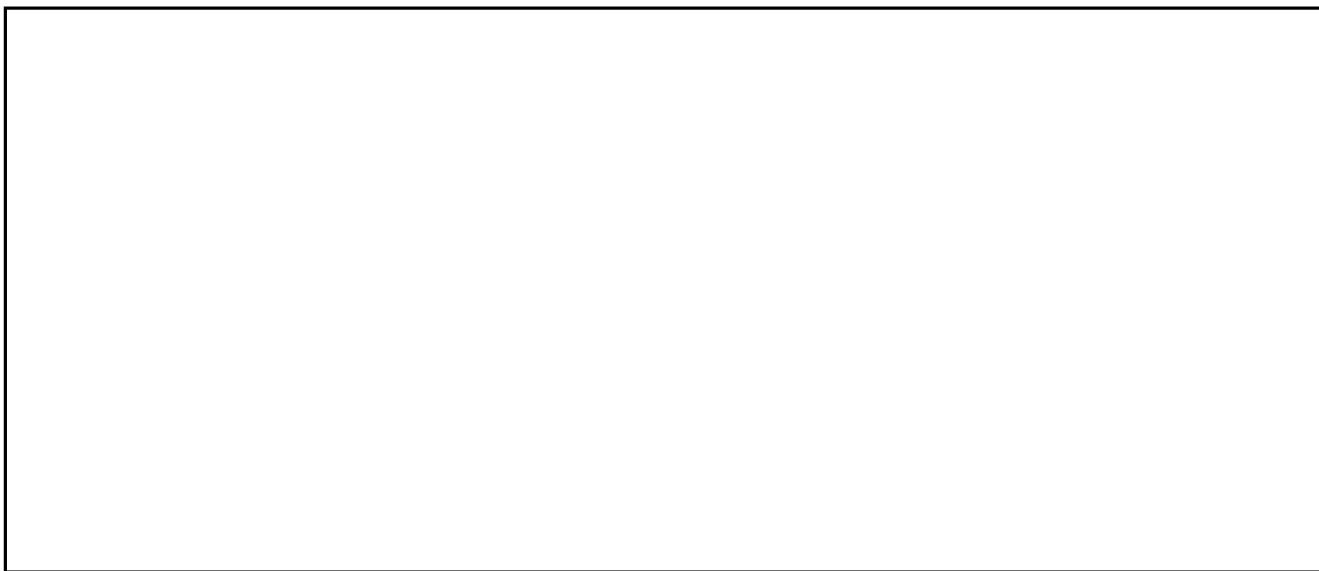
33. Mees, C. E. K. and James, T. H., op. cit., pp. 460-530.

34. Anderson, T. W., An Introduction to Multivariate Statistical Analysis, John Wiley and Sons; N. Y., (1958), pp. 281-286.

35. Simonds, J. L., "Application of Characteristic Vector Analysis to Photographic and Optical Response Data", JOSA Vol. 53, No. 8 (August 1963), pp. 968-974.

36. Ibid., p. 973.

STATINTL



42. Ibid., pp. 6-7 — 6-9.

43. Verbrugghe, R. G. L., "A New Color Print Filmstock", Journal of SMPTE, Vol. 77, No. 1 (January 1968), pp. 29-33.

44. Helgeson, G. A., op. cit., pp. 6-22.

45. Juran, J. M., Quality Control Handbook, 2nd ed. McGraw-Hill Publishing Company; N. Y., (1962), pp. 2-2 — 2-8.

46. Natrella, M. G., Experimental Statistics, NBS Handbook 91, Government Printing Office; Washington, D. C., (August 1963), pp. 3-38 — 3-39.



47. Leipnik, R. B., "Distribution of the Serial Correlation Coefficient in a Circularly Correlated Universe", The Annals of Mathematical Statistics, Vol. 18 (1947), p. 80.
48. Koopmans, T., "Serial Correlation and Quadratic Forms in Normal Variables", The Annals of Mathematical Statistics, Vol. 13 (1942), p. 14.
49. Leipnik, R. B., op. cit., p. 81.
50. Ibid., p. 83.
51. Dixon, W. J., "Further Contributions to the Problems of Serial Correlation", The Annals of Mathematical Statistics, Vol. 15 (1944), p. 126.

APPENDIX A

INTEGRAL TO ANALYTICAL DENSITY CALIBRATION  
OF THREE-COLOR TRANSPARENCY MATERIALS

The dye layers of three-color positive transparency camera original materials were isolated by the standard technique of selective exposure. Three emulsion types were utilized: [ ] SO-155, SO-151, and 8442 materials processed in a color Versamat with EA-4 chemistry with a nominal first development temperature of 100°F for the first two emulsion types and 103°F for the 8442 emulsion. A [ ] high-intensity monochromator was used as the exposing source. For the 8442 and SO-155 emulsions the monochromator slits were selected to yield a 4.8 m $\mu$  bandwidth. In selectively exposing the SO-151 material, a 9.8 m $\mu$  bandwidth was utilized.

It was realized that because of the spectral sensitivity crossovers of the three layers of each emulsion, some loss of Dmax in the isolated dye layer could be expected. The yellow dye layer suffers the least in this respect because of the sharp sensitivity drop of the blue-sensitive layer to wavelengths greater than 540 m $\mu$  (Figure A1, A2, and A3).

To minimize the loss of Dmax, the layers to be removed were exposed, not at their sensitivity peaks but at the wavelength exhibiting the greatest sensitivity differential with the layer to be isolated. The wavelengths used are listed in Table A1.

A series of trial monochromatic exposures was made to determine the minimum exposure necessary to reduce the dye density of each dye layer of each emulsion to zero. The exposures were produced by moving, at a known velocity, 3-foot lengths of 70 mm film past a 2.77-cm slit illuminated by the monochromator. Once the proper exposures had been determined for each emulsion, 100-foot lengths were exposed to give a stock supply of each emulsion in which the dye layer had been isolated.

From the stock of selectively exposed film, microstep wedges were sensitometrically exposed in each of the layers in each of the emulsion types, thus yielding 9 microstep wedges. These were then shipped to the customer's facility where the microstep wedges were traced on the [ ] Trichromatic Micro-Analyzer 1032T. The

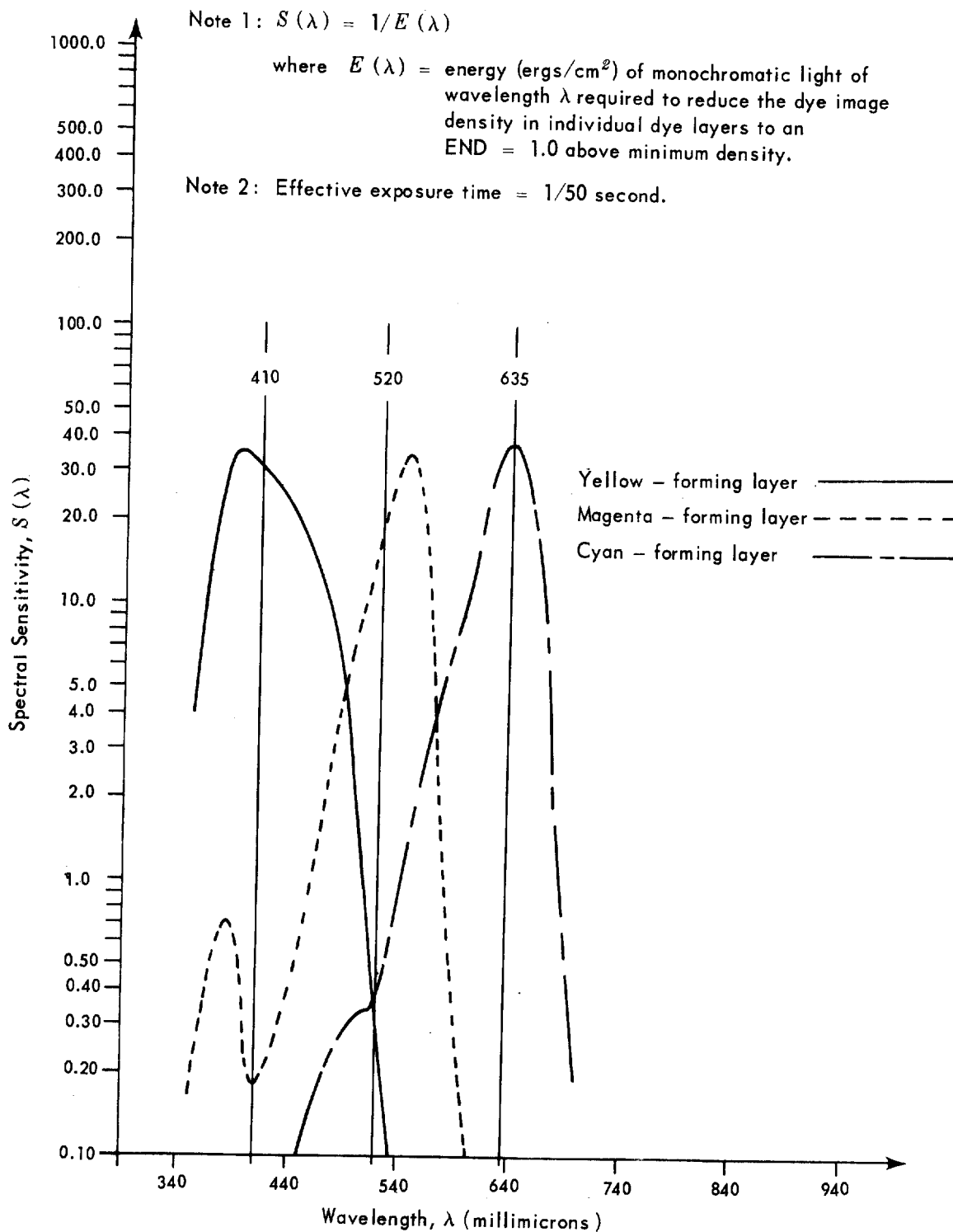


Figure A1. Spectral Sensitivity of SO-151 Emulsion

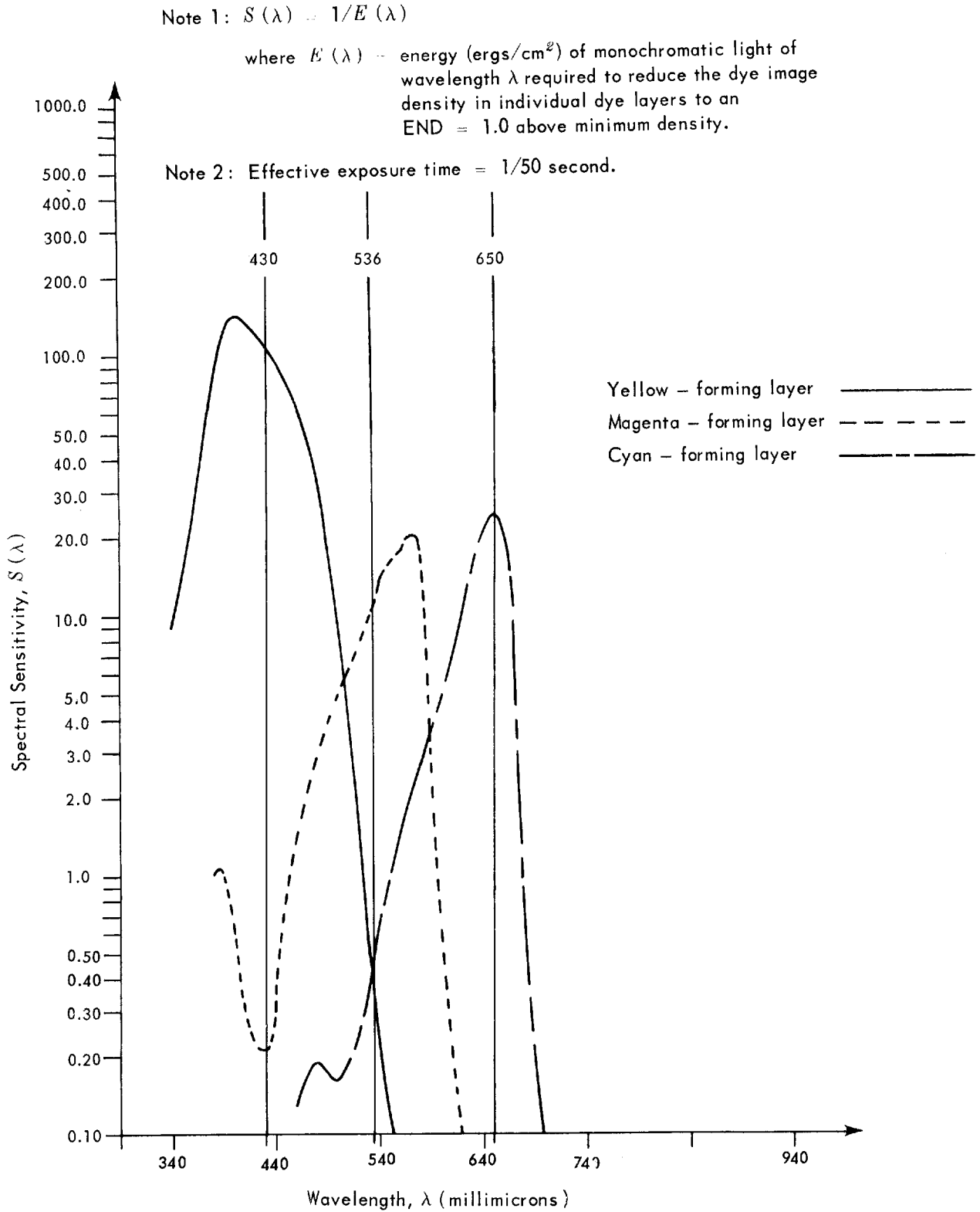


Figure A2. Spectral Sensitivity of SO-155 Emulsion

Note 1:  $S(\lambda) = 1/E(\lambda)$

where  $E(\lambda)$  = energy (ergs/cm<sup>2</sup>) of monochromatic light of wavelength  $\lambda$  required to reduce the dye image density in individual dye layers to an END = 1.0 above minimum density.

Note 2: Effective exposure time = 1/50 second.

Note 3: E-3 process.

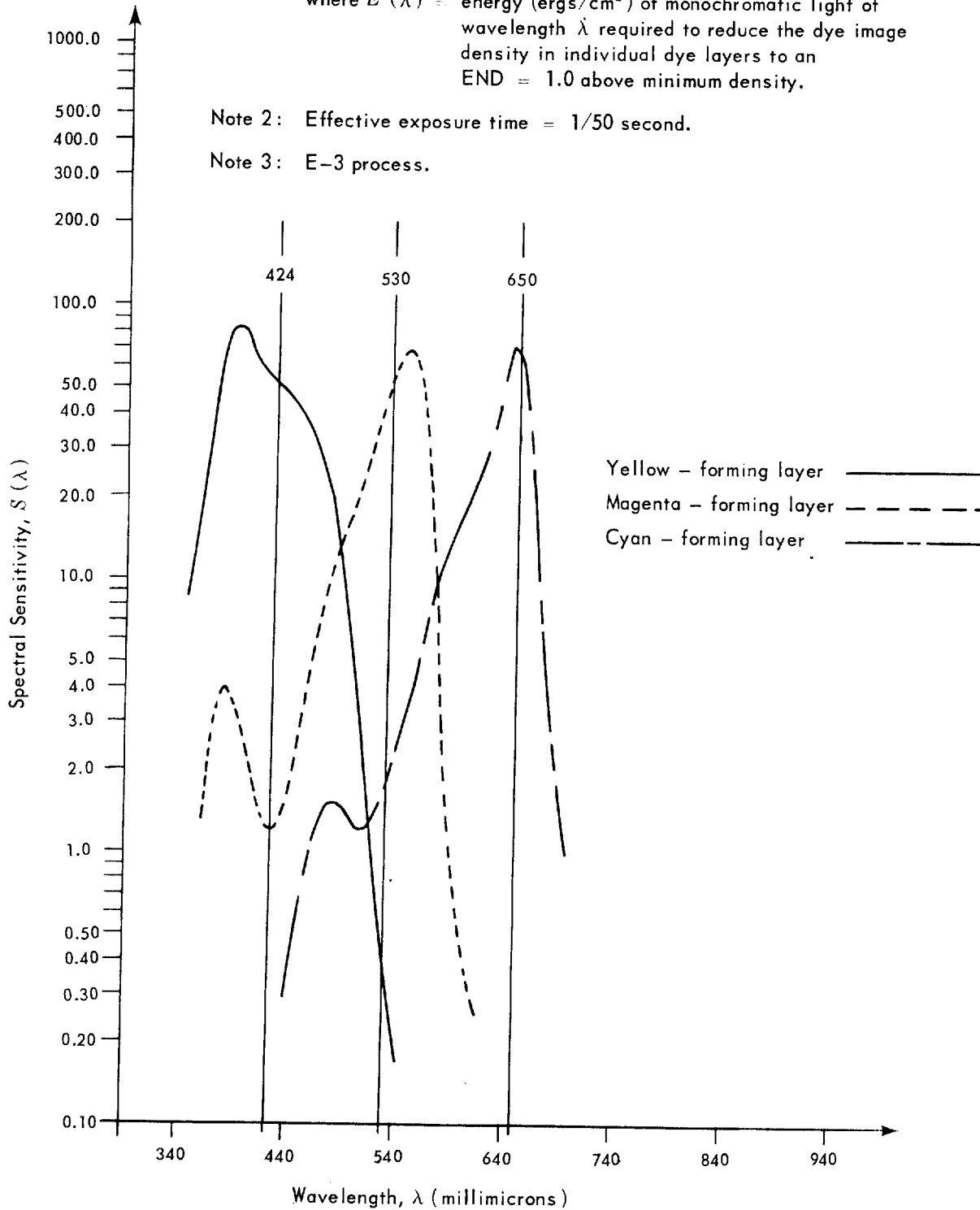


Figure A3. Spectral Sensitivity of 8442 Emulsion

TABLE A1. WAVELENGTHS USED TO ISOLATE DYES

Dye to be Isolated	Exposing Wavelength (millimicrons)		
	Blue	Green	Red
Emulsion SO-151			
Yellow	None	520	635
Magenta	410	None	635
Cyan	410	520	None
Emulsion SO-155			
Yellow	None	536	650
Magenta	430	None	650
Cyan	430	536	None
Emulsion 8442			
Yellow	None	530	650
Magenta	424	None	650
Cyan	424	530	None

digital records were undecipherable by computer because of digital equipment malfunction. The chart records were used, however, to obtain estimates of the red, green, and blue densities. Since each wedge was exposed in a single dye layer, the red, green, and blue densities were the analytical densities of the wedges. By plotting the minor densities of the dyes as a function of the major densities, the success of isolating the dye layer could be determined by the linearity of the resulting curves (Figures A4a-A12a).

From the slope of the linear portion of these curves, the entries were determined for the IFMD to AFMD conversion matrix  $A$ . The resulting matrices and their inverses are in Table A2. The characteristic curves for each of the isolated dye layers are shown in Figures A4b-A12b. It can be seen from these curves that the greatest difficulty was encountered in isolating the cyan and magenta dye layers of  SO-155.

STATINTL

TABLE A2. INTEGRAL FILTER MICRODENSITY TO ANALYTICAL FILTER MICRODENSITY CONVERSION MATRICES

NOTE

Matrices are approximations based on chart records taken from   Trichromatic Micro-Analyzer Model 1032T. They are valid only when used in working with integral densities generated by this model microdensitometer.

The emulsions from which these data were derived were processed in an  Color Versamat with EA-4 chemistry. The matrices may not be valid for these emulsions processed in a different manner or with different chemistry.

General Relation

$$\begin{bmatrix} D_b \\ D_g \\ D_r \end{bmatrix} = \mathbf{A} \cdot \begin{bmatrix} Y \\ M \\ C \end{bmatrix} \qquad \begin{bmatrix} Y \\ M \\ C \end{bmatrix} = \mathbf{A}^{-1} \cdot \begin{bmatrix} D_b \\ D_g \\ D_r \end{bmatrix}$$

SO-151

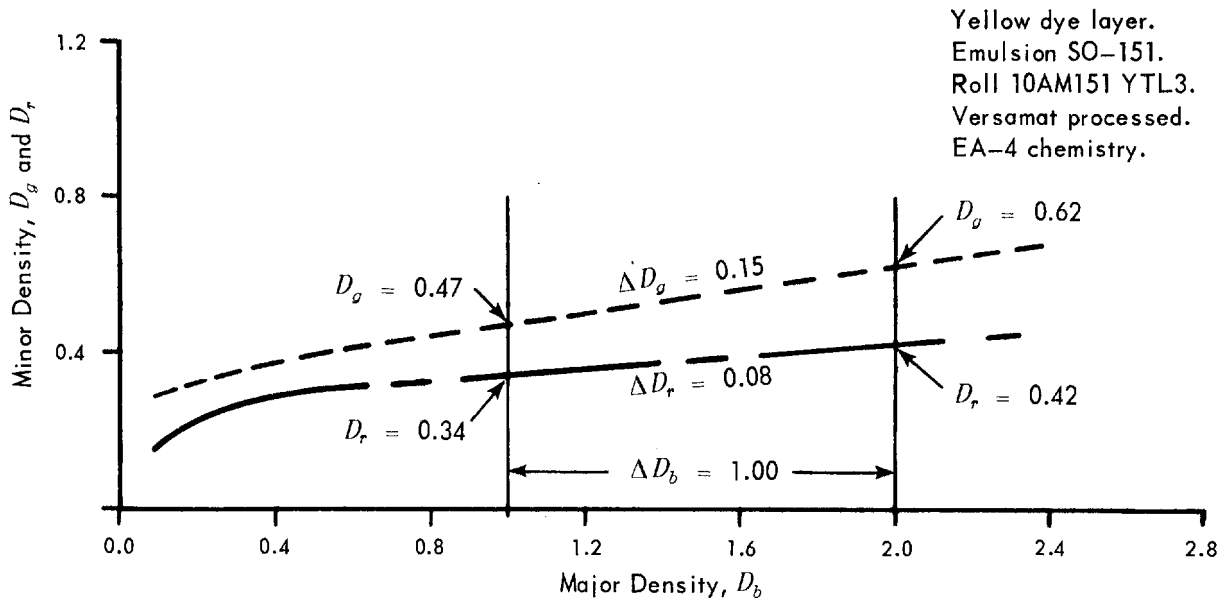
$$\mathbf{A} = \begin{bmatrix} 1.00 & 0.12 & 0.30 \\ 0.15 & 1.00 & 0.13 \\ 0.08 & 0.00 & 1.00 \end{bmatrix} \qquad \mathbf{A}^{-1} = \begin{bmatrix} 1.0425 & -0.1251 & -0.2965 \\ -0.1455 & 1.0175 & -0.0886 \\ -0.0834 & 0.0100 & 1.0237 \end{bmatrix}$$

SO-155

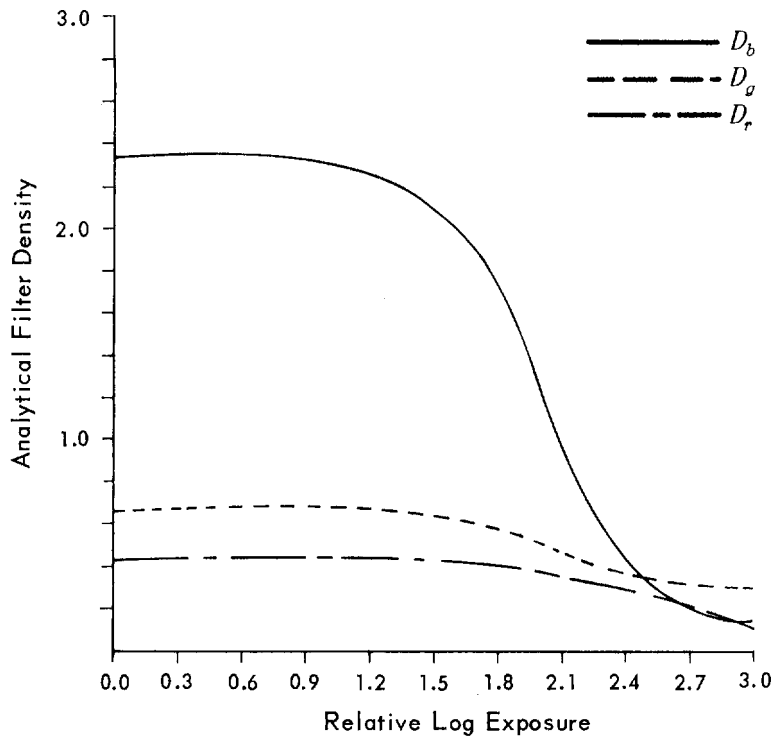
$$\mathbf{A} = \begin{bmatrix} 1.00 & 0.35 & 0.12 \\ 0.08 & 1.00 & 0.15 \\ 0.01 & 0.02 & 1.00 \end{bmatrix} \qquad \mathbf{A}^{-1} = \begin{bmatrix} 1.0295 & -0.3589 & -0.0697 \\ -0.0810 & 1.0313 & -0.1449 \\ -0.0086 & -0.0170 & 1.0037 \end{bmatrix}$$

8442

$$\mathbf{A} = \begin{bmatrix} 1.00 & 0.10 & 0.11 \\ 0.03 & 1.00 & 0.20 \\ 0.00 & 0.06 & 1.00 \end{bmatrix} \qquad \mathbf{A}^{-1} = \begin{bmatrix} 1.0029 & -0.0948 & -0.0913 \\ -0.0304 & 1.0151 & -0.1996 \\ 0.0018 & -0.0609 & 1.0117 \end{bmatrix}$$



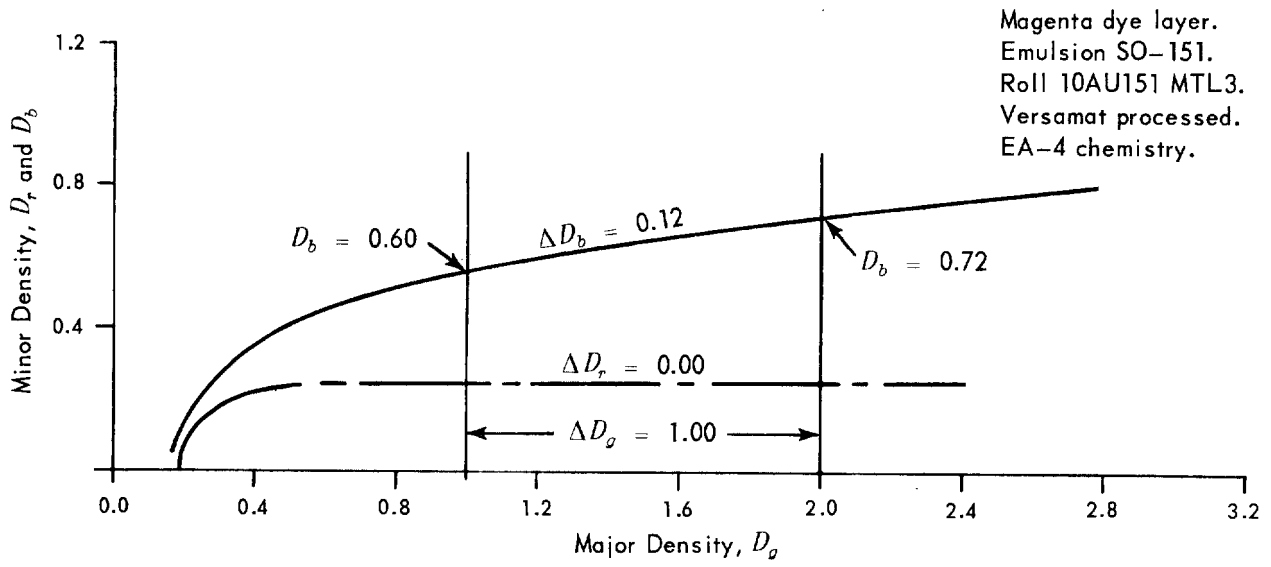
a.



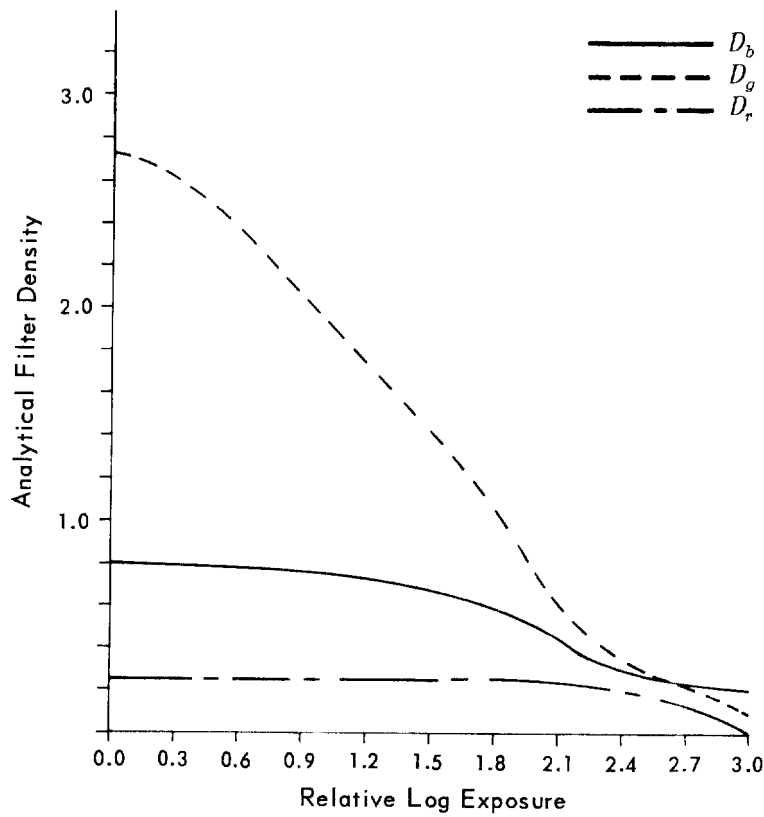
b.

Figure A4. Minor vs Major Density and Characteristic Curves





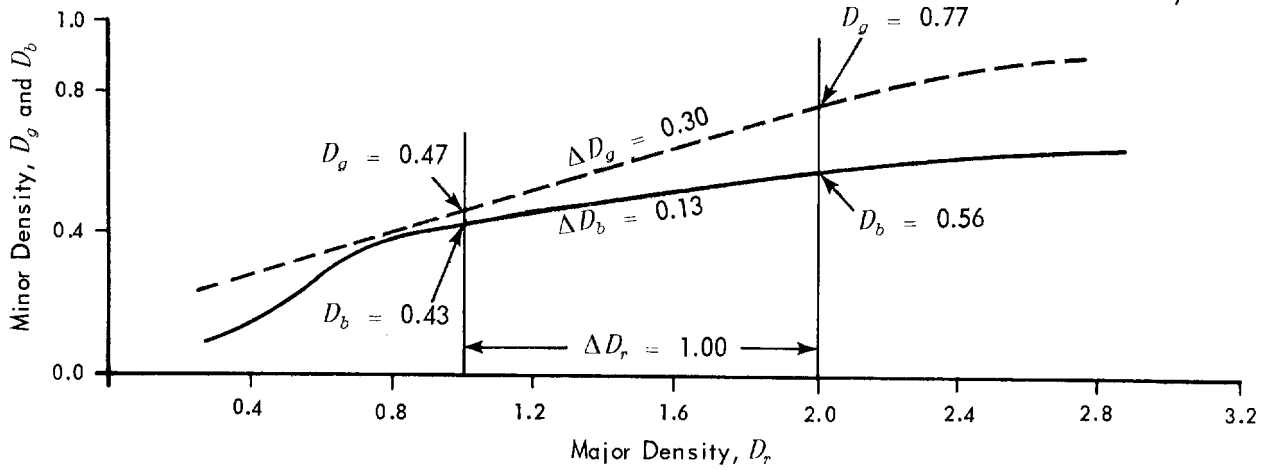
a



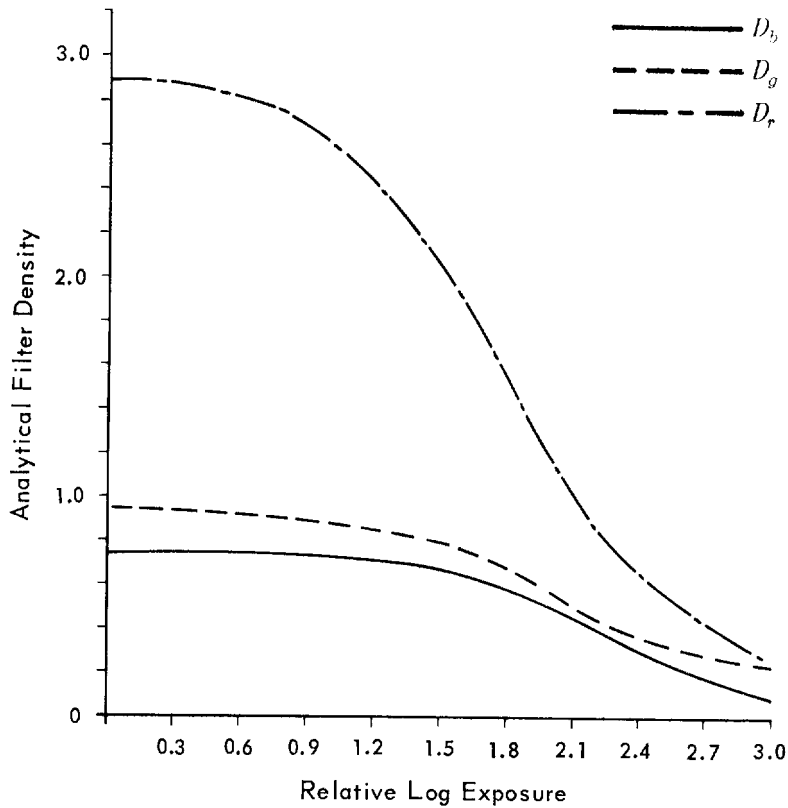
b

Figure A5. Minor vs Major Density and Characteristic Curves

Cyan dye layer.  
Emulsion SO-151.  
Roll 11AU151 CTL6  
Versamat processed.  
EA-4 chemistry.



a



b

Figure A6. Minor vs Major Density and Characteristic Curves

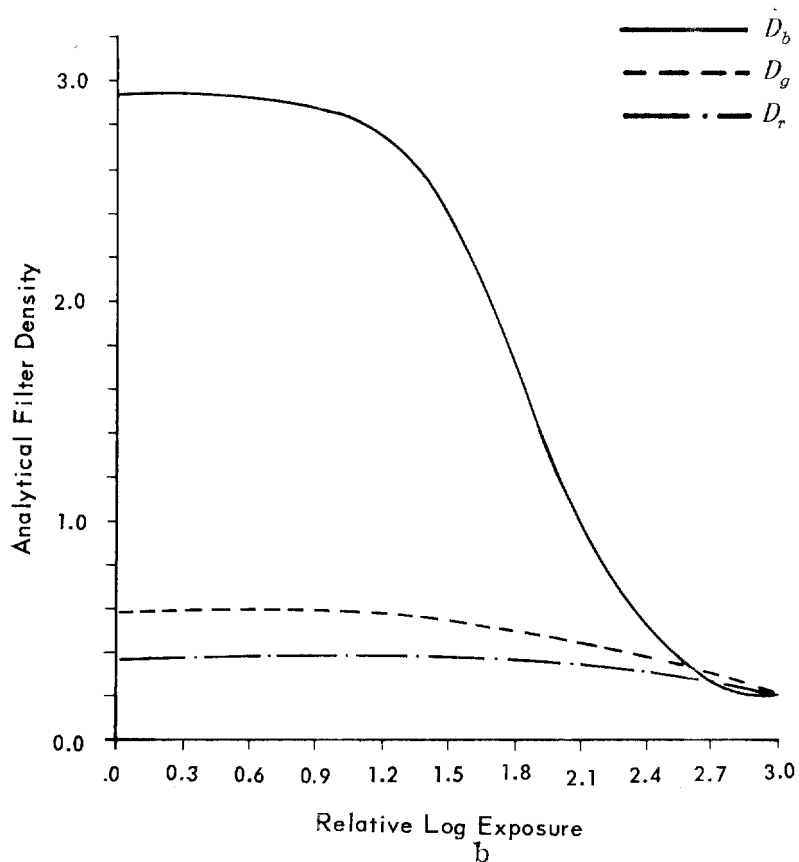
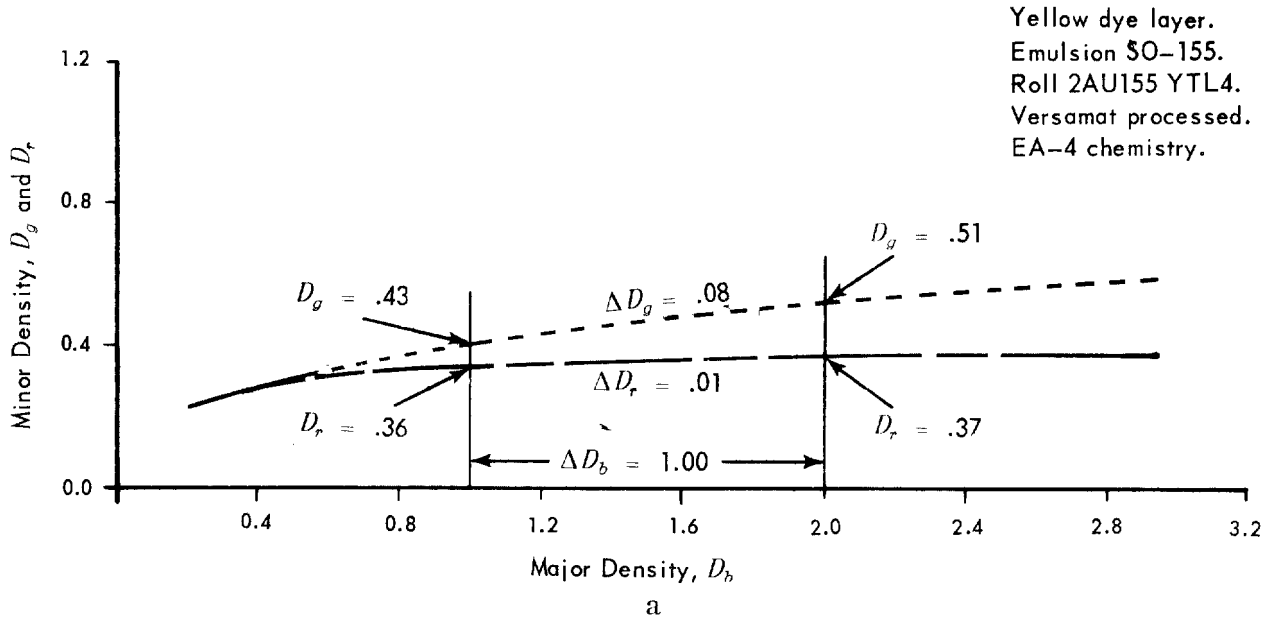
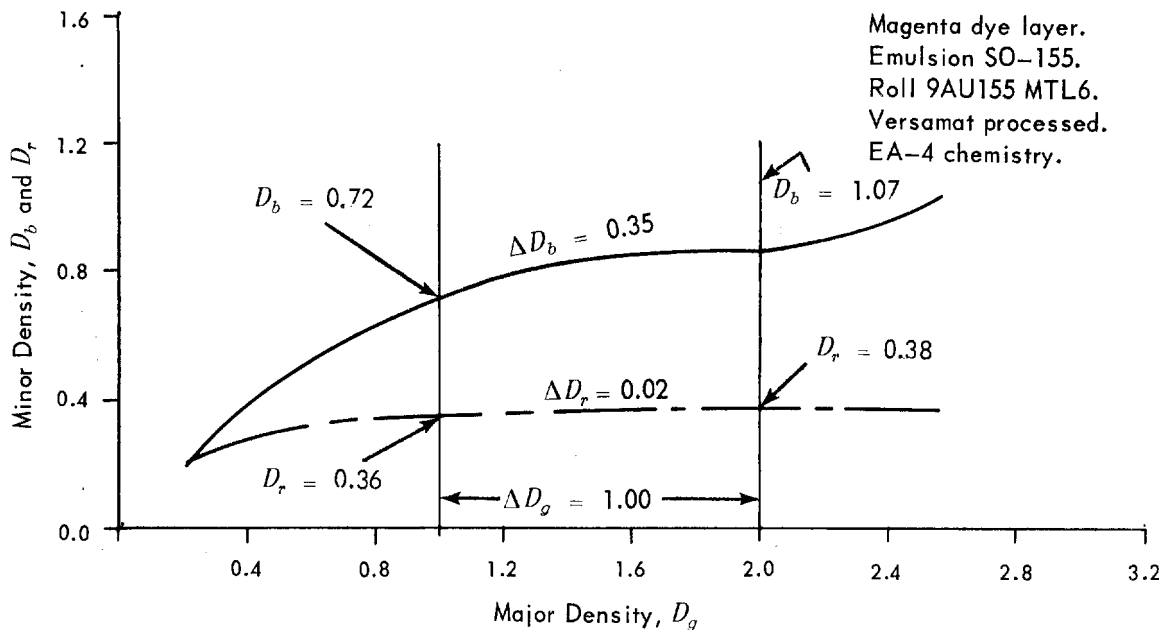
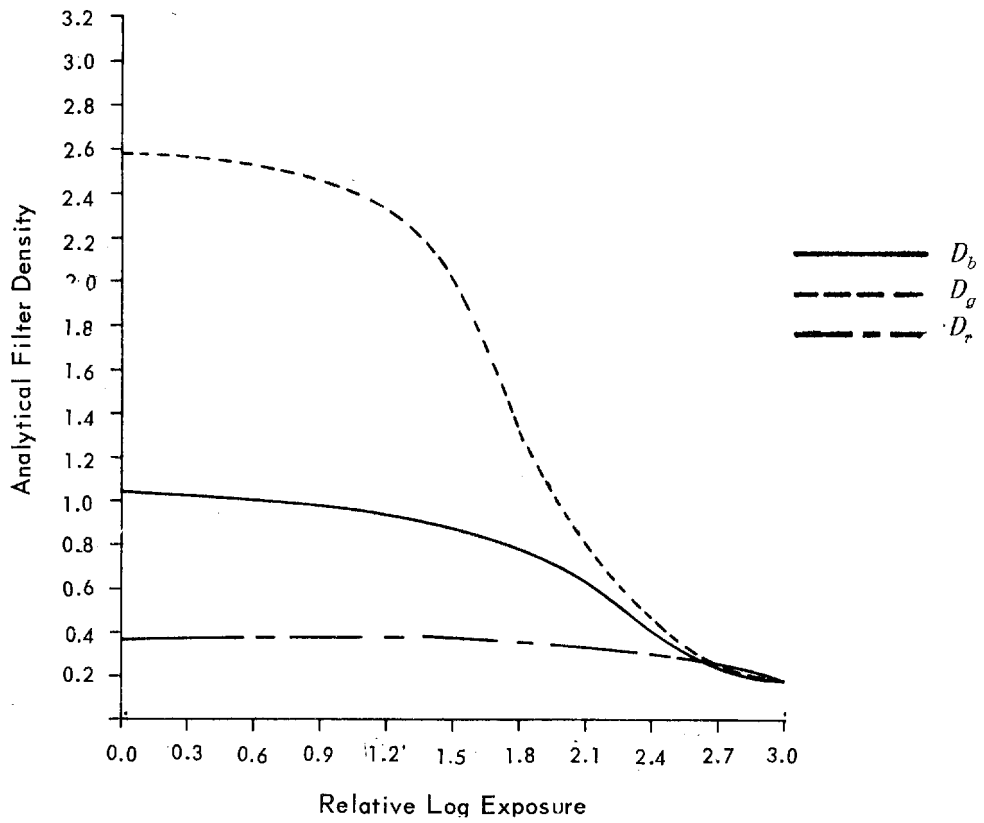


Figure A7. Minor vs Major Density and Characteristic Curves



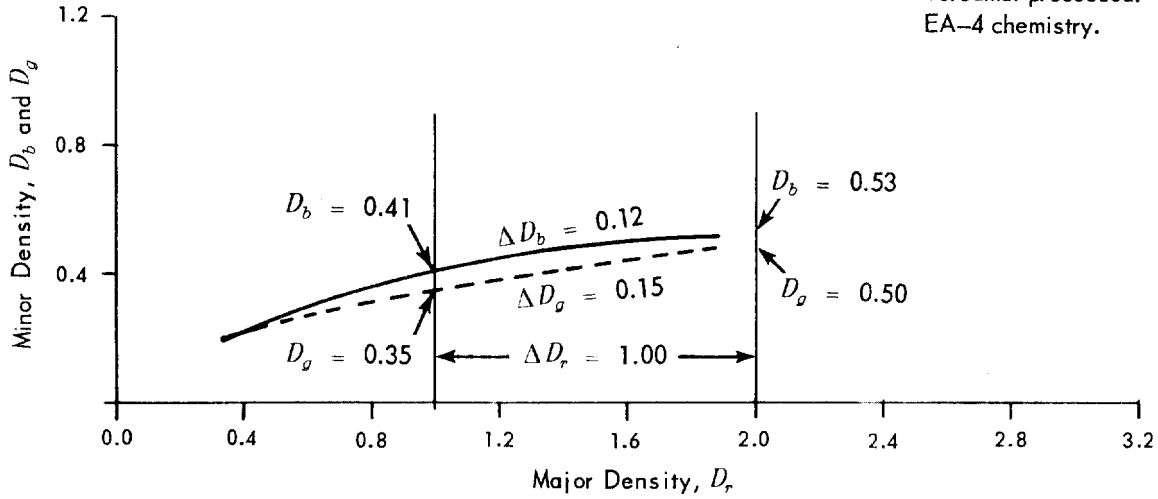
a



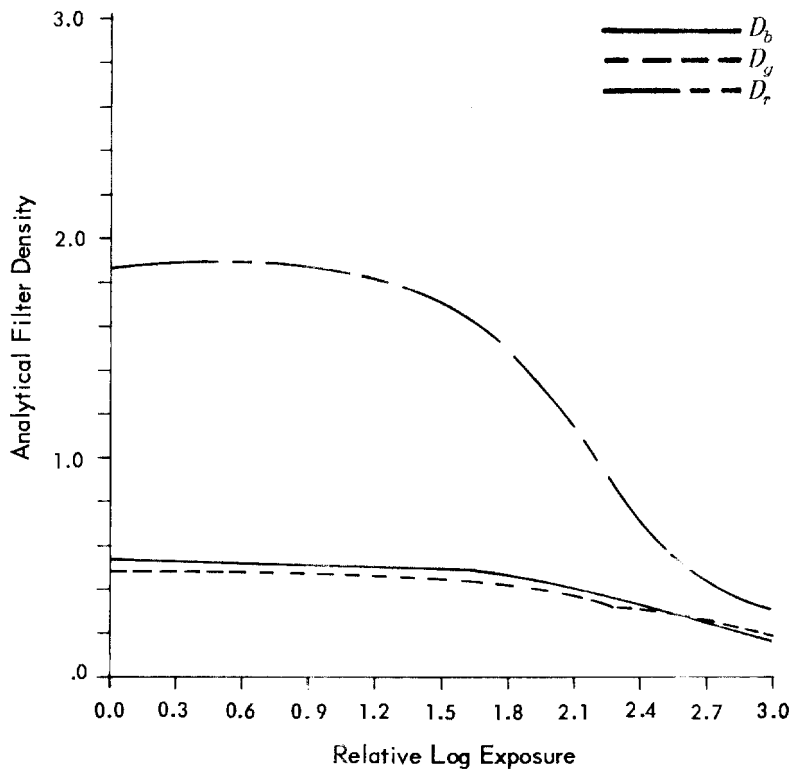
b

Figure A8. Minor vs Major Density and Characteristic Curves

Cyan dye layer.  
 Emulsion SO-155.  
 Roll 9AU155 CTL6.  
 Versamat processed.  
 EA-4 chemistry.

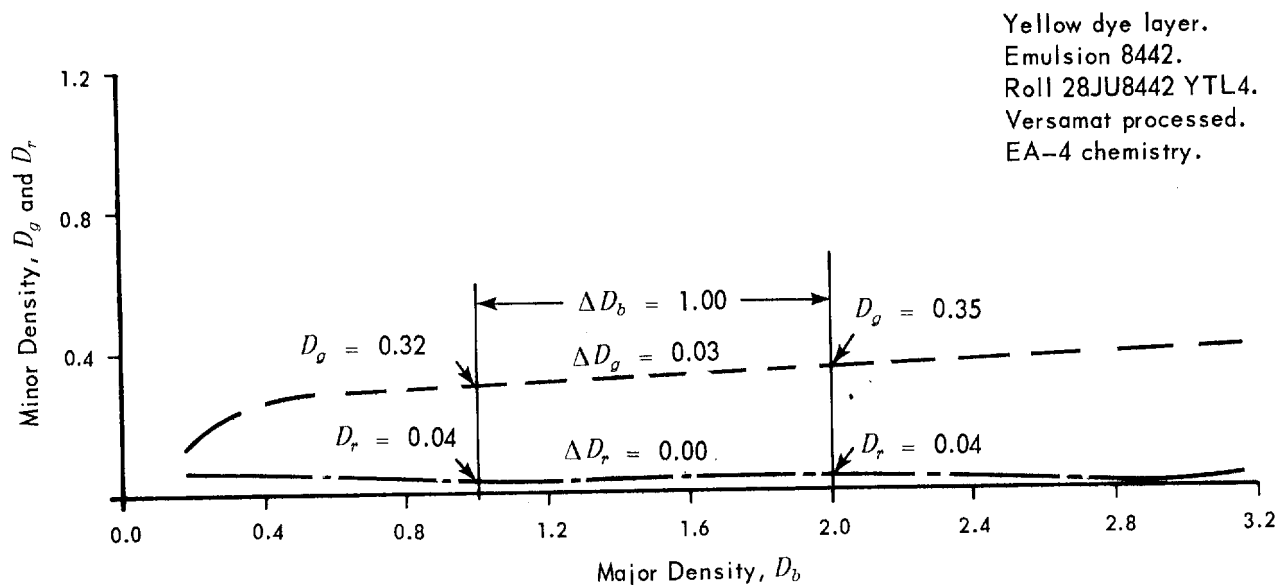


a

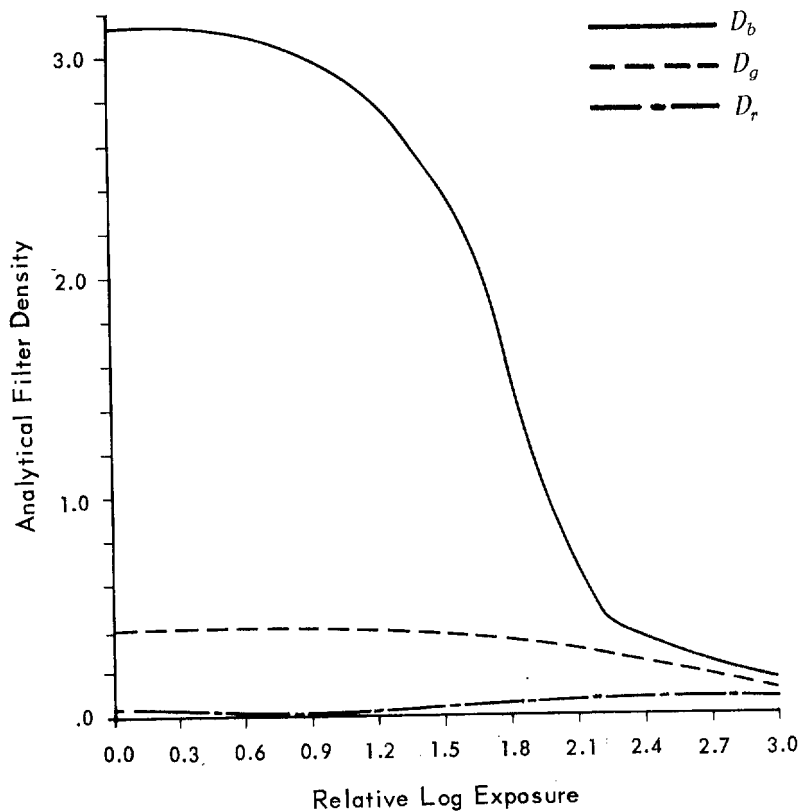


b

Figure A9. Minor vs Major Density and Characteristic Curves



a



b

Figure A10. Minor vs Major Density and Characteristic Curves

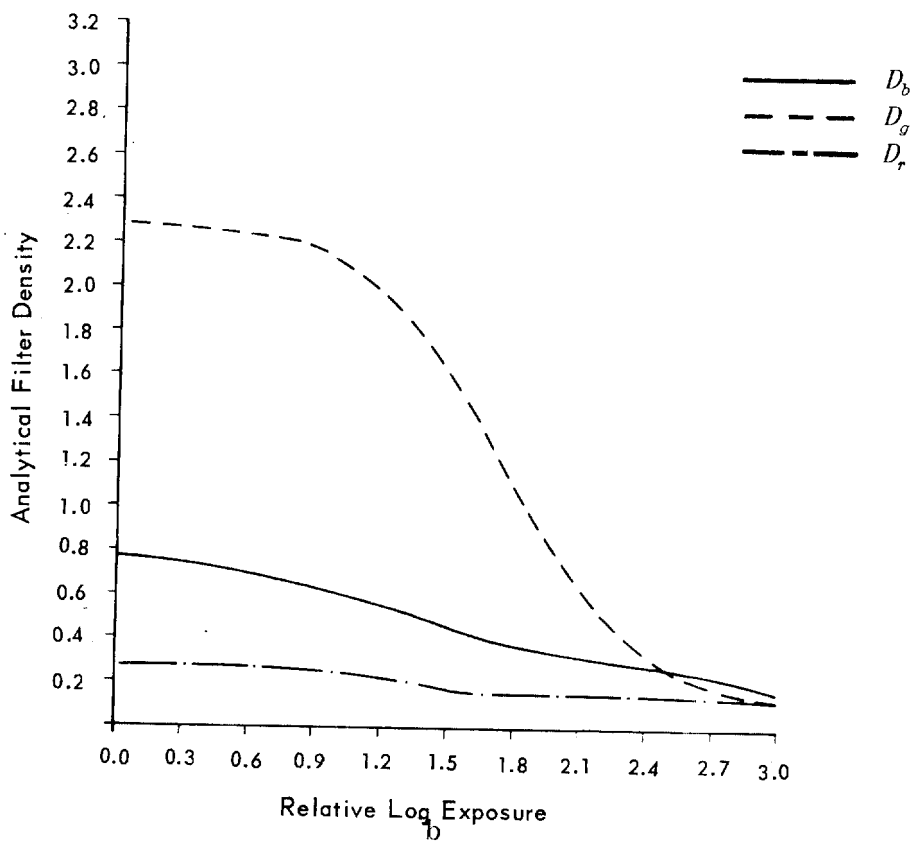
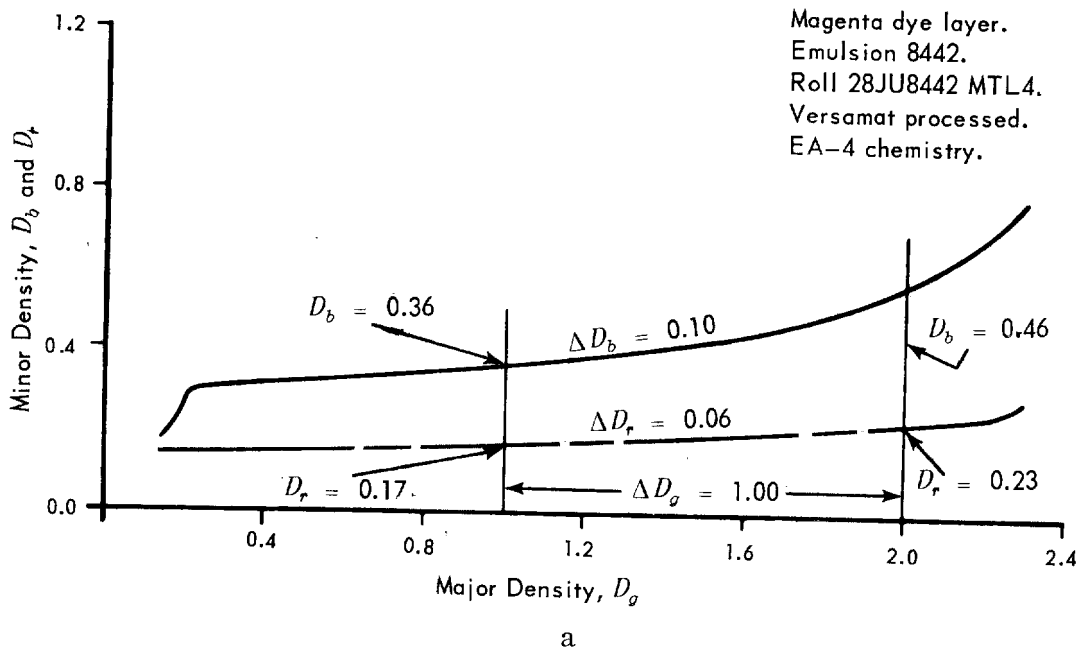
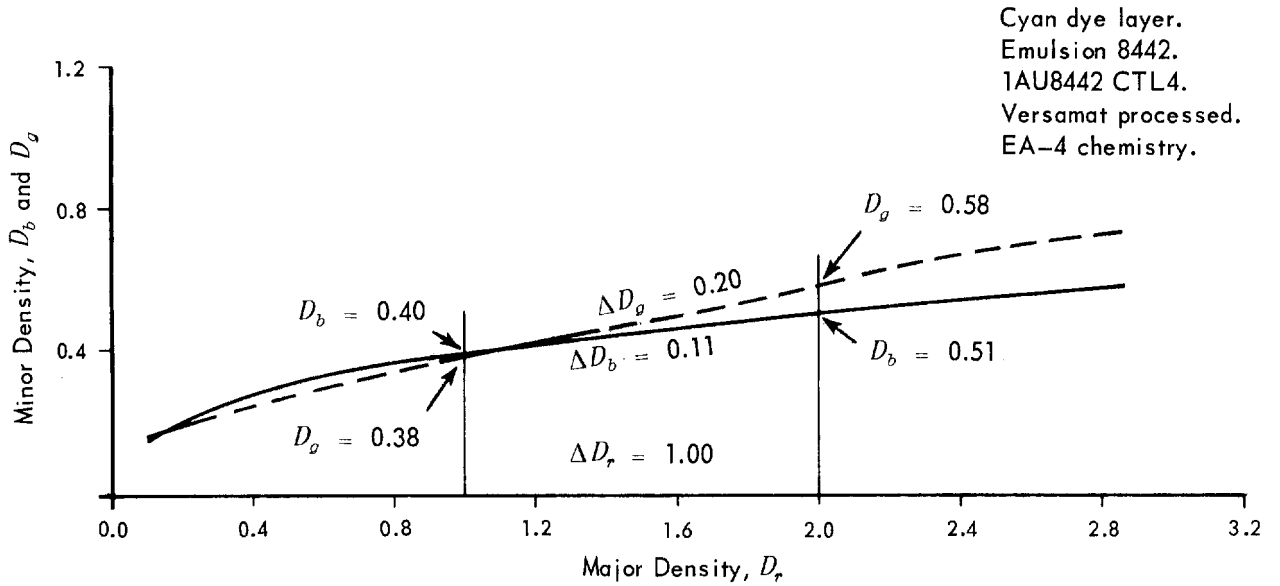
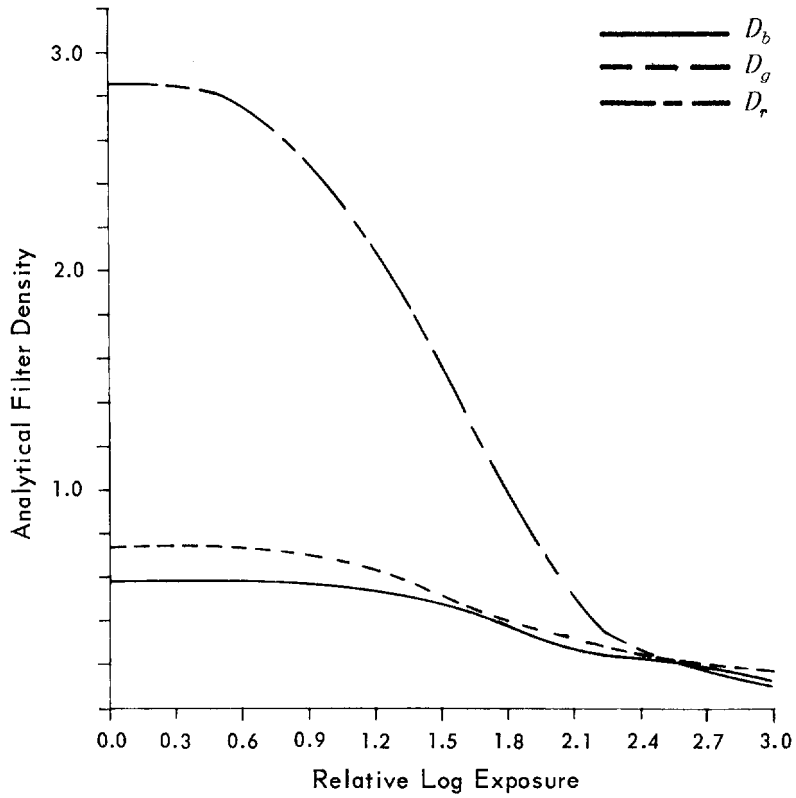


Figure A11. Minor vs Major Density and Characteristic Curves



a



b

Figure A12. Minor vs Major Density and Characteristic Curves



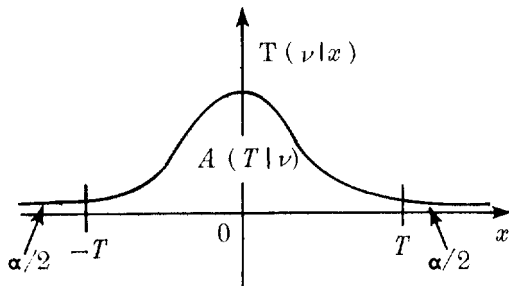
(This page is intentionally left blank. )

APPENDIX B

COMPUTATION OF ALPHA RISKS FOR VARIOUS DISTRIBUTIONS

The equations given below are easily programmed for the computation of the alpha risk. The input into the equations is the test statistic and associated degrees of freedom. It is suggested that in programming these functions all multiplication and exponential operations be performed using logarithms.

Student's *T*-Distribution<sup>1</sup>



$$A(T|\nu) = \int_{-T}^T T(\nu|x) dx$$

- where:
- $T(\nu|x)$  = Student's distribution function
  - $\nu$  = degrees of freedom
  - $|T|$  = closed domain end point over which area is computed. This *T*-value is computed by the statistical *T*-test.
  - $\alpha$  = the risk taken in rejecting the null hypothesis  $H_0$ .
  - $A(T|\nu)$  = the area under Student's *T*-distribution, bounded by  $-T \leq x \leq T$  and  $T(\nu|x)$ .

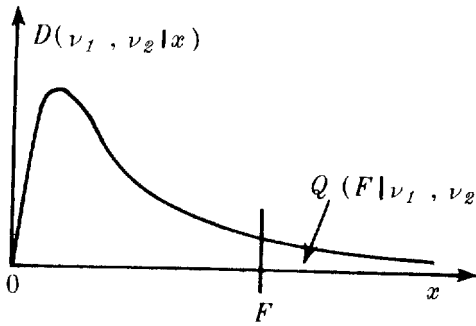
$$\theta = \tan^{-1}(T \nu^{-1/2})$$

$$\alpha = 1 - A(T|\nu)$$

$$A(T|\nu) = \begin{cases} \frac{2}{\pi} \left[ \theta + \sin \theta \cos \theta + \sin \theta \sum_{n=1}^{\frac{\nu-3}{2}} \left( \prod_{k=1}^n \frac{2k}{2k+1} \right) \cos^{2n+1} \theta \right] & (\nu > 1, \text{ odd}) \\ \sin \theta \left[ 1 + \sum_{n=1}^{\frac{\nu-2}{2}} \left( \prod_{k=1}^n \frac{2k-1}{2k} \right) \cos^{2n} \theta \right] & (\nu > 1, \text{ even}) \\ \frac{2}{\pi} \theta & (\nu = 1) \end{cases}$$

1. Abramowitz, M., Stegun, I. A. Handbook of Mathematical Functions AMS55. Washington, D. C. : Government Printing Office; (June, 1964). p. 948.

F Distribution<sup>2</sup>



$F$  = closed domain end point of integration. This is the value of the  $F$  ratio.

$D(v_1, v_2|x)$  =  $F$  variance ratio distribution function.

$Q(F|v_1, v_2) = \alpha$  = the alpha risk.

$Q(F|v_1, v_2) = \int_F^\infty D(v_1, v_2|x) dx$

$\nu_1, \nu_2$  = associated degrees of freedom.

$\nu_1$  even,  $\nu_2$  even or odd.

$$Q(F|v_1, v_2) = x^{\frac{\nu_1 + \nu_2 - 2}{2}} \left[ 1 + \sum_{n=1}^{\frac{\nu_1 - 2}{2}} \left( \prod_{k=1}^n \frac{\nu_1 + \nu_2 - 2k}{2k} \right) \left( \frac{1-x}{x} \right)^n \right]$$

where  $x = \frac{\nu_2}{\nu_2 + \nu_1 F}$

$\nu_2$  even,  $\nu_1$  even or odd

$$Q(F|v_1, v_2) = 1 - \left\{ (1-x)^{\frac{\nu_1 + \nu_2 - 2}{2}} \left[ 1 + \sum_{n=1}^{\frac{\nu_2 - 2}{2}} \left( \prod_{k=1}^n \frac{\nu_1 + \nu_2 - 2k}{2k} \right) \left( \frac{1-x}{x} \right)^n \right] \right\}$$

where  $x = \frac{\nu_2}{\nu_2 + \nu_1 F}$

$\nu_1$  and  $\nu_2$  odd

then  $Q(F|v_1, v_2) = 1 + B(v_1, v_2) - A(F|v_2)$

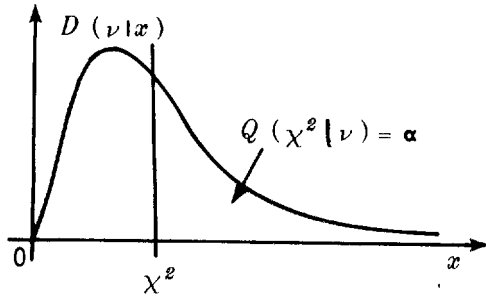
where  $\theta = \tan^{-1} \left( \frac{\nu_1 F}{\nu_2} \right)^{1/2}$  and

$$A(F|v_2) = \begin{cases} \frac{2}{\pi} \left[ \theta + \sin \theta \cos \theta + \sin \theta \sum_{n=1}^{\frac{\nu_2 - 3}{2}} \left( \prod_{k=1}^n \frac{2k}{2k+1} \right) \cos^{2n+1} \theta \right] & \text{for } \nu_2 > 1 \\ \frac{2}{\pi} \theta & \text{for } \nu_2 = 1 \end{cases}$$

$$B(v_1, v_2) = \begin{cases} \frac{2 \left( \frac{\nu_2 - 1}{2} \right)!}{\pi \prod_{j=1}^{\frac{\nu_2 - 1}{2}} \left( \frac{2j-1}{2} \right)} \left[ \cos^{\nu_2} \theta \sin \theta + \cos^{\nu_2} \theta \sin \theta \sum_{n=1}^{\frac{\nu_1 - 3}{2}} \left( \prod_{k=1}^n \frac{\nu_2 + 2k - 1}{2k + 1} \right) \sin^{2n} \theta \right] & \text{for } \nu_2, \nu_1 > 1 \\ 0 & \text{for } \nu_2, \nu_1 = 1 \end{cases}$$

2. Ibid, p. 946.

$\chi^2$  Distribution<sup>3</sup>



$D(\nu|x) = \chi^2$  distribution function

$\nu =$  associated degree of freedom

$\chi^2 =$  critical chi-square test value  
closed domain integration  
end point

$Q(\chi^2|\nu) = \alpha =$  the alpha risk

$Q(\chi^2|\nu) = \int_{\chi^2}^{\infty} D(\nu|x) dx$

$$Q(\chi^2|\nu) = 1 - \frac{(\chi^2/2)^{\nu/2} \exp(-\chi^2/2)}{\Gamma\left(\frac{\nu+2}{2}\right)} \left[ 1 + \sum_{r=1}^{\infty} \frac{\chi^{2r}}{\prod_{s=1}^r (\nu+2s)} \right]$$

for  $\nu$  even

$$\Gamma\left(\frac{\nu+2}{2}\right) = \frac{\nu}{2} !$$

for  $\nu$  odd

$$\Gamma\left(\frac{\nu+2}{2}\right) = \pi^{1/2} \prod_{h=1}^{\frac{\nu+1}{2}} \left(\frac{2h-1}{2}\right)$$

3. Ibid. pp. 940-941.

(This page is intentionally left blank.)

APPENDIX C

NOISE MEASUREMENT STUDIES PERFORMED ON COLOR MATERIALS

A study of the analytical density noise properties of SO-151, SO-155, and 8442 was initiated as a part of this program. The experimental objective was the evaluation of the complete set of analytical autocorrelation and cross correlation functions. Grainless step wedges were produced using a stock of film in which the dye layer had been isolated (Appendix A). The grainless step wedges were produced on a time scale basis since intensity modulation introduces the noise of the modulator into the system. The time of exposure of a projected beam of white light of constant intensity was varied to produce stepped exposures on the film. Cyan, magenta, and yellow grainless step wedges were shipped to the customer's facility for tracing on the [ ] Trichromatic Micro-Analyzer Model 1032T. After receipt of the digital noise traces at [ ] [ ] an effort was made to read the magnetic tapes on the [ ] IBM/360 computer system. These tapes could not be read by the computer system because of digital errors introduced by the microdensitometer system. No usable data were gathered from this experiment; hence no correlation functions were generated.

A standard black-and-white microdensitometer may be used as a trichromatic instrument; however, three scans are required to generate red, green, and blue density records. Because of this, uncertainties are introduced in the cross correlation functions due to probable record misalignment. Lack of time prevented tracing of the grainless step wedges at [ ] on the black-and-white Micro-Analyzer.

(This page is intentionally left blank.)

## APPENDIX D

RELATION BETWEEN ANALYTICAL AND INTEGRAL  
AUTO AND CROSS CORRELATIONS

The complete set of autocorrelations and cross correlations for integral filter microdensities, as formed from analytical auto and cross correlations weighted by absorption coefficients of the image-forming dyes, is listed below.

Derivations are not given; however, they follow directly the procedure established in the text (Equations (58) — (62)) and may be derived from matrix relation (68).

$$\begin{aligned} \rho_{bb}(\tau) = & a_{11}^2 \rho_{yy}(\tau) + a_{12}^2 \rho_{mm}(\tau) + a_{13}^2 \rho_{cc}(\tau) + a_{11} a_{12} [\rho_{ym}(\tau) + \rho_{ym}(-\tau)] \\ & + a_{11} a_{13} [\rho_{yc}(\tau) + \rho_{yc}(-\tau)] + a_{12} a_{13} [\rho_{mc}(\tau) + \rho_{mc}(-\tau)] \end{aligned} \quad (D1)$$

$$\begin{aligned} \rho_{gg}(\tau) = & a_{21}^2 \rho_{yy}(\tau) + a_{22}^2 \rho_{mm}(\tau) + a_{23}^2 \rho_{cc}(\tau) + a_{21} a_{22} [\rho_{ym}(\tau) + \rho_{ym}(-\tau)] \\ & + a_{21} a_{23} [\rho_{yc}(\tau) + \rho_{yc}(-\tau)] + a_{22} a_{23} [\rho_{mc}(\tau) + \rho_{mc}(-\tau)] \end{aligned} \quad (D2)$$

$$\begin{aligned} \rho_{rr}(\tau) = & a_{31}^2 \rho_{yy}(\tau) + a_{32}^2 \rho_{mm}(\tau) + a_{33}^2 \rho_{cc}(\tau) + a_{31} a_{32} [\rho_{ym}(\tau) + \rho_{ym}(-\tau)] \\ & + a_{31} a_{33} [\rho_{yc}(\tau) + \rho_{yc}(-\tau)] + a_{32} a_{33} [\rho_{mc}(\tau) + \rho_{mc}(-\tau)] \end{aligned} \quad (D3)$$

$$\begin{aligned} \rho_{bg}(\tau) = & a_{11} a_{12} \rho_{yy}(\tau) + a_{12} a_{22} \rho_{mm}(\tau) + a_{13} a_{23} \rho_{cc}(\tau) + a_{11} a_{22} \rho_{ym}(\tau) \\ & + a_{11} a_{23} \rho_{yc}(\tau) + a_{12} a_{21} \rho_{ym}(-\tau) + a_{12} a_{23} \rho_{mc}(\tau) + a_{13} a_{21} \rho_{yc}(-\tau) \\ & + a_{13} a_{22} \rho_{mc}(-\tau) \end{aligned} \quad (D4)$$

$$\begin{aligned} \rho_{bg}(-\tau) = & a_{11} a_{12} \rho_{yy}(\tau) + a_{12} a_{22} \rho_{mm}(\tau) + a_{13} a_{23} \rho_{cc}(\tau) + a_{11} a_{22} \rho_{ym}(-\tau) \\ & + a_{11} a_{13} \rho_{yc}(-\tau) + a_{12} a_{21} \rho_{ym}(\tau) + a_{12} a_{23} \rho_{mc}(-\tau) \\ & + a_{13} a_{21} \rho_{yc}(\tau) + a_{13} a_{22} \rho_{mc}(\tau) \end{aligned} \quad (D5)$$



$$\begin{aligned}
 \rho_{br}(\tau) &= a_{11} a_{31} \rho_{yy}(\tau) + a_{12} a_{32} \rho_{mm}(\tau) + a_{13} a_{33} \rho_{cc}(\tau) + a_{11} a_{32} \rho_{ym}(\tau) \\
 &+ a_{11} a_{33} \rho_{yc}(\tau) + a_{12} a_{31} \rho_{ym}(-\tau) + a_{12} a_{33} \rho_{mc}(\tau) \\
 &+ a_{13} a_{31} \rho_{yc}(-\tau) + a_{13} a_{32} \rho_{mc}(-\tau)
 \end{aligned} \tag{D6}$$

$$\begin{aligned}
 \rho_{br}(-\tau) &= a_{11} a_{31} \rho_{yy}(\tau) + a_{12} a_{32} \rho_{mm}(\tau) + a_{13} a_{33} \rho_{cc}(\tau) + a_{11} a_{32} \rho_{ym}(-\tau) \\
 &+ a_{11} a_{33} \rho_{yc}(-\tau) + a_{12} a_{31} \rho_{ym}(\tau) + a_{12} a_{33} \rho_{mc}(-\tau) \\
 &+ a_{13} a_{31} \rho_{yc}(\tau) + a_{13} a_{32} \rho_{mc}(\tau)
 \end{aligned} \tag{D7}$$

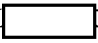
$$\begin{aligned}
 \rho_{gr}(\tau) &= a_{21} a_{31} \rho_{yy}(\tau) + a_{22} a_{32} \rho_{mm}(\tau) + a_{23} a_{33} \rho_{cc}(\tau) + a_{21} a_{32} \rho_{ym}(\tau) \\
 &+ a_{21} a_{33} \rho_{yc}(\tau) + a_{22} a_{31} \rho_{ym}(-\tau) + a_{22} a_{33} \rho_{mc}(\tau) \\
 &+ a_{23} a_{31} \rho_{yc}(-\tau) + a_{23} a_{32} \rho_{mc}(-\tau)
 \end{aligned} \tag{D8}$$

$$\begin{aligned}
 \rho_{gr}(-\tau) &= a_{21} a_{31} \rho_{yy}(\tau) + a_{22} a_{32} \rho_{mm}(\tau) + a_{23} a_{33} \rho_{cc}(\tau) + a_{21} a_{32} \rho_{ym}(-\tau) \\
 &+ a_{21} a_{33} \rho_{yc}(-\tau) + a_{22} a_{31} \rho_{ym}(\tau) + a_{22} a_{33} \rho_{mc}(-\tau) \\
 &+ a_{23} a_{31} \rho_{yc}(\tau) + a_{23} a_{32} \rho_{mc}(\tau)
 \end{aligned} \tag{D9}$$

## APPENDIX E

### PRODUCTION OF STEP WEDGES FROM NON-NEUTRAL SOURCES

In order to calibrate the exposure table generation system properly, it is necessary, as described in the main body of this report, to generate non-neutral characteristic curves on the emulsion type to be used. The resulting step wedges are read on the trichromatic microdensitometer. The step wedge integral densities are converted to cyan, magenta, and yellow analytical densities; and these, when plotted, yield the characteristic curve of each dye layer, showing the dependence of the curve shape on the color of the exposing source (see Figure 16 in text). Taking each of the dynamic transfer functions through a standard curve fitting and inversion exposure generator yields the exposure tables that are used in determining the characteristic vectors, for the emulsion being used, by principal component analysis. An example in the generation of characteristic vectors is given in Appendix F.

The non-neutral step wedges were generated using the arrangement diagrammed in Figure E1. A quartz-iodine light source illuminated a diffuse reflector. This reflector acted as a broad diffuse source illuminating a calibrated  step wedge. The step wedge was photographed, after a 90° reflection by a first surface mirror, using a standard 4 x 5-inch camera with a 70 mm back. The step wedge was reduced in size to provide a microstep wedge. A filter pack between the camera and the mirror corrected 3200°K illumination for the daylight-balanced emulsion. The emulsions used were SO-151, SO-155, and 8442; all were processed in EA-4 chemistry using a color Versamat. Altering the spectral reflectance properties of the diffuse reflector changes the spectral distribution of the neutrally modulated illumination at the film plane.

The diffuse reflectors used were Color-Aid papers. These papers are available in a multitude of hues, shades, and tints. Shades of specific hues are defined by the manufacturer as the hue plus a quantity of its complement. Tints are the hue plus white. Thirty-two color samples were chosen and were used in producing microstep wedges. Because of the variance in total energy reflected, each wedge was adjusted in exposure to produce a base plus stain estimate on the last (11th) step of the wedge and the best

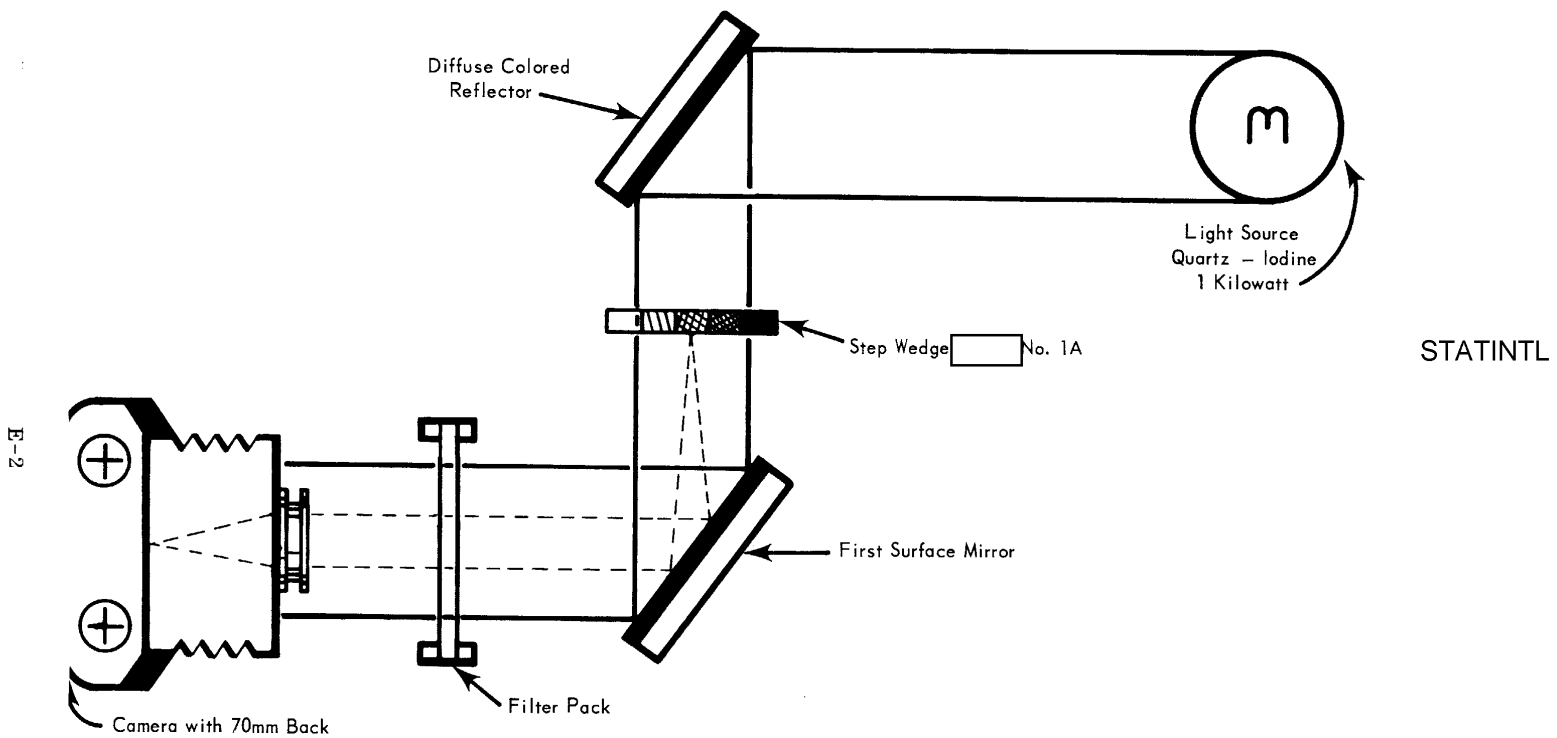


Figure E1. Optical Arrangement Used to Generate Non-Neutral Microstep Wedges

possible Dmax estimate on the first step. A listing of specific colors utilized is given in Table E1. The spectral reflectance curves for each of these samples are given in Figure E2-E33.

Each of the 32 step wedges was produced on the three previously mentioned emulsions, with the white exposure providing an estimate of the neutral dynamic response of the materials. The resulting microstep wedges were sent to the customer's facility to be traced on the  Trichromatic Micro-Analyzer Model 1032T. The resulting digital data were unusable because of microdensitometer digital equipment malfunction. Limited use of the chart records was made to estimate the step wedge densities as reported in Figure 16a, b, c in the main text. This experiment was terminated to allow correction of the operation of the microdensitometer system. Optical misalignment of the microdensitometer, plus other optical considerations (Appendix G), have delayed resumption of the experiment.

TABLE E1. LISTING OF BROAD BAND COLORS

Code: R = Red            G = Green  
       O = Orange        B = Blue  
       Y = Yellow        V = Violet

<u>BASIC HUE</u>	<u>SHADE, TINT OR HUE</u>
White	
ORO	Hue
YGY	Hue
YOY	Shade 1
YOY	Shade 2
YOY	Shade 3
YO	Shade 1
GYG	Shade 3
R	Hue
YO	Shade 2
YO	Shade 3
Y	Shade 3
O	Shade 1
O	Shade 2
O	Shade 3
YG	Hue
GYG	Hue
GYG	Shade 1
GYG	Shade 2

TABLE E1. (cont'd.)

<u>BASIC HUE</u>	<u>SHADE, TINT OR HUE</u>
RO	Shade 1
G	Hue
G	Shade 1
G	Shade 2
G	Shade 3
YG	Shade 1
YG	Shade 2
YG	Shade 3
B	Hue
BG	Hue
BV	Hue
Burnt Umber	Hue
Black	

E-5

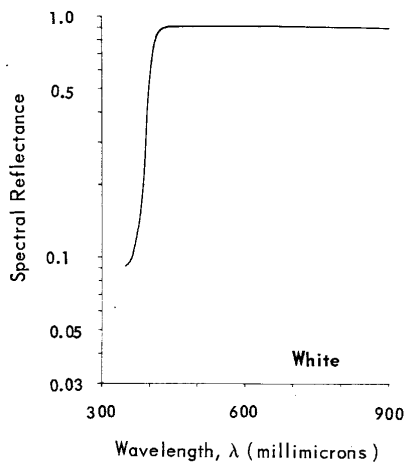


Figure E2. Spectral Reflectance Curve

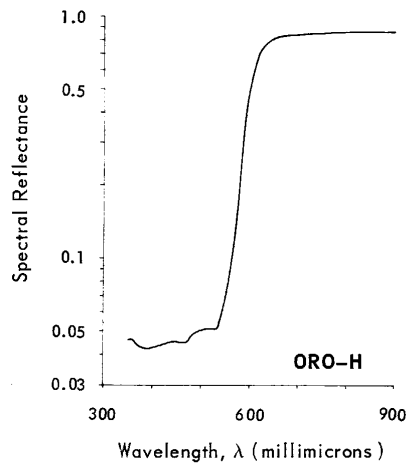


Figure E3. Spectral Reflectance Curve

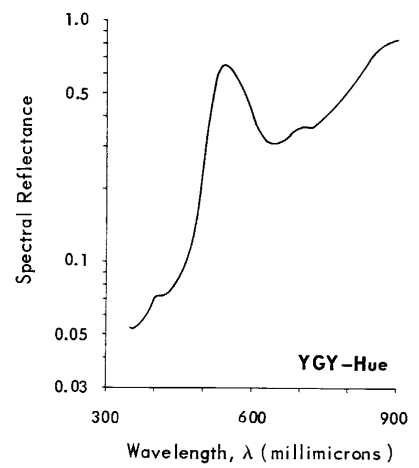


Figure E4. Spectral Reflectance Curve

E-6

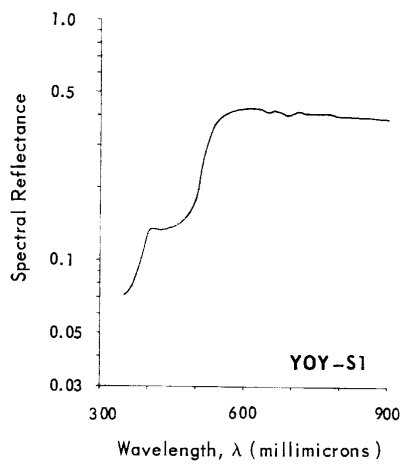


Figure E5. Spectral Reflectance Curve

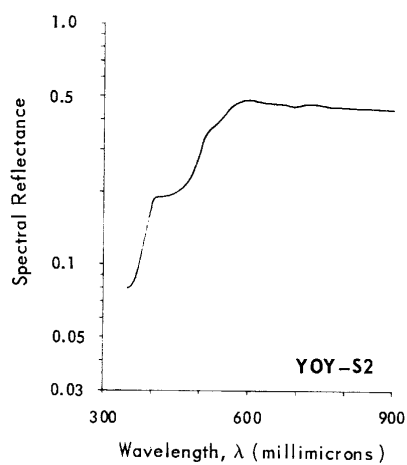


Figure E6. Spectral Reflectance Curve

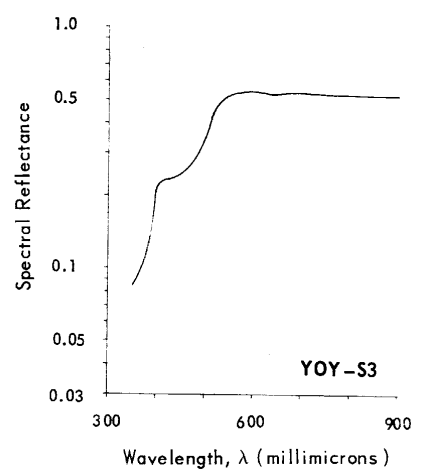


Figure E7. Spectral Reflectance Curve

E-7

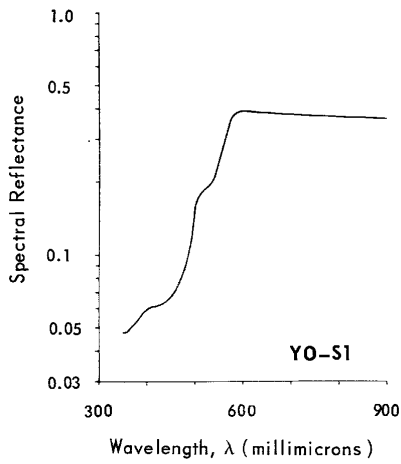


Figure E8. Spectral Reflectance Curve

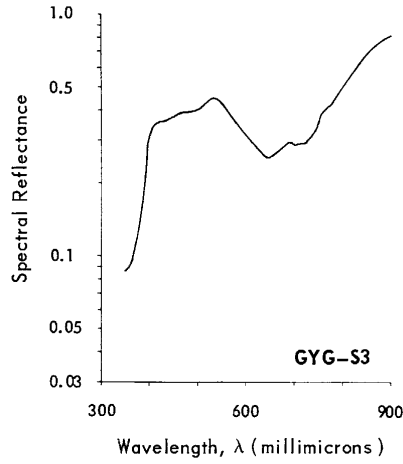


Figure E9. Spectral Reflectance Curve

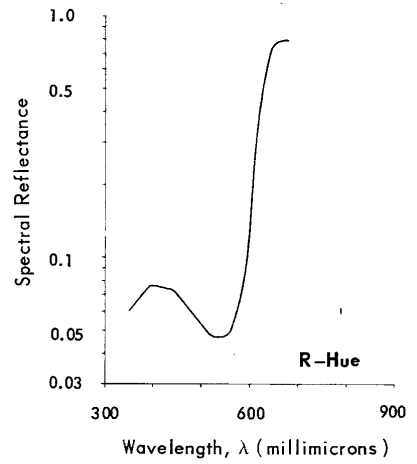


Figure E10. Spectral Reflectance Curve



E-8

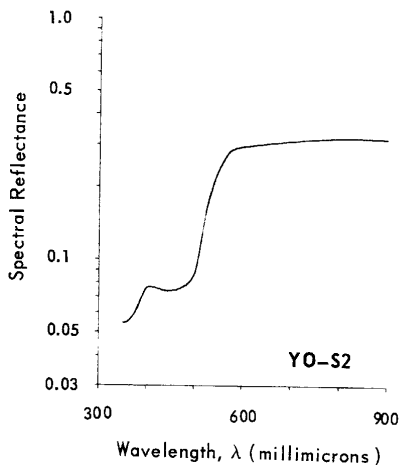


Figure E11. Spectral Reflectance Curve

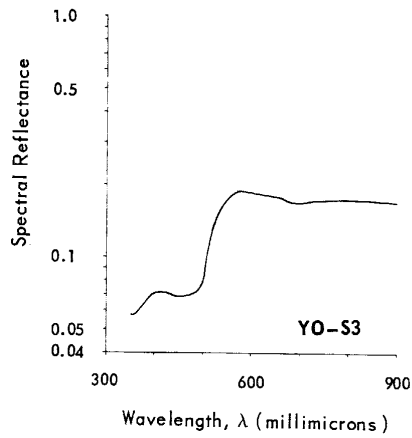


Figure E12. Spectral Reflectance Curve

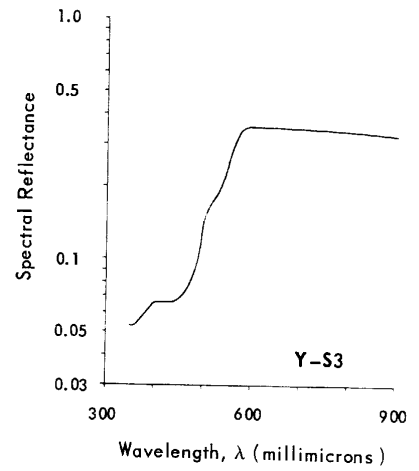


Figure E13. Spectral Reflectance Curve

6-E

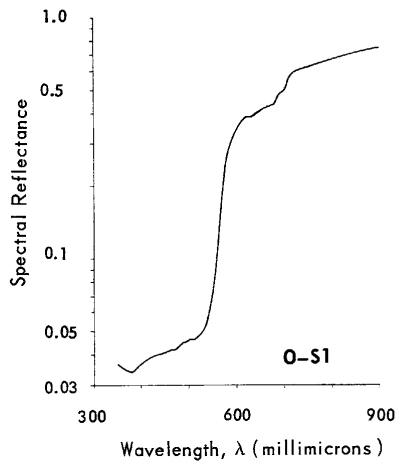


Figure E14. Spectral Reflectance Curve

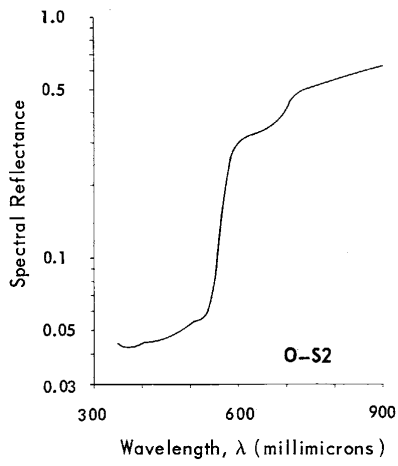


Figure E15. Spectral Reflectance Curve

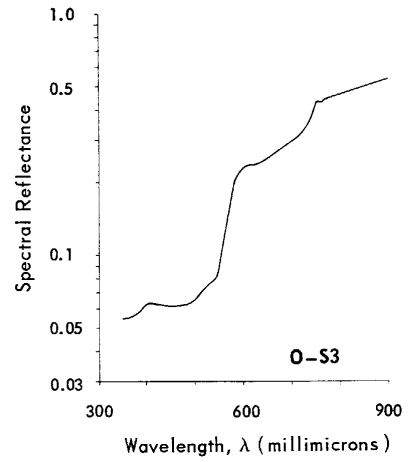


Figure E16. Spectral Reflectance Curve

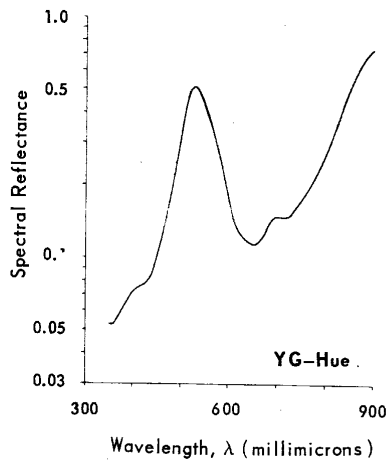


Figure E17. Spectral Reflectance Curve

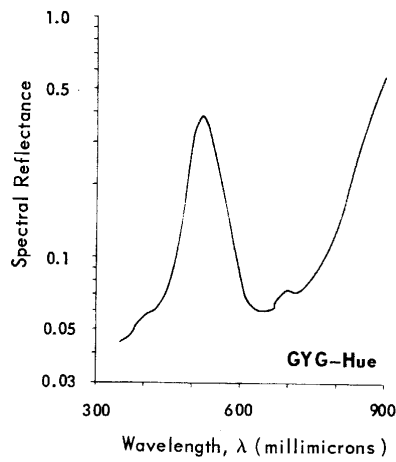


Figure E18. Spectral Reflectance Curve

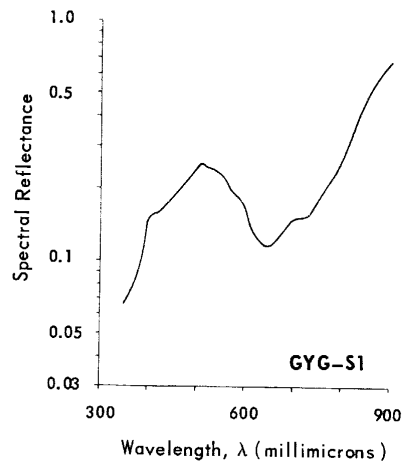


Figure E19. Spectral Reflectance Curve

E-11

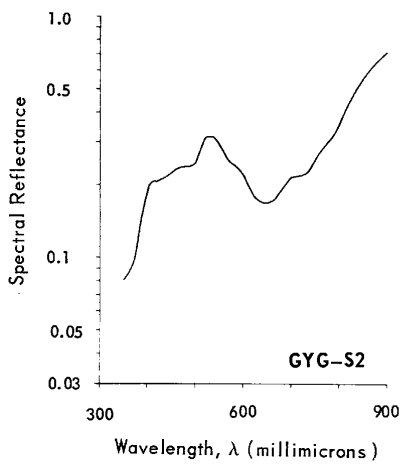


Figure E20. Spectral Reflectance Curve

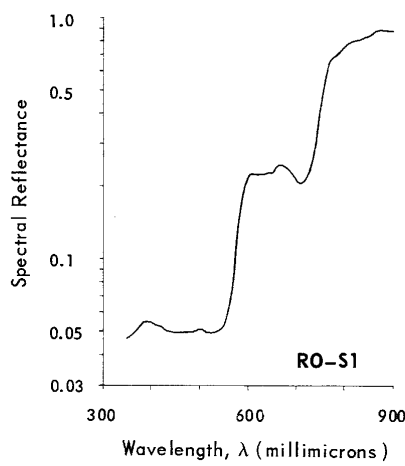


Figure E21. Spectral Reflectance Curve

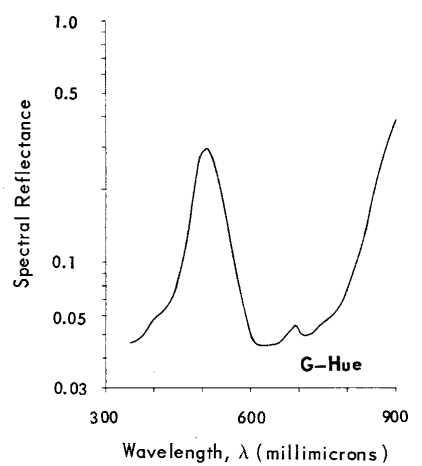


Figure E22. Spectral Reflectance Curve

E-12

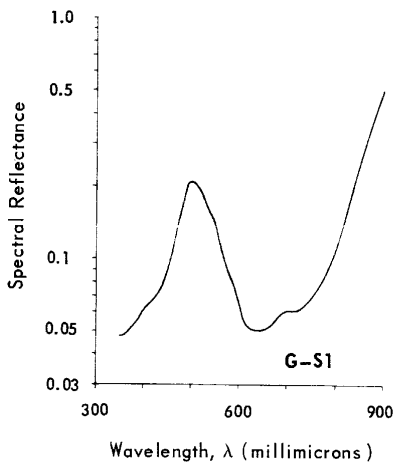


Figure E23. Spectral Reflectance Curve

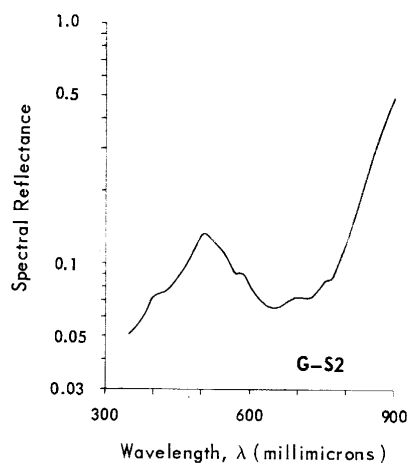


Figure E24. Spectral Reflectance Curve

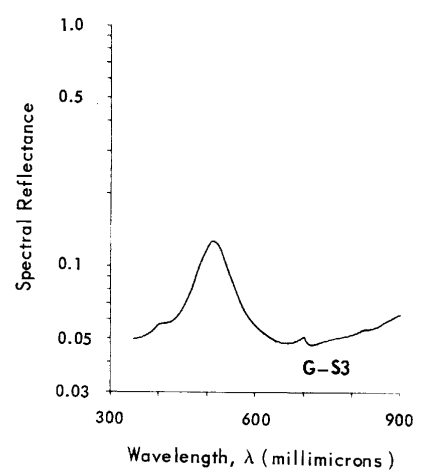


Figure E25. Spectral Reflectance Curve

E-13

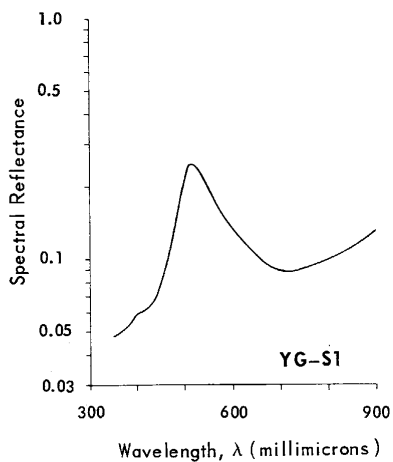


Figure E26. Spectral Reflectance Curve

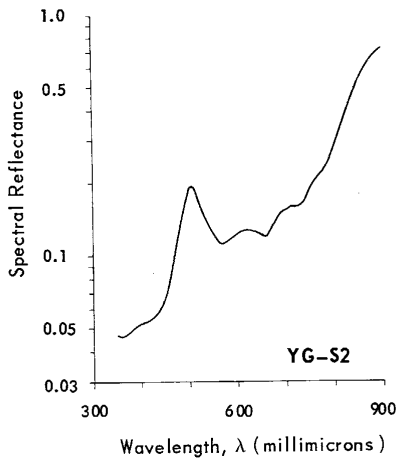


Figure E27. Spectral Reflectance Curve

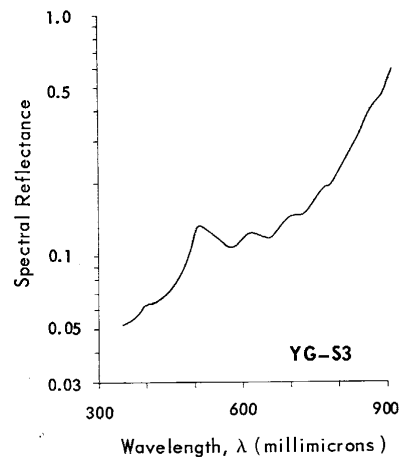


Figure E28. Spectral Reflectance Curve

E-14

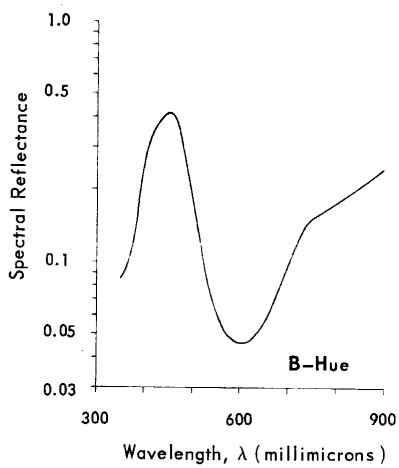


Figure E29. Spectral Reflectance Curve

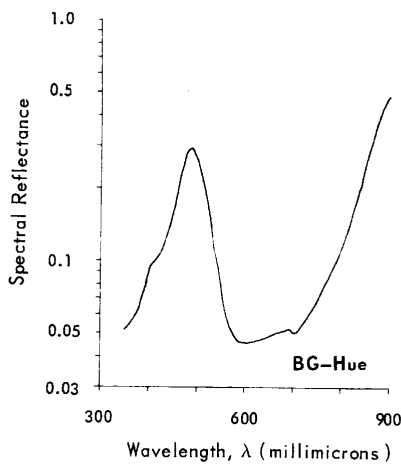


Figure E30. Spectral Reflectance Curve

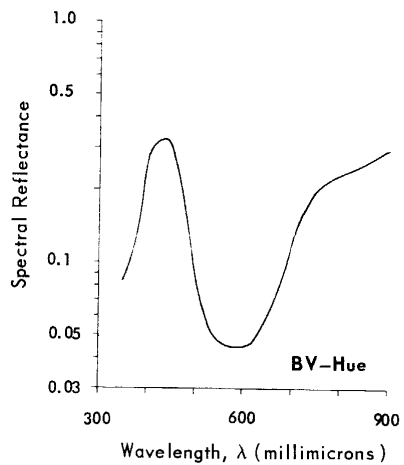


Figure E31. Spectral Reflectance Curve

E-15

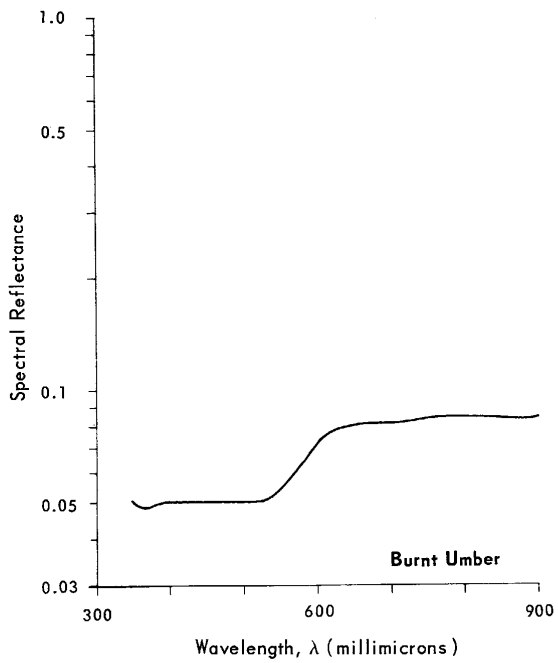


Figure E32. Spectral Reflectance Curve

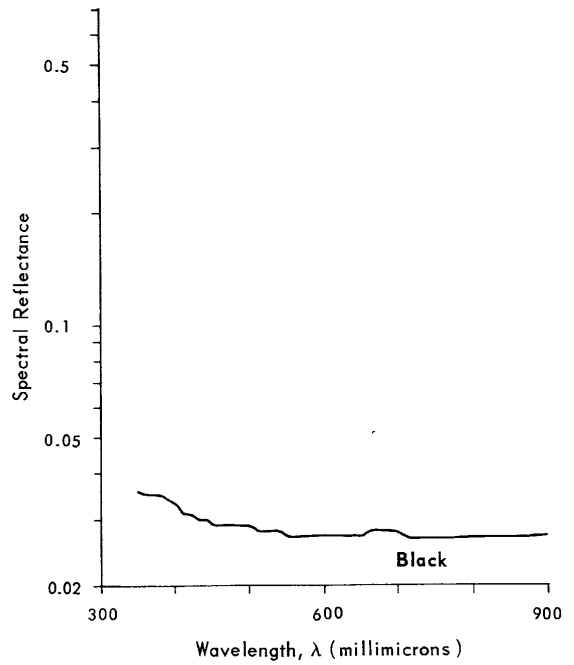


Figure E33. Spectral Reflectance Curve



(This page is intentionally left blank.)

## APPENDIX F

## SAMPLE PROBLEM IN MULTIVARIATE COMPONENT ANALYSIS

For the purpose of illustration we shall consider a sample matrix of smaller dimensions than encountered when working with effective exposure tables. Consider the 6 x 3 matrix  $E_s$  to be the sample matrix:

$$E_s = \begin{bmatrix} 1 & 2 & 3 \\ 2 & 5 & 2 \\ 2 & 6 & 1 \\ 3 & 9 & 0 \\ 4 & 12 & 8 \\ 4 & 15 & 11 \end{bmatrix} \quad \bar{E} = \begin{bmatrix} 2 \\ 3 \\ 3 \\ 4 \\ 8 \\ 10 \end{bmatrix}$$

Rather than extract a neutral, we shall extract the mean column vector  $\bar{E}$  to yield the mean corrected sample matrix:

$$P = E_s - \bar{E} = \begin{bmatrix} -1 & 0 & 1 \\ -1 & 2 & -1 \\ -1 & 3 & -2 \\ 1 & 5 & -4 \\ -4 & 4 & 0 \\ -6 & 5 & 1 \end{bmatrix}$$

The variance-covariance matrix  $S$  is computed as

$$S = PP' = \begin{bmatrix} 2 & 0 & -1 & -5 & 4 & 7 \\ 0 & 6 & 9 & 13 & 12 & 15 \\ -1 & 9 & 14 & 22 & 16 & 19 \\ -5 & 13 & 22 & 42 & 16 & 15 \\ 4 & 12 & 16 & 16 & 32 & 44 \\ 7 & 15 & 19 & 15 & 44 & 62 \end{bmatrix}$$

The trace of  $S$  is

$$\text{tr } S = \sum_{i=1}^6 s_{ii} = 158$$

Using Simond's method, we define the first estimate of the characteristic vector  $y_{(0)}$  to be

$$y^{(0)} = \begin{bmatrix} 1 \\ 1 \\ 1 \\ 2 \\ 2 \\ 2 \end{bmatrix}$$

Computing  $x^{(1)}$  we determine that

$$x^{(1)} = S y^{(0)} = \begin{bmatrix} 13 \\ 95 \\ 136 \\ 176 \\ 216 \\ 283 \end{bmatrix} \text{ and } \max x^{(1)} = 283$$

therefore

$$y^{(1)} = \frac{1}{\max x^{(1)}} x^{(1)} = \begin{bmatrix} 0.0459 \\ 0.3356 \\ 0.4805 \\ 0.6219 \\ 0.7632 \\ 1.0000 \end{bmatrix}$$

Continuing the iteration

$$x^{(2)} = \begin{bmatrix} 6.5546 \\ 38.5812 \\ 54.5945 \\ 68.0353 \\ 90.2716 \\ 119.3941 \end{bmatrix} \quad y^{(2)} = \begin{bmatrix} 0.0548 \\ 0.3231 \\ 0.4572 \\ 0.5698 \\ 0.7560 \\ 1.0000 \end{bmatrix} \quad x^{(3)} = \begin{bmatrix} 6.8274 \\ 37.5328 \\ 52.8855 \\ 65.0123 \\ 88.7204 \\ 117.7279 \end{bmatrix} \quad y^{(3)} = \begin{bmatrix} 0.0579 \\ 0.3188 \\ 0.4489 \\ 0.5522 \\ 0.7536 \\ 1.0000 \end{bmatrix}$$

$$x^{(4)} = \begin{bmatrix} 6.9203 \\ 37.1747 \\ 52.3019 \\ 63.9807 \\ 88.1900 \\ 117.1578 \end{bmatrix} \quad y^{(4)} = \begin{bmatrix} 0.0590 \\ 0.3173 \\ 0.4464 \\ 0.5461 \\ 0.7527 \\ 1.0000 \end{bmatrix} \quad x^{(5)} = \begin{bmatrix} 6.9519 \\ 37.0531 \\ 52.1037 \\ 63.6301 \\ 88.0100 \\ 116.9644 \end{bmatrix} \quad y^{(5)} = \begin{bmatrix} 0.0594 \\ 0.3167 \\ 0.4454 \\ 0.5440 \\ 0.7524 \\ 1.0000 \end{bmatrix}$$

$$\begin{array}{l}
 \mathbf{x}_{(6)} = \begin{bmatrix} 6.9630 \\ 37.0096 \\ 52.0329 \\ 63.5023 \\ 87.9452 \\ 116.8945 \end{bmatrix} \\
 \mathbf{y}_{(6)} = \begin{bmatrix} 0.0595 \\ 0.3166 \\ 0.4448 \\ 0.5432 \\ 0.7523 \\ 1.0000 \end{bmatrix} \\
 \mathbf{x}_{(7)} = \begin{bmatrix} 6.9674 \\ 36.9920 \\ 52.0043 \\ 63.4551 \\ 87.9188 \\ 116.9977 \end{bmatrix} \\
 \mathbf{y}_{(7)} = \begin{bmatrix} 0.0595 \\ 0.3161 \\ 0.4444 \\ 0.5423 \\ 0.7514 \\ 1.0000 \end{bmatrix}
 \end{array}$$

$$\begin{array}{l}
 \mathbf{x}_{(8)} = \begin{bmatrix} 6.9687 \\ 36.9629 \\ 51.9600 \\ 63.3876 \\ 87.8632 \\ 116.7977 \end{bmatrix} \\
 \mathbf{y}_{(8)} = \begin{bmatrix} 0.0596 \\ 0.3164 \\ 0.4448 \\ 0.5427 \\ 0.7522 \\ 1.0000 \end{bmatrix} \\
 \mathbf{x}_{(9)} = \begin{bmatrix} 6.9697 \\ 36.9831 \\ 51.9898 \\ 63.4294 \\ 87.9056 \\ 116.8517 \end{bmatrix} \\
 \mathbf{y}_{(9)} = \begin{bmatrix} 0.0596 \\ 0.3164 \\ 0.4449 \\ 0.5428 \\ 0.7522 \\ 1.0000 \end{bmatrix}
 \end{array}$$

$$\begin{array}{l}
 \mathbf{x}_{(10)} = \begin{bmatrix} 6.9691 \\ 36.9853 \\ 51.9934 \\ 63.4358 \\ 87.9088 \\ 116.8551 \end{bmatrix} \\
 \mathbf{y}_{(10)} = \begin{bmatrix} 0.0596 \\ 0.3165 \\ 0.4449 \\ 0.5428 \\ 0.7522 \\ 1.0000 \end{bmatrix} \\
 \mathbf{x}_{(11)} = \begin{bmatrix} 6.9691 \\ 36.9859 \\ 51.9943 \\ 63.4371 \\ 87.9100 \\ 116.8566 \end{bmatrix} \\
 \mathbf{y}_{(11)} = \begin{bmatrix} 0.0596 \\ 0.3165 \\ 0.4449 \\ 0.5428 \\ 0.7522 \\ 1.0000 \end{bmatrix}
 \end{array}$$

$$\mathbf{x}_{(12)} = \begin{bmatrix} 6.9691 \\ 36.9859 \\ 51.9943 \\ 63.4371 \\ 87.9100 \\ 116.8566 \end{bmatrix}$$

Thus,  $\mathbf{x}_{(11)}$  and  $\mathbf{x}_{(12)}$  are equal to four decimal digits after 12 iterations. The first principal root is

$$\lim_{i \rightarrow \infty} \max x_{(i)} = \lambda_1 = 116.8566$$

The percentage of the trace for the first principal root is

$$R = \frac{\lambda_1}{\text{tr } S} = \frac{116.8566}{158} = 0.7395 \text{ or } 73.95\%$$

By setting the sum of squares of the element of  $\mathbf{x}_{(12)}$  equal to  $\lambda_1$ , we obtain the first characteristic vector

$$\mathbf{v}_{(1)} = \begin{bmatrix} 0.4384 \\ 2.3267 \\ 3.2709 \\ 3.9907 \\ 5.5303 \\ 7.3513 \end{bmatrix}$$

The variance described by the first characteristic vector  $\mathbf{V}^{(1)}$  may now be removed from the variance-covariance matrix:

$$\mathbf{S}_2 = \mathbf{S} - \mathbf{V}^{(1)} \mathbf{V}^{(1)'} = \begin{bmatrix} 1.8079 & -1.0200 & -2.4339 & -6.7495 & 1.5756 & 3.7772 \\ -1.0206 & 0.5865 & 1.3896 & 3.7149 & -0.8673 & -2.1042 \\ -2.4339 & 1.3896 & 3.3013 & 8.9469 & -2.0890 & -5.0453 \\ -6.7495 & 3.7149 & 8.9469 & 26.0744 & -6.0697 & -14.3368 \\ 1.5756 & -0.8673 & -2.0890 & -6.0697 & 1.4158 & 3.3452 \\ 3.7772 & -2.1042 & -5.0453 & -14.3368 & 3.3452 & 7.9584 \end{bmatrix}$$

The second characteristic vector  $\mathbf{V}^{(2)}$  is determined in the same manner as  $\mathbf{V}^{(1)}$  except that the adjusted variance-covariance matrix,  $\mathbf{S}_2$  is used. The initial estimate  $\mathbf{y}^{(0)}$  again is arbitrary; convergence occurs in 7 iterations, yielding

$$\mathbf{x}^{(7)} = \begin{bmatrix} -10.6705 \\ 5.9144 \\ 14.2073 \\ 40.8255 \\ -9.5120 \\ -22.5608 \end{bmatrix} \text{ and } \lambda_2 = 40.8255$$

The percentage of trace now accounted for by  $\lambda_1$  and  $\lambda_2$  is

$$R = \frac{\lambda_1 + \lambda_2}{\text{tr } \mathbf{S}} = 0.9979 \text{ or } 99.79\%$$

The second characteristic vector is

$$\mathbf{V}^{(2)} = \begin{bmatrix} -1.3328 \\ 0.7387 \\ 1.7745 \\ 5.0992 \\ -1.1881 \\ -2.8179 \end{bmatrix}$$

The third characteristic root and vector would then be computed from  $\mathbf{S}_3$  :

$$\mathbf{S}_3 = \mathbf{S}_2 - \mathbf{V}^{(2)} \mathbf{V}^{(2)'}$$

Anderson's procedure requires that each iterative estimate be normalized by the square root of the sum of square of the elements

$$\mathbf{y}^{(i)} = \mathbf{x}_i (\mathbf{x}_{(i)}' \mathbf{x}_{(i)})^{-1/2}$$

This means that  $\mathbf{x}_{(i)}' \mathbf{x}_{(i)}$  converges to  $\lambda_l^2$  (the  $l$ th root) and that

$$\mathbf{B}^{(l)} = \frac{\mathbf{V}^{(l)}}{\lambda_l^{1/2}}$$

For the example just completed

$$\mathbf{B}^{(1)} = \begin{bmatrix} 0.0406 \\ 0.2152 \\ 0.3025 \\ 0.3692 \\ 0.5116 \\ 0.6800 \end{bmatrix} \quad \mathbf{B}^{(2)} = \begin{bmatrix} -0.2086 \\ 0.1156 \\ 0.2777 \\ 0.7981 \\ -0.1859 \\ -0.4410 \end{bmatrix}$$

and

$$\mathbf{B}^{(1)'} \mathbf{B}^{(1)} = \mathbf{B}^{(2)'} \mathbf{B}^{(2)} = 1$$

The weighting functions  $\mathbf{W}$  are determined as

$$\mathbf{W}^{(l)} = \frac{\mathbf{V}^{(l)'}}{\lambda_l}$$

Thus, in this example they are equal to

$$\begin{aligned} \mathbf{W}^{(1)} &= [ .0037 \quad .0199 \quad .0279 \quad .0341 \quad .0473 \quad .0629 ] \\ \mathbf{W}^{(2)} &= [ -.0326 \quad .0180 \quad .0434 \quad .1249 \quad -.0291 \quad -.0690 ] \end{aligned}$$

To determine the scalar multiplier two methods may be used. They may be related to experimental parameter through regression analysis. This means that a set of scalar multiples must be determined for a set of responses generated under condition in which the parameters are known.

Let the vector

$$\mathbf{E}_x = \begin{bmatrix} 3 \\ 2 \\ 1 \\ 0 \\ 8 \\ 11 \end{bmatrix}$$

be this set (this may be recognized as the 3rd column in the original data set.) Thus, the scalar multiplier may be generated by the equation

$$Y_x = \mathbf{W} (\mathbf{E}_x - \bar{\mathbf{E}})$$

where  $\mathbf{W}$  is the 2 x 6 array of weighting functions

$$\mathbf{W} = \begin{bmatrix} .0037 & .0199 & .0279 & .0341 & .0473 & .0629 \\ -.0326 & .0180 & .0434 & .1249 & -.0291 & -.0690 \end{bmatrix}$$

Thus,

$$Y = \begin{bmatrix} -.1458 \\ -.7043 \end{bmatrix}$$

To regenerate  $E_x$ ,  $V$ ,  $Y$  and  $\bar{E}$  are needed and are used as follows

$$E_x = V \cdot Y + \bar{E}$$

where  $V$  is the matrix comprised of characteristic vectors

$$V = \begin{bmatrix} .4384 & -1.3328 \\ 2.3267 & .7387 \\ 3.2709 & 1.7745 \\ 3.9907 & 5.0992 \\ 5.5303 & -1.1881 \\ 7.3513 & -2.8179 \end{bmatrix}$$

Regenerated  $E_x$  is

$$\text{Regenerated } E_x = \begin{bmatrix} 2.8747 \\ 2.1406 \\ 1.2735 \\ -.1731 \\ 8.0304 \\ 10.9124 \end{bmatrix} \quad \text{Actual } E_x = \begin{bmatrix} 3 \\ 2 \\ 1 \\ 0 \\ 8 \\ 11 \end{bmatrix}$$

The error in this case is rather large, being introduced by the computation of an insufficient number of characteristic vectors.

$$\text{Error} = \text{Regenerated } E_x - \text{Actual } E_x = \begin{bmatrix} -.1253 \\ .1406 \\ .2735 \\ -.1731 \\ +.0304 \\ -.0872 \end{bmatrix}$$

The above equation can be stated because the signs of the error terms suggest a higher order relationship that has not been removed from the sample matrix by the first two characteristic vectors. Although we have accounted for 99.79% of the variance by computing the first two principal roots, the remaining .21% is introducing the higher order error here observed.

APPENDIX G

OPTICAL EVALUATION AND RECOMMENDATIONS  
FOR THE

PRECISION TRICHROMATIC MICRODENSITOMETER 1032T

STATINTL

To make trichromatic microdensitometer measurements, it is necessary to form the image of a spot or a slit on the specimen to be analyzed and then collect the transmitted light on a measuring instrument to determine the modulation, or the difference of the light levels, when the specimen is in the light path and when it is removed. This theoretical consideration is simple, but in practice there exist difficulties which are not all known and which would require an empirical operational solution. By analyzing the optical parameters of the existing system, guidelines can be drawn to make an improved microdensitometer.

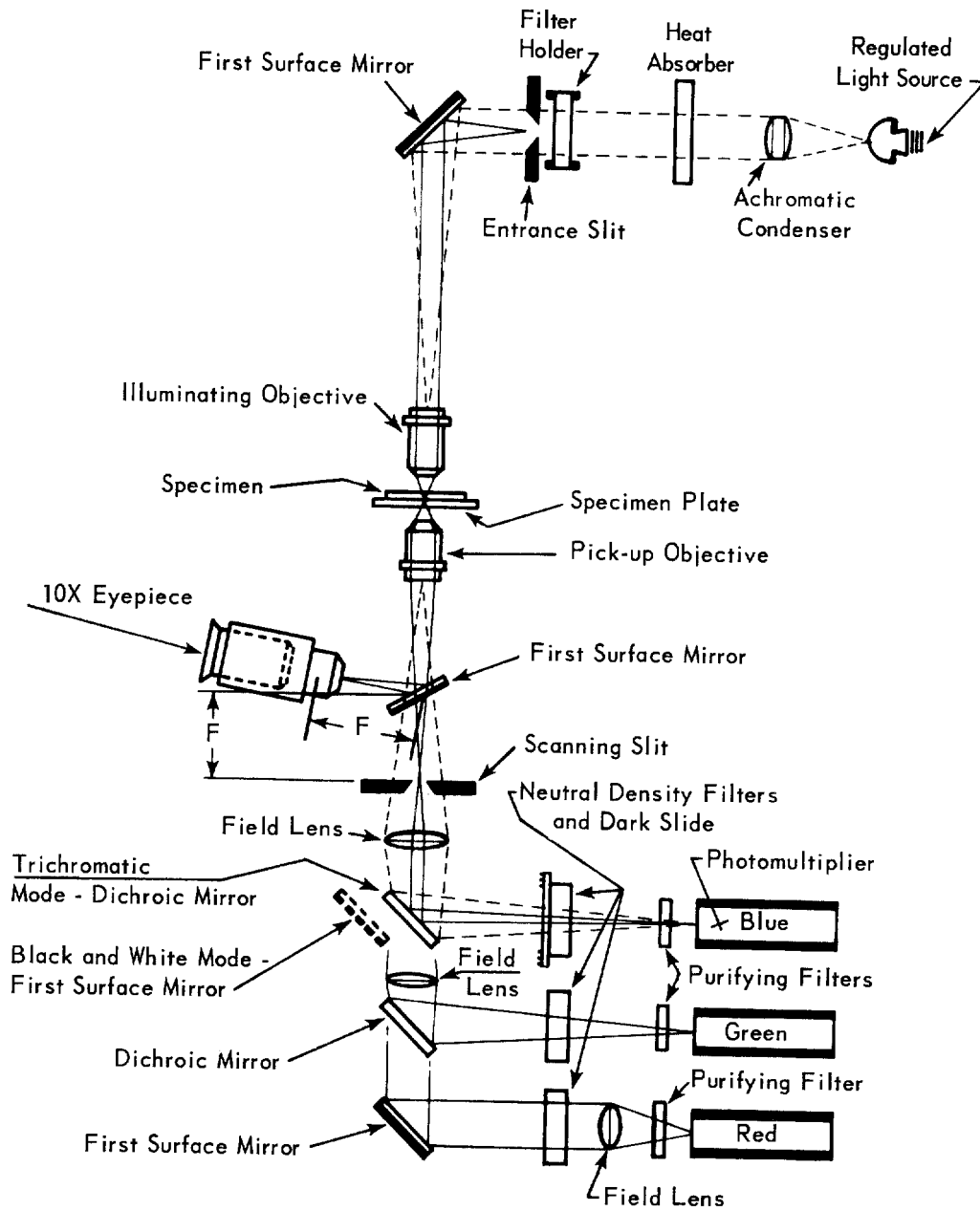
The basic optical principles for the Precision Trichromatic Microdensitometer are adequately presented in the Manual of Operating Instructions and Maintenance, dated January 1966. The schematic is repeated here in Figure G1. The condenser forms the image of the light source on the rear, or entrance pupil, of the illuminating objective, and the illuminating objective itself forms the image of the Micro-Spot or slit on the specimen. The attenuated light, after going through the specimen, enters the pickup objective, which forms the Micro-Spot or slit image on the scanning slit. From there the light (not the image) is conveyed to photomultiplier tubes via appropriate field lenses.

In practice, the difficulties associated with the accepted theoretical considerations can be divided into three groups:

1. Image forming system (Micro-Spot)
2. Specimen
3. Pickup system

In addition, there are optical differences between spot and slit image formation and they are discussed separately.





STATINTL

Figure G1. Schematic of  Trichromatic Microdensitometer 1032T

STATINTL

STATINTL

1. Micro-Spot Image Forming System: According to the [ ] manual a [ ] metallographic achromat 10/0.25 designed for 215-mm tube length has to form, on the specimen, a 2-micron diameter image of a Micro-Spot which is located in the position of the entrance slit (Figure G1). The optical distance from the Micro-Spot to the specimen is about 18 inches. If we assume about 1.5 inches from the specimen to the shoulder of the objective (working distance plus the length of the objective), we get a "tube length" or target distance of 16.5 inches or 404 millimeters. The 2-micron diameter spot on the specimen is formed by the objective of the exit pupil of the Micro-Spot, which is 50 to 100 microns in diameter. According to Ploke<sup>1</sup>, the light beam at the Micro-Spot exit aperture is more intense at the edge than in the center, and it does not form a focal point. The 10X achromat is supposed to form a 2-micron diameter image of the Micro-Spot exit pupil on the specimen at wavelengths of 443, 549, and 674 millimicrons. There is considerable doubt that this is possible. The objective has not been analyzed, and we do not know where the images form in relation to each other; however, it is known that [ ] achromats are color corrected for only two colors and spherically corrected for only one color. (See Figure G2). If only a one-color bandpass filter were used, we would expect acceptable results from the image-forming system in every required application. The deficiency of this system is increased by omitting an eyepiece, which would effect a certain amount of correction for chromatic difference of magnification<sup>2</sup>.

STATINTL

STATINTL

It is of interest to discuss the performance of the system, using comparable objectives for which the analysis data are available<sup>3</sup>. Three [ ] objectives are available and have been analyzed without eyepieces. These are:

<sup>1</sup> M. Ploke, "Light Conducting Systems with High Concentration Capability", Optica, Vol. 1, 1967, p. 25.



STATINTL

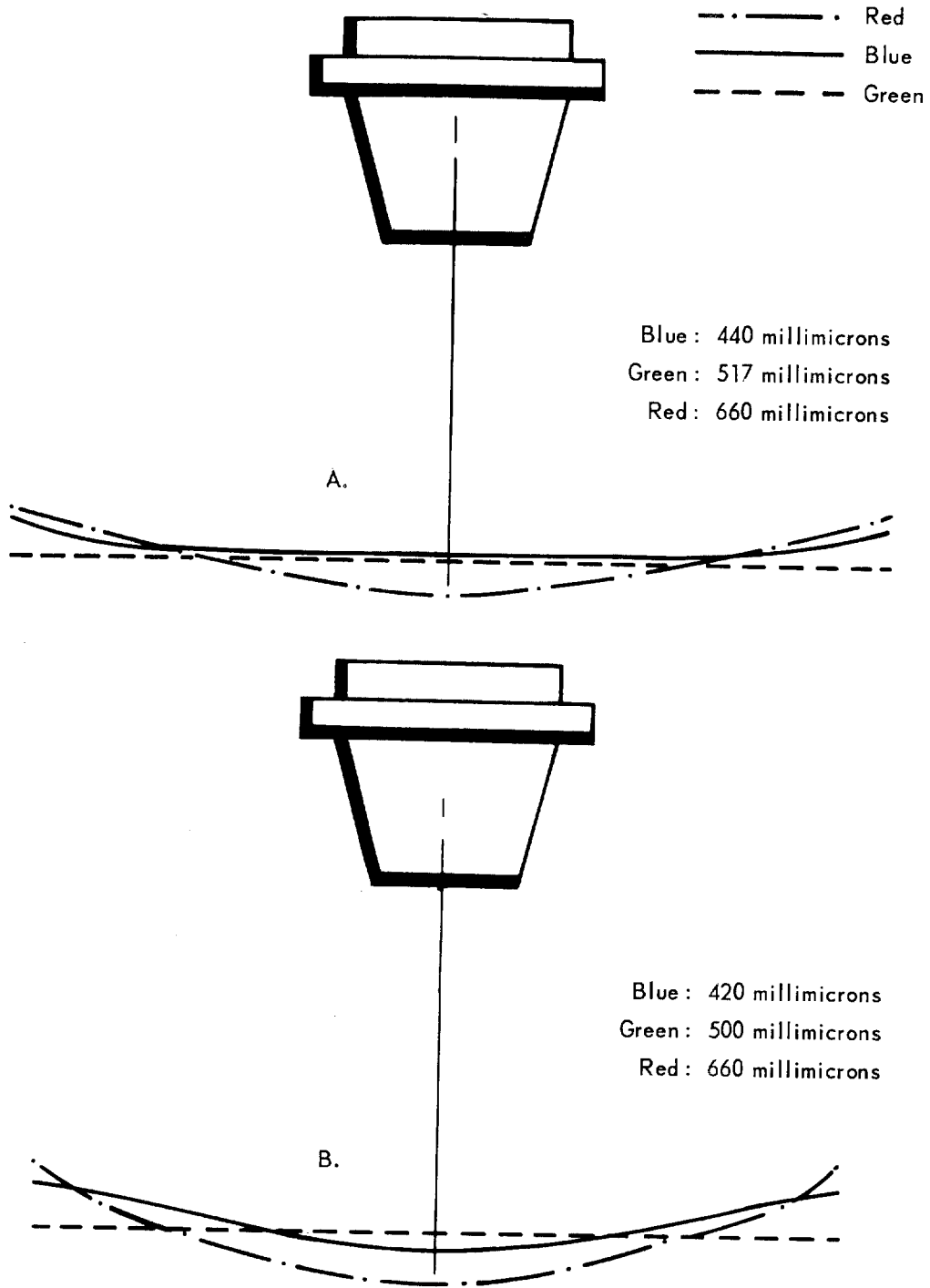


Figure G2. Schematic Representation of Wavelength Dependence of Epiplan 8 Focus

Eiplan	8/0.2
Ultrafluar	10/0.2
Eiplan	16/0.35

The Eiplans are achromats and the Ultrafluar is designed to be used in the wavelength region of 210 to 650 millimicrons<sup>4</sup>. Figure G3a shows that the focus difference between wavelengths of 443 and 674 millimicrons is 135 microns. Figure G3b indicates that the resolution diminishes from 600 to 100 lines/mm if the lens is out of focus by only 28 microns. By using Figure G4 and G5 it can easily be seen that a 135-micron out-of-focus condition cannot be tolerated for any of these objectives if a 2-micron image has to be formed.

STATINTL

The numerical aperture of the  10X achromat is 0.25 for 21<sup>5</sup>-mm tube length. A simple calculation (see Figure G6) shows that a 135-micron out-of-focus position would form a 70-micron diameter disk at the plane where the microscope is focused. This shows that it is not reasonable to form a 2-micron spot with the 10X achromat at a given surface at a given time using the wavelengths of 443, 549, and 674 millimicrons.

2. Specimen: Normally a microdensitometer is used for black-and-white film which has an emulsion thickness of 4 to 7 microns. If a Micro-Spot image is formed in the center of the emulsion, it is not out of focus by more than 2 to 3.5 microns. As Figure G3 shows, this deviation has no serious effect on the image quality. A subtractive color film like  SO-151 emulsion, however, has a four-layer emulsion, as shown in Figure G7, which has an estimated total thickness of 18 microns. It is reasonable to consider that each "dye" layer is about 5 microns thick. Furthermore, it is possible to focus the microdensitometer on the magenta dye and the image is then always less than 10 microns out of focus. The peaks of the absorption curves coincide with the transmission curves of the interference filters. This is an advisable approach to the solution of the problem.

STATINTL

---

<sup>4</sup>. K. Michel, Die Mikrophotographie, Springer Verlag, (Vienna 1962), p. 197.

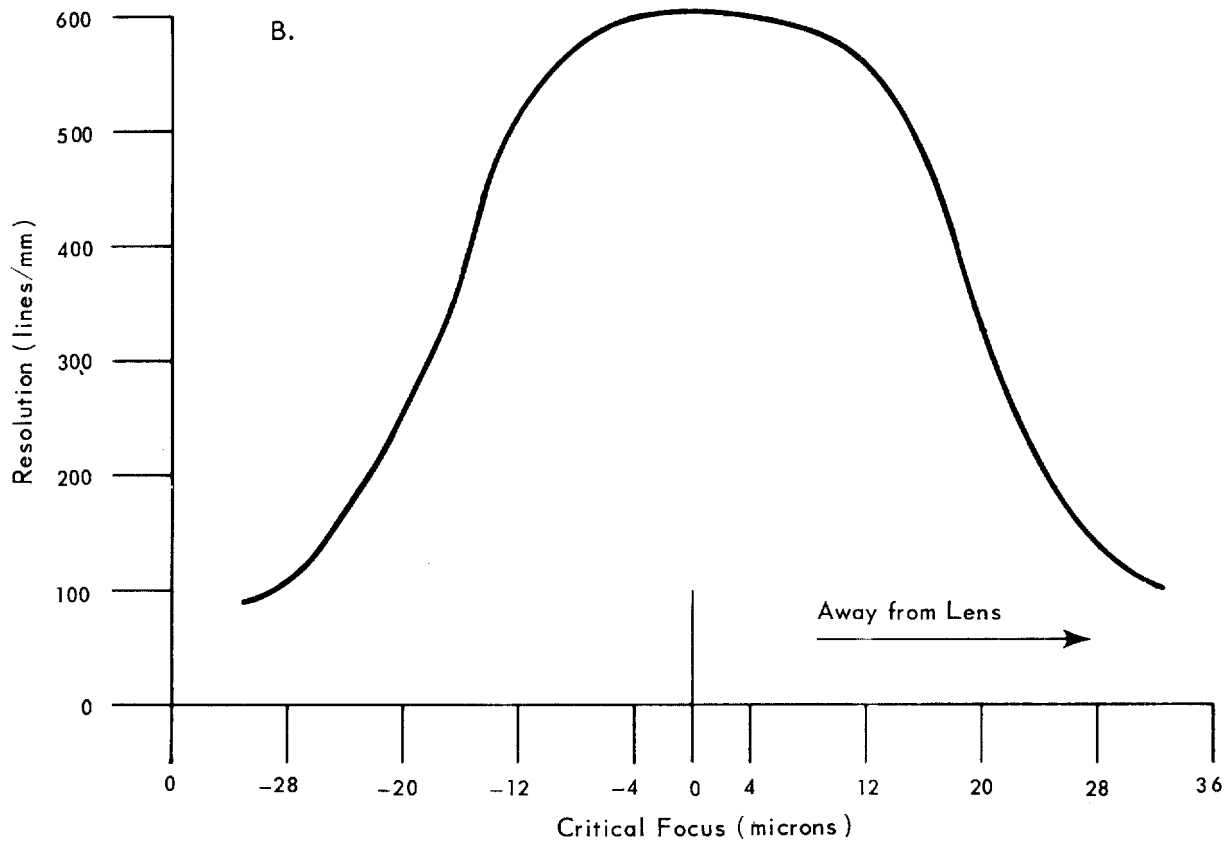
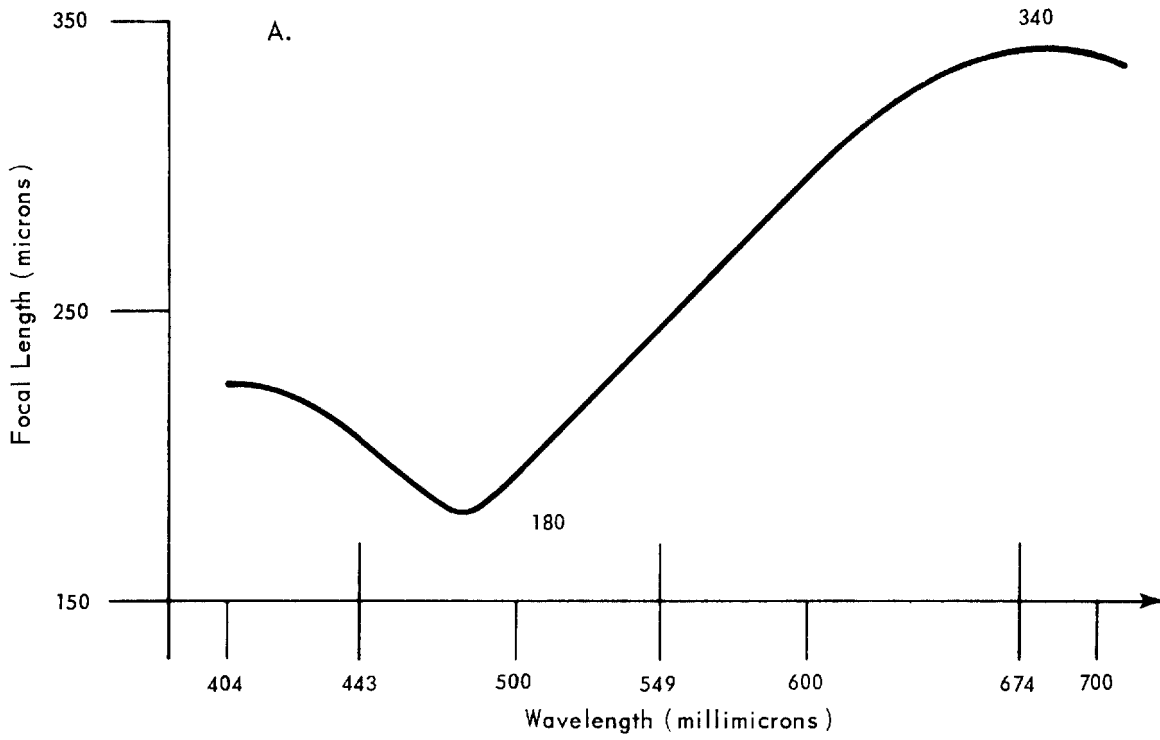


Figure G3.  Epiplan 8/0.2

STATINTL

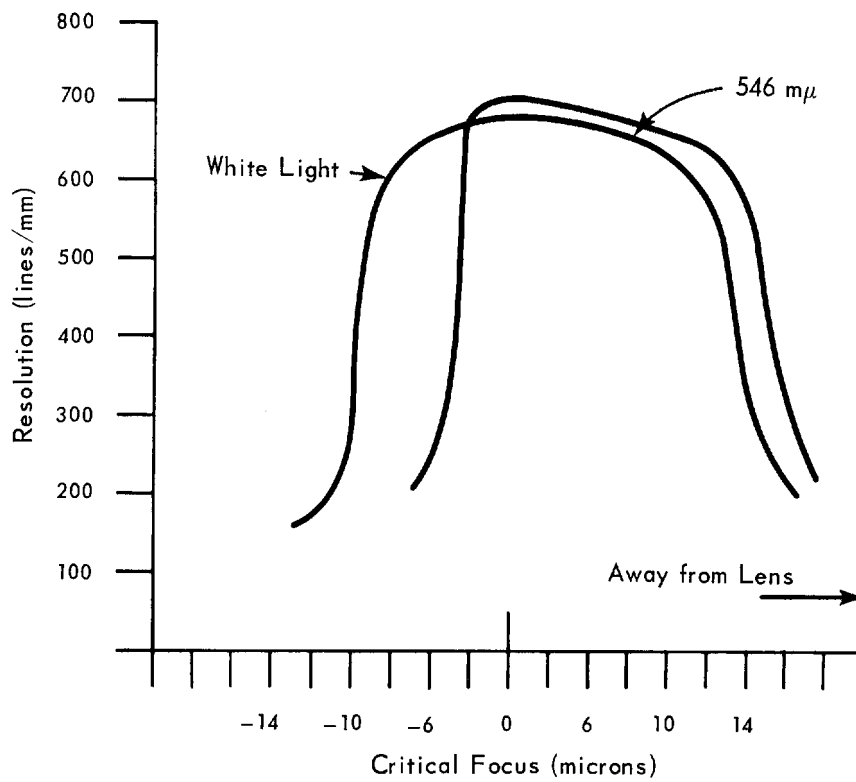
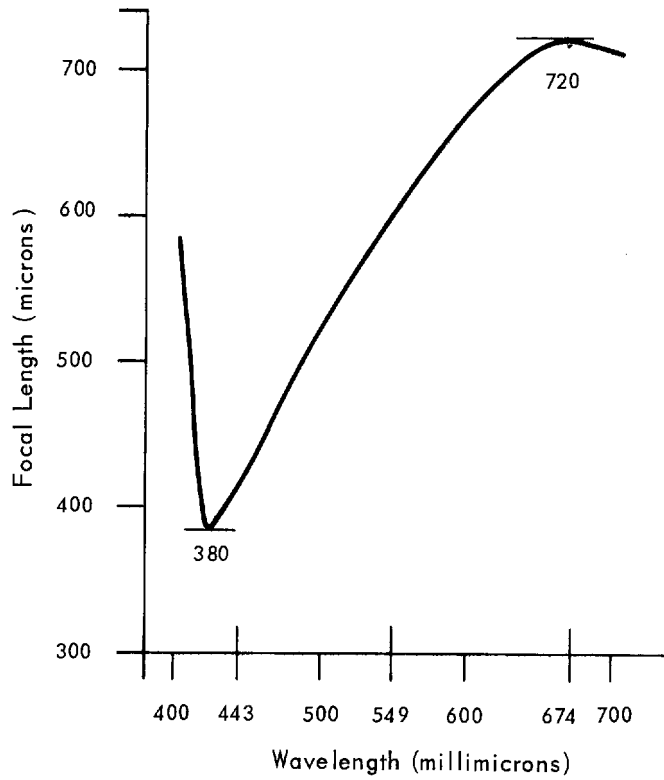


Figure G4.  Ultrafluor 10/0.2

STATINTL

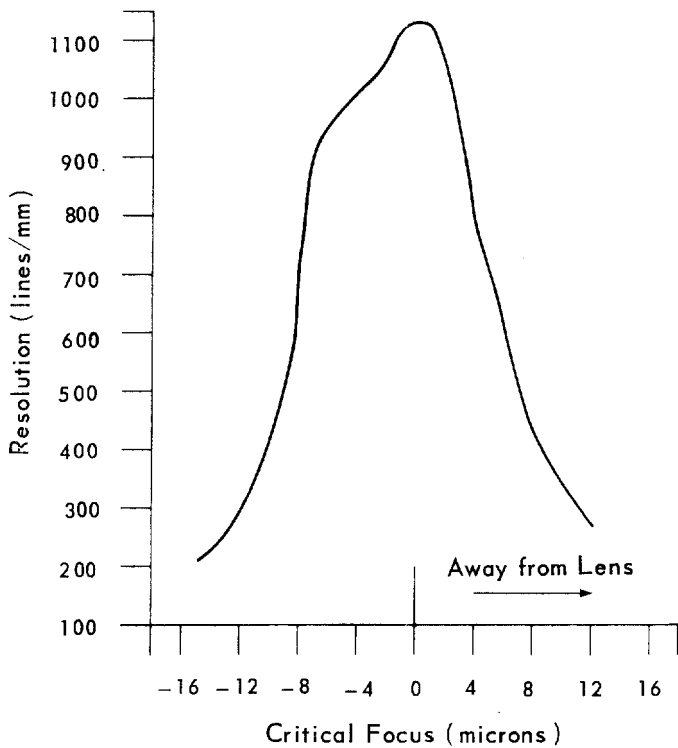
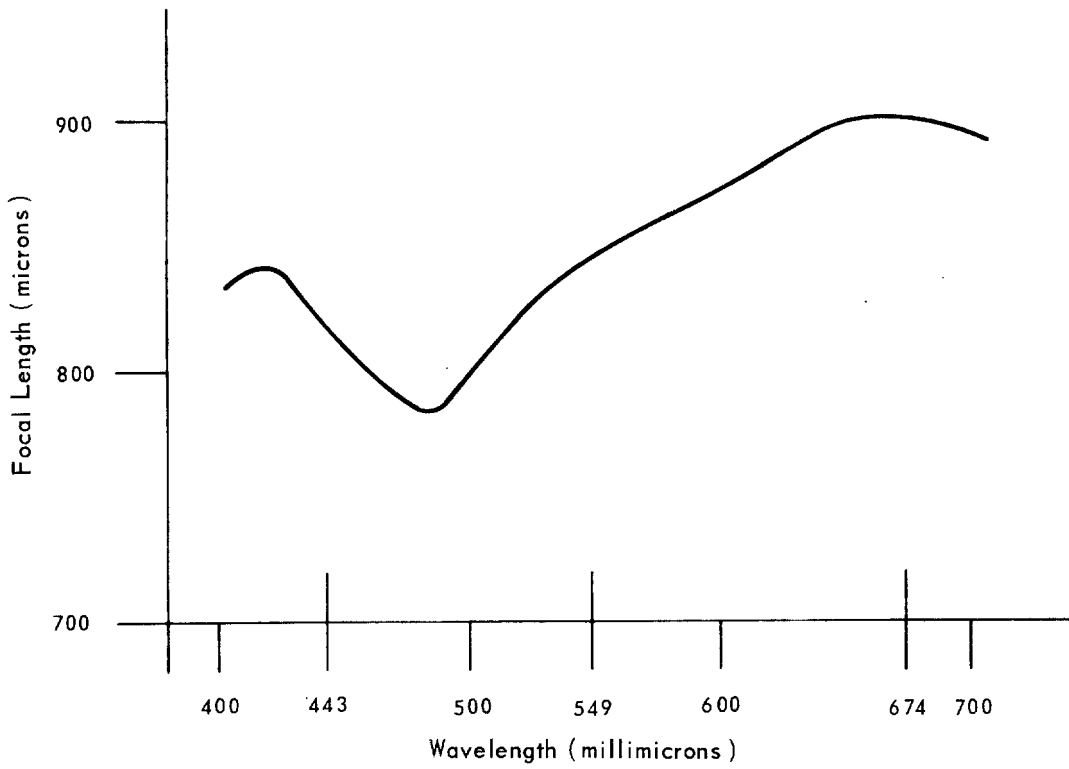


Figure G5.  Epiplan 16/0.35

STATINTL

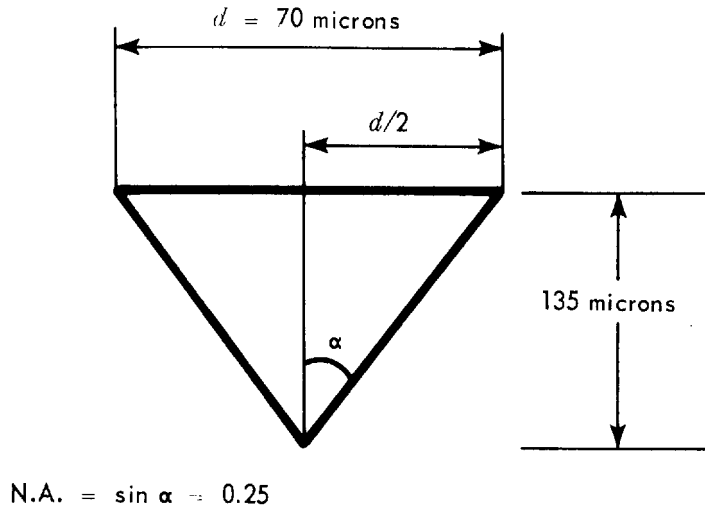


Figure G6. Defocusing Effect

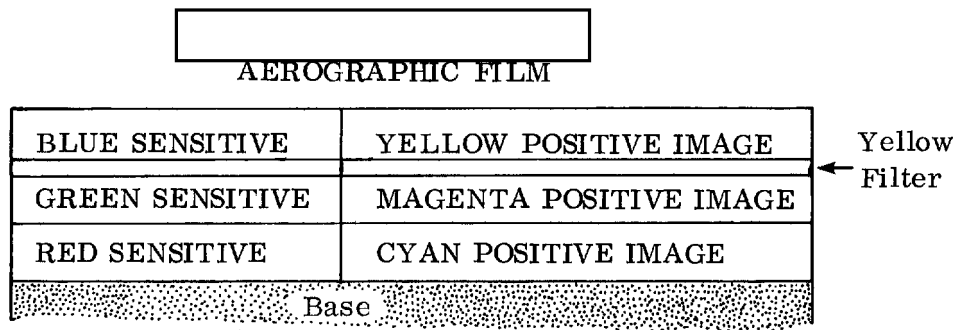


Figure G7. Schematic Representation of a Multilayer Color Film



3. The Pickup System: The illuminating objective forms the image of a spot on the specimen with the requirement that the images of all three colors lie in the same plane. The pickup objective forms the image of the same spot in the scanning slit plane. Following the same trend of thought for the pickup as for the scanning objective, we realize that our difficulties are doubled, and the pickup objective may not form an image of the spot anywhere in our system. Obviously the spots that are formed in these three-color components of white light are all of different size and of different energy distribution. It would be desirable, but not absolutely necessary, to have the same optical path length for all three colors which are being measured.

An achromatic objective is color corrected for two colors and spherically corrected for one color. This means that with an achromat it is possible to project, in one wavelength region, a slit onto a plane, so that it is sharp for its entire length. For the rest of the colors the image field has a positive curvature. This means that if the center of the slit is focused on the specimen plane, the ends are focused somewhere in space between the objective and the specimen plane. The pickup objective is positioned the opposite way; its image field is curved the opposite way and therefore cannot form a sharp image of the slit in the scanning slit plane. The problem becomes more severe in wavelength regions which are not even focused with the center in the specimen plane. The spherical aberration problem lessens, the smaller the length of the slit is in comparison to the image field.

It is obvious from the preceding analysis that an achromat is not an advisable objective to use in the discussed microdensitometer system. There are objectives available in the apochromat and planapochromat series which are color corrected for three wavelengths and spherically corrected for two wavelengths. Also available are modern objectives designed to be used without oculars. It is not known if the color correction curves of the objectives coincide with the peaks of the absorption curves of the color film. It is possible that each color filter transmission curve should peak halfway between the color correction curve of the objective and the peak of the color absorption curve of the proper dye layer.

It is advisable to review applicable objectives and select, based on manufacturer's information, the ones most appropriate for further analysis. The necessary objective

analysis data are often not available even from the manufacturers. It is therefore necessary to analyze the objectives for all the necessary data and choose the proper optics based on the analysis. The use of a Micro-Spot and slit during the analysis would add further valuable data.

To simplify the construction of the pickup system, it would be desirable to make the color separation at the light source. This would not permit three simultaneous readings during the specimen scanning, but a rotating sector wheel with color filters may make the sampling frequency sufficiently rapid for practical applications.

In order to verify the principles of our analysis, we conducted some simple tests with the  Micro-Analyzer at . The Micro-Spot system is the same as in Figure G1. The color filters which we used were always placed between the light source and the Micro-Spot assembly.

STATINTL

Two examples of all the tests performed are presented here.

Test 1

The Micro-Spot was formed in the specimen plane without using any film. The Micro-Spot image was formed, with one color filter in place, by visual inspection. The color filter was then replaced with another filter, and it was always found by visual determination that the spot was out of focus. The system was now focused again with the second filter in place and the required correction distance determined. The results are shown in the table below.

illuminating Objective	Pickup Objective	Filter 1	Filter 2	Focus Difference (microns)
Epiplan 8X	Epiplan 8X	436 m $\mu$ interference	546 m $\mu$ interference	50
Epiplan 8X	Epiplan 8X	Wratten 92	Wratten 98	44
Epiplan 8X	B and L 10X*	486 m $\mu$ interference	546 m $\mu$ interference	11

\*This objective is a  10X achromat, N. A. = 0.25, tube length = 215 mm.

Test 2

We made a set of step wedges and resolving power targets on SO-151 color film. The set consisted of three targets, each made on a different dye layer of the film. The step wedges were then traced with different filters. Two traces, both on the magenta layer, are shown in Figures G8 and G9. Figure G8 shows the target focused and traced with the green 546 millimicron bandpass interference filter, and Figure 9 shows the same target focused with a 436 millimicron bandpass interference filter and then traced with the 546 millimicron filter. As the target has a sixth root of two frequency change per element and the resolution loss is 6 elements, we can say that the resolution loss is 50 percent. Since only one emulsion layer is used, all focus differences are caused by the optics above.

These experimental results agree with and confirm our theoretical considerations.

STATINTL



Figure G8. Three-Bar Target Focused with 546 Millimicron Filter and Traced with 546 Millimicron Filter

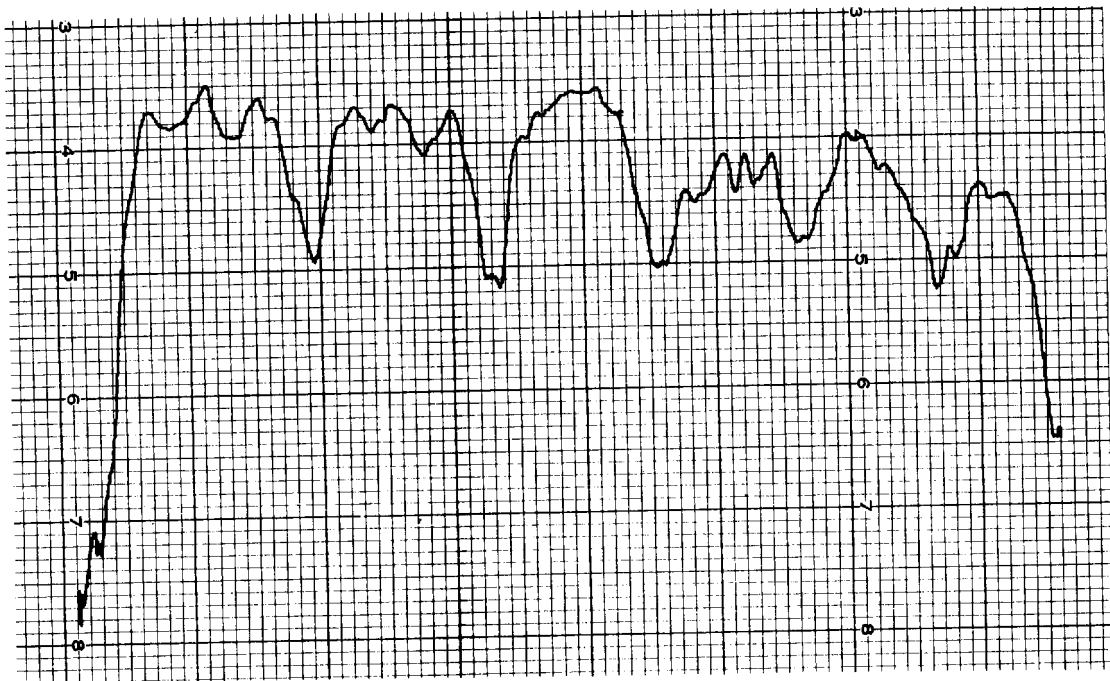


Figure G 9. Three-Bar Target Focused with 436 Millimicron Filter and Traced with 546 Millimicron Filter

STATINTL

Approved For Release 2005/02/10 : CIA-RDP78B04747A001100020006-2

Approved For Release 2005/02/10 : CIA-RDP78B04747A001100020006-2